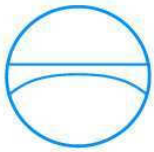

Technische Universität München

Time-Variable Gravity Field: Contributions of GOCE Gradiometer Data to Monthly and Bi-Monthly GRACE Gravity Field Estimates

Master's Thesis

Bearbeitet von: Moritz Rexer

Eingereicht am: 09. November 2012

Betreut von: Prof. Dr.techn. Mag. rer.nat. Roland Pail

Einrichtung: Institut für Astronomische und Physikalische Geodäsie

Studiengang: Masterstudiengang Geodäsie und Geoinformation
Fakultät für Bauingenieur- und Vermessungswesen

Technische Universität München
Arcisstraße 11, 80333 München

Abstract

A feasabiltiy study by Pail et al. (2011b) showed that GOCE satellite's ('Gravity field and steady-state Ocean Circulation Explorer') gradiometer data (SGG) in combination with its GPS derived orbit data (SST-hl) can be used to stabilize and reduce the (error) striping pattern in temporal (bi-monthly) GRACE satellite ('Gravity Recovery and Climate Experiment') gravity field estimates.

In the thesis, monthly and bi-monthly gravity fields for the year 2009 and 2010 are estimated on the basis of a combination of full GRACE SST-ll with full GOCE SGG normal equations. In contrast to the study of Pail et al. (2011b) focus is given to the impact of the gradiometer measurements, and whether they, solely, can improve the monthly GRACE estimates. Used GRACE normal equations from the *Astronomical Institute at the University Bern* (AIUB) are assembled up to d/o 60. Monthly GOCE SGG normal equations shall be assembled within the thesis to maximum possible d/o using the software package at the *Institute for Astronomical and Physical Geodesy* (IAPG), located at the *Techische Universität München* (TUM). For this purpose a semi-automatic outlier detection algorithm was implemented. The combinations are achieved by a variance component estimation and are investigated spatially in terms of equivalent water heights and spectrally with degree variances and degree standard deviations. Further, a method to statistically describe the extend of the the striping error in the monthly fields by means of a global RMSE is developed. Besides, the performance of gradients originating from the old and the new L1B processor is evaluated in the combinations.

Estimating monthly GOCE SGG gravity fields at high resolution (>d/o 150) is found to be a difficult task. In the investigated period stable normal equation systems could only be assembled for seven months, using old gradients, and three months, using re-processed gradients. Among those, some show remaining error structures which could not be removed in the outlier detection, as taking out more epochs perpetually led to instable normal equation systems. The officially released re-processed gradients show higher values in gradient anomalies for many epochs regarding GOCO02s, which lead to more outliers compared to the old gradients. Therefore, re-processed gradients do not show to advantage, as expected. The analysis of the striping error in the monthly and bi-monthly combinations and the comparison to GRACE-only solutions shows, that the error cannot be reduced significantly using GOCE SGG observations. The best result could be achieved for June 2010 where the RMSE reduction amounts from 2 - 7% at different degrees. In this month the GRACE solution is found to be extraordinary weak, which would explain the improvement due to GOCE SGG data. In the other months the reduction of the stripes hardly exceeds the 1% boundary at all degrees.

Kurzfassung

Eine Studie von Pail et al. (2011b) zeigt, dass die Messungen des Gradiometers (SSG) an Bord des Satelliten GOCE ("Gravity field and steady-state Ocean Circulation Explorer") in Kombination mit den GPS-bestimmten Bahnstörungen (SST-hl) benutzt werden können, um zwei-monatige Schwerefeldlösungen der Satellitenmission GRACE ("Gravity Recovery and Climate Experiment") zu stabilisieren und den Streifenfehler zu verringern.

In dieser Arbeit werden GRACE SST-ll Beobachtungen mit GOCE SGG Beobachtungen über ein- und zwei-monatige Zeiträume der Jahre 2009 und 2010 auf Normalgleichungsebene kombiniert. Im Gegensatz zur Studie von Pail et al. (2011b), in der auch GOCE SST-hl (GPS) Beobachtungen mit in die Kombination eingeflossen sind, wird in dieser Arbeit nur der Einfluss der Gradiometerbeobachtungen untersucht. Verwendete GRACE Normalgleichungen stammen aus dem *Astronomischen Institut der Universität Bern* (AIUB) und besitzen eine Auflösung von sphärisch-harmonischem Grad 60. Die Aufstellung monatlicher, möglichst hochaufösender GOCE SGG Normalgleichungen ist Teil der Arbeit und konnte am *Institut für Astronomische und Physikalische Geodäsie* (IAPG) der *Technischen Universität München* (TUM) mit der dort entwickelten Software durchgeführt werden. In diesem Zusammenhang wurde ein semi-automatischer Algorithmus zur Ausreißersuche für GOCE Gradienten implementiert. Die auf Basis einer Varianz-Komponenten-Schätzung bestimmten Kombinationen werden räumlich in äquivalenter Wasserhöhe und im Spektralraum auf Basis von Gradvarianzen untersucht. Eine speziell entwickelte, statistische Methode auf Basis eines globalen RMSE ist in der Lage, den Fehler in den monatlichen Feldern zu quantifizieren. In der Arbeit soll zudem das Ausmaß der Verbesserung durch die neue L1B Prozessierung in den Kombinationen untersucht werden.

Die Schätzung von monatlichen, hochauflösenden (>G/O 150) Schwerefeldlösungen rein aus Gradientenbeobachtungen stellt sich als eine schwierige Aufgabe heraus. In dem untersuchten Zeitraum konnten stabile Normalgleichungen nur für sieben Monate unter Verwendung von altem Gradienten und drei Monate unter Verwendung von reprozessierten Gradienten aufgestellt werden. Unter diesen befinden sich auch einige, in denen keine vollkommen fehlerfreie Lösung möglich war, da die Herausnahme weiterer, vermeintlicher Außreißer stets zu einer Instabilität der Systeme führte. Die offiziellen, re-produzierten Gradienten zeigen nicht das erwartete Ausmaß an Verbesserung in den Lösungen, da signifikant weniger Beobachtungen in die Schätzung eingehen. Dies ist auf eine erhöhte Anzahl von Ausreißern, die auf Basis von Gradienten Anomalien bezüglich GOCO02S detektiert werden, zurückzuführen.
Die Untersuchung des Streifenfehlers in den kombinierten ein- und zwei-monatigen Feldern zeigt bezüglich reiner GRACE Felder keine signifikante Verringerung bzw. Verbesserung. Bestenfalls, im Monat Juni (2010), kann der RMSE Wert um 2-7 % für unterschiedlichhohe Auflösungen reduziert werden. Eine plausible Erklärung dafür ist die verhältnismäßig schlechte GRACE Lösung in diesem Monat. In anderen Monaten ist durch die Kombination mit GOCE SGG kaum mehr als 1% RMSE Verringerung zu beobachten.

Contents

I Introduction **7**

1 Motivation 7

2 Temporal gravity variations from space 7

3 Aims of thesis 9

II Modeling temporal gravity variations on Earth and gravity field parameters **12**

4 The Earth's gravity field and its temporal variations 12

5 Spherical harmonic series expansion and gravity functionals 14
5.1 Geoid heights and gravity anomalies 15
5.2 Equivalent water heights 17

6 Gravity signal and error parameters 17
6.1 Degree variances 18
6.2 Degree (error) median 18
6.3 Degree standard deviation 19

III The satellite missions GOCE and GRACE and related gravity recovery methods **20**

7 GRACE 20
7.1 GRACE mission concept 20
7.2 Gravity recovery from GRACE observables 21
7.2.1 Single satellite approach 21
7.2.2 Baseline approach 21
7.2.3 Celestial mechanics approach 22
7.3 GRACE error structure and its handling 23
7.3.1 Dealiasing 23
7.3.2 De-striping – filter techniques 24

8 GOCE 25
8.1 GOCE mission concept 25
8.2 Gravity Recovery from GOCE observables 26
8.2.1 Direct method (DIR) 27
8.2.2 Time-wise method (TIM) 27
8.2.3 Space-wise method (SPW) 28
8.3 Outlier detection methods for GOCE gravity gradients 28
8.3.1 Tracelessness condition 29
8.3.2 Gravity gradient anomalies 29

8.4 Regularization . . . 29
8.5 GOCE time-wise processing at IAPG . . . 31

9 Variance component estimation 34

10 Least - squares parameter elimination for normal equations 35

IV Estimation and analysis of combined monthly and bi-monthly fields from GOCE and GRACE 37

11 Description of data 37
11.1 GRACE data . . . 37
11.2 GOCE data . . . 37
11.3 Consistency regarding time variable gravity signals . . . 39

12 Methodology and processing 39
12.1 GRACE data pre-processing . . . 41
12.2 GOCE data pre-processing . . . 42
12.2.1 Inclusion of non-tidal time variable signal . . . 42
12.2.2 Outlier detection . . . 42
12.2.3 Assembling of normal equations . . . 47
12.2.4 Regularization and solving GOCE SGG NEQs . . . 48
12.2.5 Parameter elimination . . . 49
12.3 Optimal combination of GOCE and GRACE on basis of normal equations . . . 51
12.4 Quality evaluation methods for gravity field estimates . . . 52

13 Results 53
13.1 GRACE SST-ll gravity field solutions . . . 53
13.2 GOCE SGG gravity field solutions . . . 57
13.3 Combined gravity field solutions from GRACE and GOCE . . . 61
13.3.1 Monthly combined solutions . . . 62
13.3.2 Bi-monthly combined solutions . . . 66

V Conclusion 68

VI Outlook 71

VII Annex 72

Acknowledgments 72

Abbreviations 73

References 75

List of Figures 78

List of Tables 80

Appended Figures 81

Appended Tables 87

Part I

Introduction

1 Motivation

GRACE is the satellite which today can observe temporal gravity variations globally with the highest spatial resolution. Furthermore, it provides the only observation technique which is able to resolve the variations temporally and spatially in a way that it becomes interesting for analysis in hydrology, climatology, oceanography, and related fields. Hence, an improvement of the performance of GRACE regarding the detection of time variable signals would be a real benefit not only from a geodetical perspective, but also for all applications relying on GRACE data.
The core idea for the improvement arises from the fact that the GRACE anisotropic errors significantly evolve from the GRACE observation configuration (along-track ranging) and not from the observations themselves. Full covariance propagation to a GRACE variance-covariance matrix gives evidence that the striping pattern already becomes visible in the geoid height errors at a spherical-harmonic degree and order of 30 to 40 (see, e.g, Pail et al. (2011b), and Mayer-Gürr and Kurtenbach (2010)). GOCE, another satellite measuring the gravitational potential, is actually dedicated to observe the static part of the Earth's gravity field, and has not been designed to resolve temporal time variable gravity signals (see ESA (1999)). One of the strengths of GOCE, however, lies in its highly isotropic error behavior. In this sense, GOCE gradient data is complementary to GRACE and may improve GRACE temporal gravity field estimates by reducing the striping pattern in affected spherical harmonic coefficients, as Pail et al. (2011b) already showed in a case study.

2 Temporal gravity variations from space

Beginning in the 1980's, the observation of gravity from space started a new era in the detection of temporal gravity variations. In contrast to ground-based gravity measurements with gravimeters, which can provide local (point-wise) measurements of gravity variations with a very high accuracy at high temporal sampling intervals, satellite-based measurements provide information about large-scale variations of the entire Earth. Of course, even today, satellites do not reach the accuracy of ground-based measurements simply due to thefact that the gravitational potential V decreases inversely with the distance r to Earth following $V \sim \frac{1}{r}$ (see Heiskanen and Moritz (1967)). Thus, a satellite is sensitive to the gravity signal at satellite height, which is of a much lower magnitude than it is at the Earth's surface.

The first observations of time variable gravity signals based on satellites were given by Satellite Laser Ranging (SLR), ground based measurements to satellites evaluating the traveltime of a laser beam. Remarkable results have been achieved by SLR tracking of the two NASA satellite missions launched in 1976 (LAGEOS)[1] and 1993 (LAGEOS II) [1]. However, due to the flight height of about 6000 km over ground, SLR measurements could mainly provide information about the temporal variation of the strongest acting signal, the Earth's changing oblateness (which mainly is expressed by the C_{20} coefficient). Apart from that, only information of a few

[1] LAGEOS 1/2 : http://ilrs.gsfc.nasa.gov/satellite_missions/list_of_satellites/lag1_general.html

other low-frequency harmonics could be derived (see Wahr (2007)).

The next important satellite in chronological order which was able to gather information about the Earth's gravitational field was the German mission *Challenging Microsatellite Payload* (CHAMP), launched in 2001 [2]. The gravity field solutions from this mission are based on the analysis of kinematic orbits, which are derived from GPS phase measurements. An accelerometer on board of the satellite could for the first time correct the disturbing effect of non-gravitational forces. The mission significantly contributed to the knowledge of the static part of the gravity field up to a spherical harmonic degree of about 60. In contrast, most geophysical signal spectra are below the CHAMP error level, and monthly results do not seem to reflect physically meaningful gravity variations, even for the lowest harmonics (see Sneeuw et al. (2005)). However, some studies show that under certain circumstances temporal gravity variations can be extracted from CHAMP observables in the low harmonics. An investigation of 2.5 years of CHAMP data by Reiberger et al. (2005) showed that temporal gravity variations derived from CHAMP are restricted to longest wavelengths (degree/order 4, half wavelength 5000 km) and time resolutions of more than three months. Prange (2010) presents sophisticated procedures which may enable the detection of most prominent seasonal gravity signal (e.g., in the Amazonas river basin) with a low resolution up to spherical-harmonic degree 10.

In 2002, the *Gravity Recovery And Climate Experiment* (GRACE) mission consisting of two satellites, which are still in operation, was launched jointly by NASA, DLR (*Deutsches Zentrum f ur Luft und Raumfahrt*) and GFZ (*Deutsches GeoForschungsZentrum*) [3]. Due to it's innovative and unique *satellite-to-satellite tracking* technique in *low-low mode* (SST-ll) and its low, near-polar orbit (see section 7), this mission can provide monthly global gravity field solutions up to a maximum spherical harmonic degree of 120. This equals to a spatial resolution for monthly fields of about 170 km on the Earth's surface. Hence, GRACE was the first mission to provide profound, globally consistent information about temporal changes of the Earth's gravity field. GRACE gravity field products find application in current analysis of global and regional mass (re-)distribution in the fields of climatology, hydrology, geophysics and cryosphere studies. Generally, the mass variations caused by the continental water cycle are the dominant signal component after subtracting contributions from the atmosphere and the oceans. This makes hydrology to the primary area of application (Werth et al. (2009)). However, GRACE gravity solutions suffer from an erroneous striping pattern which is caused by the satellite-to-satellite tracking only in along-track direction and aliasing effects resulting from high-frequency mass variations signal. These effects lead to anisotropically correlated noise of the potential coefficients and require adequate filtering and decorrelation techniques for the reconstruction of mass signal (see section 7.3).

The latest gravity field satellite mission to follow GRACE is ESA's *Gravity field and steady-state Ocean Circulation Explorer* (GOCE) mission, launched in 2009 [4]. This mission is dedicated to the determination of the static part of the gravity field using GPS and the first satellite-borne gradiometer ever flown, which facilitates direct measurements of gravity gradients along three axes (see section 8).

[2]CHAMP : http://op.gfz-potsdam.de/champ/
[3]GRACE : http://www.csr.utexas.edu/grace/
[4]GOCE : http://www.esa.int/SPECIALS/GOCE/index.html

The question whether GOCE is able to contribute to the estimation of time variable gravity fields has been a topic of research since the mission's acceptance. Before the operational phase of GOCE Jarecki et al. (2005) dealt with investigations on the necessity of de-aliasing of temporal gravity changes in GOCE gradiometric data. The study is based on simulations of the impact of (model derived) mass variations in different earth parts (Atmosphere, Hydrosphere, Cryosphere and Solid Earth) on the radial GOCE gradiometer component *Vrr*. Their analyses show that modeled hydrological and ice mass changes are neither critical for GOCE gradients in terms of amplitude ($<$ 1mE) nor do the timescales of the changes fit into the gradiometer's measurement bandwidth ($5 \cdot 10^{-3}$ Hz to $1 \cdot 10^{-1}$ Hz, see ESA (1999)). In the same way, modeled gradients from oceanic and atmospheric mass changes as well as changes due to ocean and solid Earth tides are below the gradiometer's performance, regarding spectral considerations. In conclusion, a reduction of geophysical effects which are causing mass and gravity fluctuations in the system Earth is not necessary for GOCE gradients, because their impact is negligible. However, de-aliasing can lead to an improvement of the stochastic behaviour of the gradiometer. In another study by Peters et al. (2001) similar results with focus on the impact of atmospheric mass changes only could be achieved. In simplified estimations of the PSD's of daily gravitational signals mapped into GOCE-like gradients, they found the influence generally to be under the GOCE error PSD. But they also found that the removal of the effects are necessary as small parts of the effects may be sensed and show potential for systematic errors when it comes to the determination of the static part of the gravity field. Especially affected are the along-track and radial gradient components.

A first analysis on the potential improvement of time variable GRACE gravity field estimates through GOCE was done by Pail et al. (2011b). The study is based on real observations and aims to determine (1) the contribution of GOCE data to GRACE fields and (2) whether standalone time variable solutions from GOCE orbit information are solvable. In the investigations focus is given to the fact that the error structure in GRACE is highly anisotropic, whilst the error structure of the GOCE gradiometer is isotropic. Additionally the authors expect GOCE to deliver some valuable information because they found that signals from geophysical models tend to be underestimated in terms of amplitude. They show that GRACE is able to resolve time variable signal (in areas of Greenland, Ganges, Amazon) up to degree 50-60, but the striping effect start already at degree 30 - 40. Hence, the reduction of the striping pattern through an inclusion of GOCE might improve the time variable solution in this domain. In core, the analysis of a pure bi-monthly GRACE solution in comparison to a combined bi-monthly GOCE (SGG + SST-hl) and GRACE solution for the months November and December 2009 show, that the GRACE striping pattern can be reduced significantly between the degrees 30 and 40. However, the high impact of GOCE may partly be due to the fact that the quality of the GRACE solution in the observed two months was worse than usual because GRACE flew a 7-days sub-cycle.

3 Aims of thesis

In this thesis the impact of GOCE gradiometer observations on GRACE monthly and bi-monthly gravity field estimates shall be investigated. As shown above, it has been proven that GOCE gradiometer (SGG) data together with GOCE GPS (SST) data can improve GRACE SST temporal gravity estimates. The role of the gradiometer solely, however, remains unclear. For this purpose monthly and bi-monthly GOCE SGG normal equations shall be assembled for the year 2010 from ESA's officially released gradient products. The positive or negative contributions

of those normal equations when combined with corresponding monthly or bi-monthly GRACE normal equations shall be examined. GRACE normal equations used for the combination are provided by the Astronomical Institute in Bern. In the investigation special attention is given to the impact of GOCE L1B processing in the combination. The performance of GOCE gravity gradients processed according to a newly developed enhanced procedure (Stummer et al. (2011)) is compared to the performance of gradients originating from the old procedure.
GOCE SGG normal equations shall be processed according to the time-wise strategy because it is the only GOCE processing procedure not including external information. This is essential because including external information would make the determination of the true impact of the gradiometer impossible.

In the context of the investigations it shall be dealt with the following questions:

- Can GOCE SGG normal equations be assembled for monthly periods?
- Can GOCE SGG help to improve monthly and bi-monthly GRACE gravity field estimates?
- Is there additional benefit due to the new L1B - processing strategy?
- Is the striping pattern inherit to GRACE solutions reduced significantly due to GOCE gradiometer data?
- Can we get rid of the necessity to apply de-striping procedures? Is there benefit for regional analysis of water storage changes?
- How can the quality of monthly GRACE solutions and accordingly the extent of the striping error be assessed and quantified?
- Is there benefit only for weak GRACE solutions? To what extent is the 7-days sub-cycle degrading the GRACE solution?

In order to find answers to these questions it will be proceeded in the following way :

In part II a general understanding of gravity variations of the Earth's gravity field is provided together with the basics for globally modeling temporal gravity variations in a spherical-harmonic approach. Common methods to evaluate spherical-harmonic gravity field estimates in spatial and spectral domain are presented, likewise.
Part III introduces both satellite mission concepts and typical gravity recovery methods. In this context the GRACE error type is described together with some de-aliasing and de-striping methods to cope with it. Further, outlier detection methods for GOCE gradients and regularization approaches which are both needed to process GOCE SGG gravity field estimates are presented. Then the software used to process GOCE gradient data following the time-wise method is explained. In the end of this part two methods which find application in the combination of GOCE SGG with GRACE SST normal equations, a least-squares parameter elimination and a variance component estimation, are introduced.
In part IV the initial data sets and single steps which are needed to get from the given data-sets to the combined GOCE SGG - GRACE SST gravity field solutions are described. Hand-in-hand with the methodological description, in each step preliminary results and arising issues are discussed. Finally, the resulting combined monthly and bi-monhtly gravity field solutions are

presented and analyzed qualitatively as well as quantitatively.
In part V the results are summarized and a conclusion is drawn regarding the initially posed questions and aims.
At the end of the thesis the references, a list of frequently used abbreviations, a list of figures and a list of tables is appended together with some large figures and tables.

Part II

Modeling temporal gravity variations on Earth and gravity field parameters

In this part of the thesis not only a common understanding of temporal gravity variations on Earth and its sources shall be given, but also the basics for modeling and visualizing global temporal gravity variations are introduced. First, in section 4 the reasons for changes in the gravity field of the Earth are described, and the different sources are categorized by their temporal behavior. Second, in section 5 the basic mathematical model for describing gravity and gravity variations in a global approach, the spherical harmonic series expansion, is introduced. The model allows the expression of the gravity field in terms of different gravity functionals which are introduced likewise. In section 6 common parameters for describing gravity signal and errors in the frequency domain, so called degree variances, are defined.

4 The Earth's gravity field and its temporal variations

Changes of the Earth's gravitational field do either refer to processes related to the gravitational attraction of sun and moon (and other planets) or to mass transports within geophysical fluids. Direct tides resulting from the gravitational attraction of other celestial bodies appear at different periods (most dominant: diurnal and semi-diurnal period), spatial scales and with a magnitude up to $10^{-7}g$, where g denotes the mean gravity acceleration (see Torge (1980) in Peters et al. (2001)). Meanwhile, direct tides are very well known and can be eliminated from measurements using tide models (see Peters (2007)). Therefore, direct tides will be neglected from all upcoming discussions although they are omnipresent. The effect of tidal deformation produced by tidal forces on solid Earth, ocean, and atmosphere, and the processes in geophysical fluids, however, will be considered.

In principle, all mass transports and all density changes below, at, and above the Earth's surface cause a change in the Earth's gravity field. But not all of those processes are relevant considering up-to-date measurement accuracies and observation techniques. Table 1 gives an overview of sources causing gravitational variations regarding their spatio-temporal characteristics and their magnitude, expressed in geoid heights. In the following, the individual processes will be classified by their temporal behavior as suggested by Peters (2007), and their effects are explained:

Instantaneous and irregular variations
Earthquakes and volcanic eruptions are the most prominent sources for variations of this class. As they appear instantaneously, they cannot be modeled, and gravitational variations always refer to the pre-event and post-event state of the gravity field. Locally, significant changes in the gravitational field can be measured. (c.f Peters (2007))
Today, there exist various studies that show that GRACE is sensitive for earthquakes, e.g., for the Sumatra-Andaman earthquake (see, e.g, Han et al. (2006), and Chen et al. (2007)).

Daily up to yearly periodical variations
Referring to table 1 all variations caused by tidal deformation, atmosphere, ocean and continental hydrology can be found within daily up to yearly periods.

Source, Process	Spatial Scale [km]	Dominant Periods	Dimension in Geoid Heights [mm]
Solid-earth and ocean tides	50 - 5000	daily, semi-daily semi-monthly	100 - 150
Atmosphere	20 - 2000	yearly, seasonal, daily	15
Ocean currents	100 - 1000	yearly, seasonal	10
Ocean surface	100 - 1000	decades	1 - 3 p.y.
Continental water	10 - 8000	yearly, seasonal	10 - 12
Cryosphere	100 - 1000	seasonal, decades	1 - 3 p.y.
Earthquakes	10 - 1000	single events	0.5
Volcanic Eruptions	10 - 100	single events	0.5
Glacial isostatic adjustment	1000 - 10000	secular	1 - 2 p.y.
Plate tectonics	>500	secular	?
Core and Mantle	>5000	secular	0.005

Table 1: Temporal gravity variations and their characteristics (Peters, 2007) (modified)

Among those, the most dominant impact on the gravitational field is given by tidal deformation and ocean tides with $100 - 150[mm]$ geoid height variation. Due to the attraction of sun and moon, the solid Earth body and the ocean surface is deformed following the periods of their ephemerids. In principle, also atmosphere masses are affected by the attraction. Due to the low density of the atmosphere, the gravitational impact is smaller. Nowadays, solid Earth tides as well as pole tides can be sufficiently modeled for most applications using relatively simple models (see IERS Conventions (Petit and Luzum, 2010)). Pole tides is an effect that describes the polar motion induced (centrifugal force) additional ocean tides, and is of minor amplitude. Polar motion is the movement of the celestial pole around the figure axis of the earth (conventional pole) and is dominated by the 14-month *Chandler wobble* period and annual variations. Ocean tides, however, require a more complex modeling, but models also reach high spatial resolutions ($0.25°$ *to* $0.125°$). In polar regions, the lack of altimeter measurements leads to a poor accuracy of those models of around 10 *cm*. Coastal areas are likewise determined with poorer quality in ocean models, due to more complex currents and uncertainties regarding water depth, water temperature and salinity. Also, altimetry delivers less valuable information in coastal areas because the technique faces issues, such as restrictions due to the swath width.

One order of magnitude below the tidal effects are gravity variations caused by mass transports in the atmosphere, ocean and continental hydrosphere. The mass signals from these components are dominated by an annual and a semi-annual period. The three components are deeply connected within the hydrological circle, which is mainly driven by solar radiation. Processes like evaporation, precipitation, water storage (e.g., clouds, ground water, soil moisture, water bodies, ice) account for most gravitational variations. Furthermore, atmosphere and ocean show strong interaction, as parts of the atmospheric loading are compensated by the ocean.
Gravity variations from those components can be subdivided into the direct effect of mass attraction and the indirect (smaller) effect of mass loading (*loading effect*). Loading leads to a deformation of the body of the solid Earth, which leads to a change in the gravity field.

In the atmosphere processes like humidity changes, wind, evaporation and precipitation cause mass transport and change the gravity field with daily, seasonal and yearly periods. In the ocean water mass changes due to currents, and in- and outflow cause variations with annual and seasonal periods. Often, because of heavy interactions between ocean and atmosphere, both components are investigated together and modeled in coupled models (oceanic models require atmospheric parameters as input). Continental hydrosphere describes the cosmos of water stored in surface water bodies (e.g., lakes and rivers), ground water, soil humidity, snow and ice canopy as well as water stored in plants. A lot of efforts have been made to describe the Earth's hydrosphere in models. Differences between the models exist, e.g., models like GLDAS (*Global Land Data Assimilation Center*), LaD (*Land Dynamics Model*), CPC (*Climate Prediction Center*) and WGHM (*Water Gap Hydrology Model*) do not all include all kinds of continental water storage. Further, hydrological models do not reach the temporal ($< 1\ day$) and spatial resolution ($< 1°$) of atmosphere and ocean models. Often snow masses in Antarctic or Greenland are missing completely due to rare observations in these areas. However, within regional analysis of water storage changes within river catchments the models show good correlation with water storage changes derived from GRACE measurements (c.f. Peters (2007)). Furthermore, hydrological models can be improved using GRACE data, as shown in Güntner (2008).

Long periodic and secular variations

This group of mass variations comprises effects related to changes of the cryosphere and to effects underneath the Earth's surface. All the effects have in common that they lead to changes in the gravity field which can only be recognized as trends in measurements over many years.
Melting and accumulation of ice masses influences the sea level and lead to the post-glacial rebound of the elastic Earth body (glacial isostatic adjustment (GIA)). The changes of glacial ice masses mainly go in hand with the global, cyclic changes of warm periods and ice ages with periods of one or more millenniums. When glaciers are melting and the surface load is reduced, the Earth's surface bounces upwards slowly and leads to almost secular changes in the gravity field. The consequence of the melting of ice masses on land is an augmentation of the water mass in the oceans. There is evidence that the sea level within such a cycle can change for more than 100 meters. Note, that the sea level change is caused by mass variations in the ocean and thermal expansion.
The processes underneath the surface which can lead to mass variations are mantle convection, plate tectonics and processes within the Earth's core. Those effects happen in timescales of millions of years and they are most relevant for the state of the static part of the gravity field. (see Peters (2007))

5 Spherical harmonic series expansion and gravity functionals

The Newtonian gravity potential V of the Earth can be described as series of dimensionless spherical harmonic coefficients $\bar{C}_{nm}$ and $\bar{S}_{nm}$ of degree n and order m. It can be retrieved from the coefficients with the series expansion

$$V(\lambda,\phi,r) = \frac{GM}{R}\sum_{n=0}^{\infty}(\frac{R}{r})^{n+1}\sum_{m=0}^{n}\bar{P}_{nm}(cos(\phi))[\bar{C}_{nm}cos(m\lambda)+\bar{S}_{nm}cos(m\lambda)] \tag{1}$$

for any point on and above the Earth, where λ, ϕ and r is the triplet of spherical coordinates, R is the semi-major axis of the Earth, GM denotes the gravitational constant times the mass

of the Earth; $\bar{P}_{nm}$ are the normalized associated Legendre functions of degree n and order m (see, e.g., Heiskanen and Moritz (1967)). Due to the fact that the coefficients of the series are dimensionless, any other gravity field functional (e.g., gravitational acceleration or gravity gradients) can be derived by the choice of the right dimensioning factors and transfer coefficients (see Peters (2007)).
Changes in the gravitational field ΔV over the period t can be described likewise as changes in the spherical harmonic coefficients $\Delta\bar{C}_{nm}$ and $\Delta\bar{S}_{nm}$. In a general so-called Eulerian approach, these changes can be regarded as density distribution variations $\Delta\rho$ of the Earth over time, from which the spherical coefficients can be retrieved following the equation

$$\left.\begin{matrix}\Delta\bar{C}_{nm}(t)\\ \Delta\bar{S}_{nm}(t)\end{matrix}\right\} = \frac{1}{2n+1}\frac{1}{M}\iiint_{\Sigma}(\frac{r}{R})^n\Delta\rho(\phi,\lambda,r,t)\bar{P}_{nm}(cos(\phi))\left\{\begin{matrix}cos(m\lambda)\\ sin(m\lambda)\end{matrix}\right\}d\Sigma \qquad (2)$$

(see Wahr and M. (1998)). Under simplifying assumptions that all mass redistributions happen in a thin layer of thickness $H << R$, the surface density change $\Delta\sigma$ can be introduced as the product of the layer's height H and the density $\Delta\rho$. Then the direct gravitational attraction of the surface mass accounts for changes in the potential through

$$\left.\begin{matrix}\Delta\bar{C}_{nm}(t)\\ \Delta\bar{S}_{nm}(t)\end{matrix}\right\} = \frac{3}{4\pi R\bar{\rho}(2n+1)}\iint_{\sigma}\Delta\sigma(\phi,\lambda,t)\bar{P}_{nm}(cos(\phi))\left\{\begin{matrix}cos(m\lambda)\\ sin(m\lambda)\end{matrix}\right\}d\sigma \qquad (3)$$

following equation 2, where $4/3\pi G\bar{\rho} \approx M$ and $\bar{\rho}$ is the constant mean density of the Earth. However, the indirect effect of the surface mass, which loads and deforms the underlying solid Earth, is not yet included in equation 3. This indirect effect leads to a lowering of the bigger direct effect. Using the *Love* numbers k'_n of degree n for surface loadings, which express the elastic behavior of the Earth, the total effect of surface masses on the potential can be described by

$$\left.\begin{matrix}\Delta\bar{C}_{nm}(t)\\ \Delta\bar{S}_{nm}(t)\end{matrix}\right\} = \frac{3(k'_n+1)}{4\pi R\bar{\rho}(2n+1)}\iint_{\sigma}\Delta\sigma(\Phi,\lambda,t)\bar{P}_{nm}(cos(\phi))\left\{\begin{matrix}cos(m\lambda)\\ sin(m\lambda)\end{matrix}\right\}d\sigma \qquad (4)$$

(cf. Wahr and M. (1998)). Equation (4) and (1) then give a simplified model for changes of the gravitational potential due to surface mass changes.

Temporal gravity changes, as well as surface mass changes, from GRACE satellite data can be derived from the observed changes in the spherical harmonic coefficients $\Delta\bar{C}_{nm}(t)$ and $\Delta\bar{S}_{nm}(t)$. They can be obtained by the subtraction of the spherical harmonic coefficients of a mean (stationary) gravity field from the gravity field coefficients estimated from (GRACE) gravity observations over a certain period of time. In the case of GRACE coefficients can be estimate already from one month of data (hence the temporal resolution of GRACE is one month) and mainly seasonal changes and trends can be detected in the gravity field.

5.1 Geoid heights and gravity anomalies

Geoid heights and *gravity anomalies* are the typical gravity functionals in geodesy which are used to describe the gravity on Earth. The geoid describes the equipotential surface which approximates the mean sea level and can be considered as a hypothetical ocean covering the whole earth at rest (without any dynamics). Geoid heights N define the geometrical height of the geoid above a reference ellipsoid at any point on earth. Gravity anomalies $\Delta g = g - \gamma$ describe the difference between the measured gravity g and the normal gravity γ (c.f. Heiskanen

and Moritz (1967)).

Both, geoid heights and gravity anomalies are derived from the disturbing potential $T = W - U$, where W denotes the (real or observed) gravity potential (incl. centrifugal potential) of the Earth and U describes the normal potential. The normal potential is the potential of a reference ellipsoid and is described by 4 gravitational parameters, e.g., by the geodetic reference system of 1980 (GRS80). Sound explanations on the derivation of both functionals from the disturbing potential in spherical harmonic notation are for example given by Hofmann-Wellenhof and Moritz (2006) and Torge (2003). Here only the basic formulas shall be given.

The disturbing potential T at the point P in spherical harmonic notation can be written as

$$T_P = \frac{GM_0}{R} \sum_{n=2}^{\infty} \left(\frac{R}{r_p}\right)^{n+1} \sum_{m=0}^{n} \bar{P}_{nm}(cos(\phi_p)) \left[\delta\bar{C}_{nm} cos(m\lambda_p) + \delta\bar{S}_{nm} sin(m\lambda_p)\right] \tag{5}$$

where r_p, ϕ_p and λ_p describe the spherical coordinates of the point P and $\delta\bar{C}_{nm}$ / $\delta\bar{S}_{nm}$ the residual coefficients after subtraction of the coefficients of the normal potential. The expansion starts at degree $n = 2$, because a perfect consistency of the masses of the normal ellipsoid and the Earth's body and identical centers of gravity are presumed.

The geoid heights N are related to the disturbing potential by *Bruns formula* which reads

$$N = \frac{T}{\gamma} \tag{6}$$

and in spherical harmonic notation the geoid heights can be expressed in spherical approximation by

$$N_P = R \sum_{n=2}^{\infty} \sum_{m=0}^{n} \bar{P}_{nm}(cos(\phi_p)) \left[\delta\bar{C}_{nm} cos(m\lambda_p) + \delta\bar{S}_{nm} sin(m\lambda_p)\right] \tag{7}$$

for any point P on the surface of the Earth ($r_p = R$).

Gravity anomalies Δg can be written as

$$\Delta g = g_P - \gamma_Q \tag{8}$$

and denote the difference of the measured gravity g_P at a point P on the Earth's surface and the normal gravity γ_Q on the reference ellipsoid. The relation to the disturbing potential T is then given by

$$\Delta g = -\frac{\partial T}{\partial R} + \frac{1}{\gamma}\frac{\partial \gamma}{\partial R}\, T. \tag{9}$$

Expressed in spherical harmonic notation the gravity anomalies read

$$\Delta g = \frac{GM}{R^2} \sum_{n=2}^{\infty} (n-1) \sum_{m=0}^{n} \bar{P}_{nm}(cos(\phi_p)) \left[\delta\bar{C}_{nm} cos(m\lambda_p) + \delta\bar{S}_{nm} sin(m\lambda_p)\right] \tag{10}$$

for any point P on the geoid ($r_p = R$).

5.2 Equivalent water heights

In order to treat hydrological and oceanic gravity variations, we usually do not use functionals like geoid heights or gravity anomalies, but rather *equivalent water heights (EWH)* are used. They actually describe the pressure p, which acts on a certain area through the gravitational attraction g of a water layer of height h and density ρ_{water} ($p = h \cdot \rho_{water} \cdot g$) (see Wahr and M. (1998)). The unit of EWH is normally chosen as millimeters of water column [mm WC] or surface density [$\frac{kg}{m^2}$] where

$$1[mmWC] = \frac{1kg}{1m^2} \tag{11}$$

with a water density ρ_{water} of 1000 [$\frac{kg}{m^3}$]. If water height changes $\Delta\kappa$ in mm are available globally (from models or satellite observations), spherical coefficient changes can be computed as follows:

$$\left.\begin{matrix}\Delta\bar{C}_{nm} \\ \Delta\bar{S}_{nm}\end{matrix}\right\} = \frac{3}{4\pi R\bar{\rho}(2n+1)} \iint_\sigma \Delta\kappa(\phi,\lambda,t)\bar{P}_{nm}(cos(\phi))\left\{\begin{matrix}cos(m\lambda) \\ sin(m\lambda)\end{matrix}\right\} d\sigma \tag{12}$$

Likewise, the EWH changes $\Delta\kappa$ can be retrieved from the potential coefficient changes by the spherical harmonic synthesis

$$\Delta\kappa(\phi,\lambda,r) = \frac{R\bar{\rho}}{3} \sum_{n=0}^{\infty}(2n+1) \sum_{m=0}^{n} \bar{P}_{nm}(cos(\phi))[\Delta\bar{C}_{nm}cos(m\lambda) + \Delta\bar{S}_{nm}cos(m\lambda)] \tag{13}$$

as shown by Wahr and M. (1998). The inclusion of the coefficients of degree $n = 0$ and $n = 1$ requires a discussion. The C_{00} coefficient, when investigating gravity changes of the entire system Earth, does not change, as it represents the total Earth's mass. However, looking at just one component of the system, e.g., the oceans, the mass is not constant as the ocean exchanges water with the atmosphere. Consequently, here, changes $\Delta\bar{C}_{00}$ in the gravity are possible. The values of the $n = 1$ coefficients are proportional to the position of the Earth's center of mass relative to the chosen coordinate system. All those terms are zero, under the assumption that the instantaneous center of mass always coincides with the coordinate system's origin. Again, looking just at one component, the terms do not vanish. For example, the redistribution of ocean masses can change the center of mass of the ocean (c.f. Wahr and M. (1998)).

With equations 12 and 13, equivalent water heights can also be interpreted as the height of a water layer above a certain area, which needs to be removed or restored to explain a certain change in gravity. Throughout the thesis, when EWH find application, the variations in $n = 0$ and $n = 1$ coefficients are set to zero, because those terms are not provided for GRACE solutions.

6 Gravity signal and error parameters

In this section other methods for the description of gravity fields and gravity field changes are introduced, which do not refer to the spatial domain like the gravity functionals described in previous sections.
Different signal and error parameters for gravity fields on the basis of spherical harmonic coefficients (see section 5) are defined, which play an important role in the validation and quality assessment of gravity field solutions.

6.1 Degree variances

Assessing coefficients per degree allows a much better interpretation than the visualization of all spherical coefficients. Degree variance as described in Gruber (2011) are based on a degree-wise summation of the squared spherical harmonic coefficients. Degree variances c_n^2 describing the signal (energy) content of a gravity field per degree n are given by

$$c_n^2(\bar{C}_{nm}, \bar{S}_{nm}) = \sum_{m=0}^{n} (\bar{C}_{nm}^2 + \bar{S}_{nm}^2). \tag{14}$$

In order to relate degree variances to other gravity functionals, scaling factors have to be introduced, e.g., degree variances for geoid heights [m] are given by

$$c_n^2\{N\} = R^2 \; c_n^2(\bar{C}_{nm}, \bar{S}_{nm}) \tag{15}$$

where R is the radius of the Earth.

The error behavior of a gravity field model can likewise be expressed through degree variances of the formal errors σ^2 of the coefficients (*error degree variances*) :

$$c_{error,n}^2(\bar{C}_{nm}, \bar{S}_{nm}) = \sum_{m=0}^{n} (\sigma^2(\bar{C}_{nm}) + \sigma^2(\bar{S}_{nm})). \tag{16}$$

Other related error parameters based on degree variances are cumulative error degree variances, omission error and commission error. The cumulative error degree variances are the accumulated sum of error degree variances up to a certain maximum degree N. The commission error is the cumulative geoid error up to a certain degree. The omission error describes the loss of signal which is caused by the omission in terms of a spherical harmonic series expansion beyond a maximum degree N. All the signal of a hypothetical series expansion from degree $N+1$ up to infinity is then defined as omission error

$$c_{omission,N}^2 = \sum_{n=N+1}^{\infty} \sum_{m=0}^{n} (\bar{C}_{nm}^2 + \bar{S}_{nm}^2). \tag{17}$$

Signal degree variances can also be retrieved from models and serve as a good first quality indicator when compared to calculated degree variances. Model degree variances can be derived from *Kaula's rule* which is given by

$$c_n^2 = \frac{1.6 \cdot 10^{-10}}{n^3} \tag{18}$$

while there exist more complex models like the *Tscherning/Rapp model* (see Gruber (2011)), which shall not be explained here.

6.2 Degree (error) median

The *degree median* is one method to overcome the problem of polar gaps in gravity field models due to imperfect global data acquisition, when it comes to the illustration of gravity fields in terms of degree variances (c.f. Sneeuw (2000)). The coefficient in the center of value-sorted coefficients per degree is taken as representative (median) value.

This parameter is only applicable to the absolutes of the variations of coefficients (Peters (2007)). This means one usually subtracts the coefficients of a reference gravity model in order to get the variations of the coefficients to the reference. If the reference gravity model is known to be of higher quality, the variations show the error of the investigated gravity coefficients. Computing the degree median out of the absolute values of the errors results in the *degree error median*.

6.3 Degree standard deviation

In order to visualize the differences between a gravity field and a reference field (e.g. from ICGEM) the *degree standard deviation* is a practicable parameter. It computes the standard deviation of the coefficient differences per degree under inhibition of the polar gap problem, which is inherent to GOCE observables. The degree standard deviation is defined in Pail et al. (2012) as

$$\sigma_n = \sqrt{\frac{1}{2(n - m_{min,n}) + 1} \sum_{m=m_{min,n}}^{N} [(\bar{C}_{nm} - \bar{C}_{nm}^{ref})^2 + (\bar{S}_{nm} - \bar{S}_{nm}^{ref})^2]} \tag{19}$$

with the spheric harmonic coefficients $\bar{C}_{nm}^{ref}$ and $\bar{S}_{nm}^{ref}$ of a reference field and the minimal order $m_{min,n}$, which is not affected by the polar gap any more. The rule of thumb for the undistorted minimal order

$$m_{min,n} = \Theta_0 * n \tag{20}$$

where Θ_0 denotes the size of the polar gap ($\frac{\pi}{2} - I$, I : satellite inclination) in radians, is defined in Sneeuw and Gelderen (1997). The polar gap of GOCE mission ($I = 96.70°$) accounts for $\Theta_{0,GOCE} = 6.7°$ (see also section 8.4).

Part III

The satellite missions GOCE and GRACE and related gravity recovery methods

In this part the mathematical background and tools for retrieving the Earth's gravity potential and its temporal variations in terms of a spherical harmonic analysis from the measurements of both satellites shall be provided.
First, the GRACE mission concept and the measurement principle is presented (see section 7). In this context three possible ways of deriving gravity from GRACE via a generalized orbit determination problem, the *single satellite approach* (see section 7.2.1), the *baseline approach* (see section 7.2.2), and the *celestial mechanics approach* (see section 7.2.3) are introduced. Then the reasons for the erroneous striping pattern in GRACE solutions and one simple method to cope with it, *Gaussian smoothing*, are explained.
Second, the mission concept of GOCE (see section 8) and gravity recovery from the observables with three different approaches, the *direct approach* (see section 8.2.1) , the *time-wise approach* (see section 8.2.2), and the *space-wise approach* (see section 8.2.3) are presented. Different methods to treat with outliers in GOCE gradient timeseries are given in section 8.3. In section 8.4 regularization methods for dealing with the GOCE-type ill-posed normal equations are described. The working principle of GOCE SGG processing software used at IAPG is explained in section 8.5.
In the end of this part the formulas of a *variance component estimation* (see section 9) for optimally combining GRACE and GOCE normal equations and the formulas for a least-squares parameter elimination (see section 10) are given.

7 GRACE

7.1 GRACE mission concept

The GRACE satellite mission was jointly launched by NASA and the German Space Agency DLR in March 2002. The design of the mission, which consists of two identical satellites following each other in a distance of about 220km in an altitude of less than 500 km, makes it very useful for the observation of time variable gravity. The core instrument on board of each satellite is a microwave (K-band) ranging system, which is able to continually measure the distance between the two satellites with a very high accuracy. The microwave satellite-to-satellite tracking system (SST-ll) guarantees relative positioning with an uncertainty of less than $\frac{1}{100}$ of the thickness of human hair (less than a micron). As the distance between both satellites is heavily related to the current attraction and acceleration of each satellite in the gravity field of the Earth, temporal and spatial gravity changes can be detected analyzing the distance variations. Additionally, the GRACE satellites are equipped with an accelerometer accounting for the measurement and correction of non-gravitational forces (e.g., atmospheric drag) in post-processing. Further, each spacecraft has an on-board GPS receiver, which delivers the orbital position and orbital movement in the global GPS reference frame. The GPS satellite-to-satellite measurements (SST-hl) themselves can be used to solve for low gravity field harmonics and to stabilize the SST-ll solutions in this domain.
All this raw data, called Level-1 data, is made commonly available and may be used to solve for gravity fields. Further, several project-related processing centers such as the *Center for Space*

Research (CSR) at the University of Texas, the *GeoForschungsZentrum* (GFZ) in Potsdam or the *Jet Propulsion Laboratory* (JPL) provide spherical harmonic solutions of monthly averaged gravity fields (up to d/o = 120), called Level-2 data. (see Wahr (2007))

7.2 Gravity recovery from GRACE observables

Generally, gravity field parameters are retrieved from GRACE Level-1 observables (see section 7) using various forms of a generalized orbit determination problem.
The orbit determination problem is following the equation of motion of a low orbiting satellite including all perturbing accelerations (see, e.g., Jäggi et al. (2009) or Jäggi et al. (2010)) which reads in the inertial frame as

$$\underline{\ddot{r}} = -GM\frac{\underline{r}}{r^3} + \underline{f_1}(t, r, \dot{r}, q_1, ..., q_d), \tag{21}$$

together with a set of initial conditions $r^k(t_0) = r^k\ (E_1, ..., E_6; t_0)$, $k = 0, 1$ where E_i with $i \in [1, 2, ..., 6]$ describe the 6 Keplerian elements for epoch t_0. GM denote the gravitational constant times the mass of the Earth, and q_j with $j \in [1, 2...3]$ are additional unknown dynamical parameters. Among those perturbing accelerations which act on a low earth orbiter (LEO) we find the gravity field parameters. The gravity field parameters refer to the series of normalized spherical harmonic coefficients described in Heiskanen and Moritz (1967) from degree 2 up to degree 90.

7.2.1 Single satellite approach

In the *single satellite approach* described in Jäggi et al. (2009) first pseudo-observations are determined from precise point positioning as a time series of epoch-wise coordinate triplets of kinematic positions and its error estimates (covariance information). Then normal equations are set up for the unknown gravity field coefficients on a daily basis with the pseudo-observations weighted according to their covariance information. This is done using equation 21 simplified to an orbit improvement process where the actual orbit $r_j(t)$ with $j \in \{a, b\}$ of each of the two satellite A and B is expressed as a truncated Taylor series of the form

$$r_j(t) = r_{j0}(t) + \sum_{i=1}^{n_j} \frac{\delta r_{j0(t)}}{\delta p_{ji}} \Delta p_{ji} + \sum_{i=1}^{n_c} \frac{\delta r_{j0(t)}}{\delta p_{ci}} \Delta p_{ci} \tag{22}$$

with respect to the n_i unknown arc-specific orbit parameters p_{ji} and to the n_c unknown gravity field coefficients p_{ci} (see Jäggi et al. (2010)). Applying numerical integration techniques, observation equations can be formulated which are needed to set up the normal equations in a standard least-squares adjustment approach. Obtained normal equations can then be accumulated to weekly, monthly and annual systems and can be inverted to retrieve the spherical harmonic coefficients and full covariance information. To be precise, only corrections to an a priori static gravity field are estimated in the approach.

7.2.2 Baseline approach

A slight modification to this method is given by the *baseline approach* (see Jäggi et al. (2009)), where differenced GPS observables are used to generate the LEO positions together with its covariance information. This procedure can provide kinematic orbits with a few mm precision

and reduced-dynamic orbits with sub-mm precision in an extended Kalman filter environment or with similar techniques. The method qualitatively shows independence regarding the chosen reference trajectory needed for reduced-dynamic orbits.
In both above described approaches K-band data serves as independent, direct source of validation for the kinematic distance between both GRACE A and B. K-band range residuals can be used in order to determine systematic errors of the kinematic orbit determination and to separate those errors from systematic errors occurring during gravity field recovery.

7.2.3 Celestial mechanics approach

Another method to retrieve the Earth's gravity field parameters using both GRACE observations types is the *Celestial Mechanics Approach*. Here, the inter-satellite K-band range-rate measurements (SST - ll) are used as observations and the GPS-derived kinematic positions (SST - hl) are introduced as pseudo-observations in a generalized orbit determination problem (see Jäggi et al. (2010)). On the basis of a priori orbits, daily normal equations for both types of (pseudo-) observations are set up into independent systems. A differential orbit improvement process with the actual distance $r_a(t) - r_b(t)$ between both satellites A and B may be expressed as a truncated Taylor series of the unknown parameters. The Taylor expansion follows the expression

$$\begin{aligned} r_a(t) - r_b(t) = r_{a0(t)} - r_{b0(t)} \\ + \sum_{i=1}^{n_a} \frac{\delta r_{a0(t)}}{\delta p_{ai}} \Delta p_{ai} \\ - \sum_{i=1}^{n_b} \frac{\delta r_{b0(t)}}{\delta p_{bi}} \Delta p_{bi} \\ + \sum_{i=1}^{n_c} \frac{\delta r_{a0(t)} - \delta r_{b0}(t)}{\delta p_{ci}} \Delta p_{ci} \end{aligned} \tag{23}$$

and is used to formulate the observation equations for the least-squares adjustment (see Jäggi et al. (2010)). Finally, combined systems from SST-hl and SST-ll are created for each daily arc. After a pre-elimination of arc-specific parameters the combined systems can be again accumulated to daily, monthly and annual systems. Inversion of the system can be done without any regularization.

Within the *Celestial Mechanics Approach* as proposed by Jäggi et al. (2010) GRACE accelerometer data is neglected and short-term mass variations are not included in the models. However, these model shortcomings are both compensated to a big part by the introduction of empirical parameters, so called pseudo stochastic pulses.

Other spherical harmonic approaches exist (e.g. see Jekeli (1999), Visser et al. (2003), Han et al.(2005) and Schmid et al. (2006) in Wahr (2007)) but are not further explained here. Apart from spherical harmonic approaches there exist also so called *mascon* solutions. Those *mascons* refer to uniformly spread mass anomalies of consistent shape at the Earth's surface and are often used to estimate regional mass anomalies reducing leaking effects. (c.f Wahr (2007))

For further details on the gravity recovery methods for GRACE the author recommends the cited publications.

7.3 GRACE error structure and its handling

GRACE monthly gravity field solutions suffer from erroneous stripes when explored spatially e.g. in geoid heights. Two error sources for those stripes can be classified.
First, the GRACE observation type - the along track ranging (SST-ll) - leads to a highly anisotropic error structure in the error estimates obtained in the gravity recovery procedure. Rigorous covariance propagation to the full GRACE variance-covariance matrix of the monthly ITG-GRACE2010s model to different maximum degrees could show that the striping pattern already occurs at degrees 30 to 40 (Pail et al., 2011b). There it is stated, that error estimates only reflect the GRACE measurement type and the orbit configuration, so a significant part of the stripes is related to it and not to the observations themselves (right-hand side of the normal equation system).
Second error source for the stripes is aliasing of short periodic signal (e.g. , from atmosphere or ocean) affecting the true observations (right hand side). The twin satellites mainly sense gravity along their orbit, thus the measurements reflect the instantaneous gravity on Earth at the time the satellites pass. Without correction (using geophysical models) in so called *de-aliasing* procedures, those effects alias into the monthly fields.

When it comes to retrieving mass variations, e.g., the ones of hydrological nature from GRACE monthly spherical harmonic solutions, the spherical harmonic coefficients can not be used right away. For example the analyses of hydrological mass variations in large river catchment areas (scales of 500km) afford clean monthly fields in these spatial scales. The corresponding coefficients at that degrees (d/o 30 to d/o 40), however, suffer from the striping pattern due to the GRACE error structure. Thus the spherical harmonic coefficients of the GRACE gravity field solution need to be subject to certain procedures in order to overcome the signal distortion through short periodic signals (aliasing) and the anisotropic error behavior. In section 7.3.1 the general principle of eliminating aliasing effects is described exemplary by the GFZ GRACE data processing. Section 7.3.2 is dedicated to some known de-striping and decorrelation filter techniques.

7.3.1 Dealiasing

As explained above, short periodic gravity fluctuations need to be removed within the GRACE data processing in a *de-aliasing* procedure. The sources for those variations generally are tides, and variations in atmosphere, oceans, and continental water storage (see section 4). Seasonal gravity variations are not corrected for because GRACE monthly fields shall help to determine the latter.
In Gruber and Flechtner (2007) the overall GRACE data analysis and the principle of GRACE de-aliasing for the monthly GFZ *GRACE Satellite-only Model* (GSM) (release 01 to 04) is explained. Within the processing the time variable gravity variations are interpreted as disturbing forces acting on the satellites. Those forces need to be known, externally, in order to be corrected for. Geophysical models can provide the necessary potential coefficients, describing the impact of the disturbing forces. Different tide models find application in the de-aliasing, accounting for direct tides, ocean tides, solid Earth tides and pole tides (all explained in 4). The variations of atmosphere and ocean are corrected for in terms of potential coefficients derived from the ECMWF (*European Center for Medium Range Weather Forecast*) atmosphere models and the OMCT (*Ocean Model for Circulation and Tides*) ocean models. Those potential coefficients are better known as the *atmosphere and ocean de-aliasing level-1B products* (AOD1B). Details on

their calculation and usage are found in Flechtner (2007) (AOD1B product description document).

7.3.2 De-striping – filter techniques

According to Werth et al. (2009) in their sound evaluation of GRACE filter tools from a hydrological perspective, filtering of GRACE spherical harmonic coefficients aims at three different benefits: 1) Smoothing the original data to a lower spatial resolution. Neglecting suppression of high resolution coefficients is indispensable, knowing that noise is rising towards higher degrees. Furthermore, evaluation of water mass changes is mostly done in large-scale river basins, hence a high resolution is not necessary. 2) Removal of the striping artifacts of GRACE gravity data. The artifacts are the result of an-isotropically correlated noise in the coefficients. Needed decorrelation techniques can be interpreted as filters. 3) Minimizing the leakage error. The term leakage refers to signal outside the region of interest leaking inside and to signal variability inside the region, which both need to be damped. Filters can be characterized in terms of (an-)isotropic behavior, degree and order dependence, and inclusion of decorrelation methods. In their study Werth et al. (2009) evaluated six different filter methods which find usage in the calculation of GRACE terrestrial water storage (TWS) changes for correspondence with TWS changes from various hydrological models. Different filter techniques deal differently with GRACE error and leakage effects. The selection of an appropriate filter method mainly is a balance of remaining satellite errors and spatial resolution. Besides, the optimal choice may vary for different basin size, shape, and location as well as signal type and intensity (c.f. Werth et al. (2009)).

Gaussian smoothing, a very simple and commonly used filter, and its spherical harmonic presentation shall be introduced here. In Wahr and Molenaar (1998) the application of this filter to GRACE data is described based on the filter coefficients presented by Jekeli (1981). Jekeli's Gaussian averaging function $W(\alpha)$ (normalized that the global integral of the averaging function equals 1) can be written as

$$W(\alpha) = \frac{b}{2\pi} \frac{exp\ [-b(1 - cos(\alpha))]}{1 - e^{-2b}} \tag{24}$$

where α denotes the angle from the filter core to another point on the Earth's surface in radians. The distance on the Earth's surface in meters can be calculated via the semi-major axis a of the Earth's body by $a \cdot \alpha$. The parameter b defines the strength of the smoothing inversely by the filter radius r following

$$b = \frac{ln(2)}{1 - cos(r/a)} \tag{25}$$

where r is the distance on the Earth's surface where the averaging function has dropped to half of its value.
The degree dependent smoothing coefficients W_n (normalized that the global integral of the averaging function equals 1) can be computed recursively with the relation

$$W_{n+1} = -\frac{2\ n+1}{b}\ W_n + W_{n-1} \tag{26}$$

where n is the spherical harmonic degree. The low degree filter coefficients can be derived by

$$W_0 = \frac{1}{2\pi} \tag{27}$$

and

$$W_1 = \frac{1}{2\pi}\,[\frac{1+e^{-2b}}{1-e^{-2b}} - \frac{1}{b}]. \tag{28}$$

Other GRACE filter techniques exist, e.g., degree and order dependent filters by Swenson and Wahr (2002), an empirical decorrelation method by Swenson and Wahr (2002), time dynamic filter by Seo et al (2006), and a decorrelation method by Kusche (2007). They are all investigated in Werth et al. (2009). Details on these filters are not given here but can be found in the cited literature.

8 GOCE

8.1 GOCE mission concept

The GOCE satellite mission, which delivers data since November 2009, is the first core satellite mission defined in ESA's *Living Planet* program (ESA (1999)). The mission aims to determine the stationary part of the Earth's gravity field - geoid heights and gravity anomalies - globally with a very high accuracy and spatial resolution. Therefore, it flies at a very low altitude of 260 km (to sense a greater gravitational attraction) on a sun-synchronous orbit (inclination of 96.7°) [5]. The scientific goal is the determination of gravity anomalies with an accuracy of $10^{-6}\dot{g}$ (which corresponds to 1 $mgal$) and the geoid with $1-2$ cm accuracy, with a spatial resolution of better than 100 km half wavelength (ESA (1999)). The newly derived gravity information is complementary to data of other gravity field satellite missions and thus is of importance for science and applications concerning various Earth processes (e.g., solid earth physics, oceanography, geodesy and glaciology) (see Gruber et al. (2009)).

The core instrument on board of the spacecraft to measure gravity is a 3-axis *satellite gravity gradiometer* (SGG) (see figure 1), which is a unique technique in space. It consists of three pairs of orthogonally mounted accelerometers in 50 cm distance with their axes approximately arranged in along track (x-axis), cross track (y-axis) and radial (z-axis) direction. This gradiometer allows the direct measurement of the second order derivatives of the gravitational potential - the differences of the accelerations acting at the locations of the accelerometers - along the above defined axes. The differences stem from the fact that the gravitational signal along the orbit is influenced by all attracting earth masses (e.g. mountains, valleys, ocean ridges, etc.) and the accelerometers are sensitive enough to measure the variation of this attraction over a distance of 50 cm (ESA, 1999). Non-gravitational attraction (e.g., air drag) is ideally eliminated in the differences (differential mode accelerations), because all accelerometers inside the gradiometer are affected by the same non-gravitional attraction. Further, the direct measurement of the linear disturbing accelerations (common mode accelerations) allows the instantaneous compensation (and minimization) of the drag effect with the satellite's drag-free control system via ion-thrusters. Due to the fact, that each accelerometer suffers of one less sensitive axis, the arrangement of the accelerometers was done in a way, that the diagonal components V_{xx}, V_{yy} and V_{zz} of the gravity tensor and the off-diagonal component V_{xz} can be determined with high precision (Gruber et al., 2009). Among the three main diagonal components, however, the V_{zz} component performs worse by a factor of two due to yet unknown reasons (see Pail et al. (2011a)). The off-diagonal tensor elements V_{xy} and V_{yz} can only be determined with lower precision (Gruber et al., 2009) and are in consequence not used for gravity recovery (see Pail et al. (2011a)). The gradiometer measurements are very precise only within the systems measurement

[5] http://www.esa.int/SPECIALS/GOCE/SEMD304XQEF_0.html

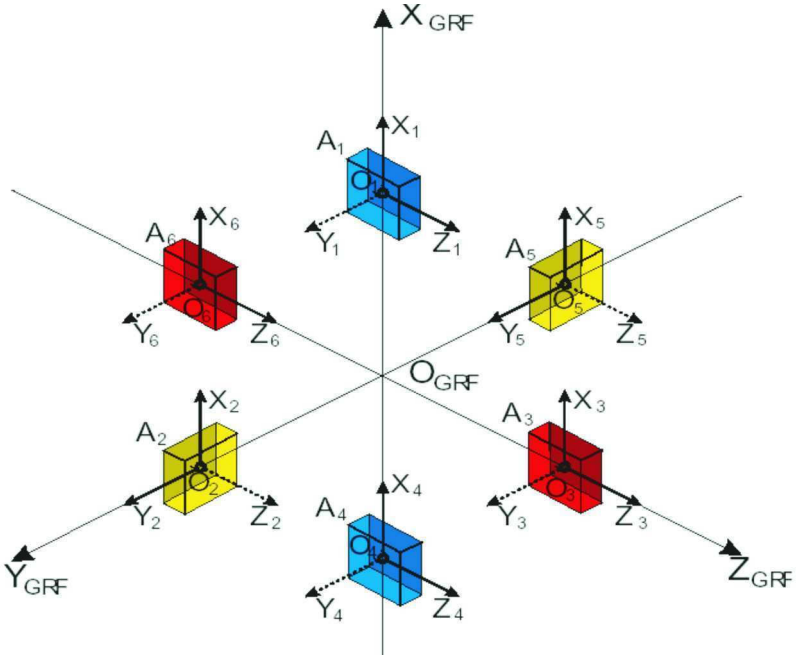

Figure 1: Scheme of GOCE gradiometer with 6 accelerometers and the axes defined in the Gradiometer Reference Frame (GRF); solid arrows denote the sensitive axes of the accelerometers, dashed arrows denote the less sensitive axes;

bandwidth between 5 and 100 mHz and therefore require adequate filtering before usage (see Pail et al. (2011a)).
With the on-board GPS receiver the satellite is equipped with a second, complementary gravity sensor device (similar to the CHAMP mission, see section 2). The information gathered from the GPS receiver accounts for the long-wavelength part of the gravity field, which lies outside of the measurement bandwidth of the gradiometer. From a joint analysis of both on-board gravity sensor devices the GOCE-only gravity field models can be derived (see section 8.2.1, 8.2.2 and 8.2.3).

8.2 Gravity Recovery from GOCE observables

GOCE gravity recovery can be done independently for both on board gravity sensor concepts, the satellite-to-satellite tracking in the high-low mode (SST-hl) via GPS receivers and the satellite gravity gradiometer (SGG), but is mostly done in combination as they are complementary. The data of the SST-hl sensor only accounts for low frequencies of the gravitational field. In contrast, the high frequencies of the gravity field can be determined from the gravity gradient tensor measured with the SGG.

For the SST-hl observables gravity recovery can be realized via orbital analysis. Similar to GRACE (or CHAMP) type SST-hl observables gravity field coefficients can be estimated from GOCE type SST-hl observations using techniques like the *single satellite approach* as described in section 7.2. Alternatively, the GOCE type SST-hl can be solved with the *energy conservation approach* or *energy integral method*, which are not further explained here.

As defined in the GOCE mission selection manuscript (see ESA (1999)) three complementary techniques have been foreseen and were later implemented by the European GOCE Gravity consortium (EGGc) to compute a gravity field from GOCE type observations: the *direct method* (DIR), the *time wise method* (TIM) and the *space wise method* (SPW). They mainly differ in usage of the SST-hl observations, in modeling the stochastic behavior of the gradiometer, in the general computional domain (time or space), spatial resolution, inclusion of external information and in combination of the information of the two sensor concepts. In the sections 8.2.1, 8.2.2, and 8.2.3 the principle and characteristics of these methods will briefly be outlined.

8.2.1 Direct method (DIR)

Within the *direct method* gravity recovery is based on different approaches for the individual releases. In release 1, which shall be explained here, the least-squares solution of the inverse problem is done with a Cholesky decomposition (see Bruinsma et al. (2010)). EIGEN-51C served as a priori model for the SST processing and as background model for the SGG processing. The SST processing and SST normal equation set-up relies on an orbit determination problem based on dynamic orbit computation in an iterative least-squares adjustment (up to d/o 120). The noisy SGG observations are filtered using a band pass filter aiming to suppress signal outside the measurement bandwidth to less than 0.1mE. From the filtered SGG observations normal equations are derived for each SGG component in a single step (up to d/o 240). Normal equations for both data types are computed in daily (24h) manner and before inversion the normal equation batches are stacked together for the whole period. For optimal combination, the information of the yy-component and the SST matrix is down-weighted by a factor of 0.5 empirically. The solution of the DIR-method requires a spherical cap regularization, which constrains the solution in the unobserved polar caps to the used a priori model (EIGEN-51C) (see Pail et al. (2011a)). It was shown (see Gruber et al. (2011)) that the models from this approach outperform others above degree 150 when it comes to comparisons with terrestrial gravity data, due to the fact that this information is already contained in the EIGEN-51C prior model.

8.2.2 Time-wise method (TIM)

The main goal of the *time-wise method* is to derive a gravity field model which is independent of any external or a priori information (see Pail et al. (2010)). One difference to the DIR method is that the SST processing is done via the *energy integral method* (up to d/o 100) which reduces the available information in the low degrees by a factor of $\sqrt{3}$, when used in a unique scalar equation. Again, in order to be independent from any biases towards a GRACE prior model, not the reduced dynamic orbits (SST_PRD) but the kinematic orbit positions (SST_PKI) are used, which show a worse performance. The SGG data in this approach is filtered regarding its entire spectra using an ARMA filter model, which corresponds to a complete decorrelation of the signal. The disadvantage is that those filter models are complex and require longer warm-up periods, so more data remains unused. Within the approach a so called *tuning machine*, which iteratively solves the field in an approximation, delivers optimum regularization and weighting parameters, SGG ARMA filter models and undetected outliers. With the filtered main diagonal gradients V_{xx}, V_{yy} and V_{zz} the full normal equations are assembled (up to d/o 224). SGG and STT normal equations are combined using *variance component estimation* (see section 9) and regularized using two approaches before solving. (c.f. Pail et al. (2011a))
A pure GOCE-only field, as derived from the TIM approach, offers the possibility to discover inconsistencies regarding comparisons to gravity fields derived from other satellites and terres-

trial gravity data. However, as GRACE information is missing, the models from this approach show a significantly lower performance in the low frequencies (see Pail et al. (2011a)).
In the last decades, efforts have been made to make use of the sensor fusion concept of the satellite with its complementary sensor data, in order to achieve a GOCE-only gravity field model. According to Pail et al. (2010) various approaches have been proposed to handle the demanding numerical and computational task evolving from the enormous normal equation systems of the SGG observation type. A gravity field complete up to degree and order 250 requires to solve 63.000 unknown spherical harmonic coefficients, which leads to the inversion of a normal equation matrix of about 30 GB size. A software solving this task in a parallel processing strategy using the *time-wise method* on a Linux-PC cluster is described in section 8.5.

8.2.3 Space-wise method (SPW)

The concept of the *space-wise approach* (see Migliaccio et al. (2010)) differs with respect to the above mentioned approaches, as a gravity model is derived from previously gridded gravity gradients. In this approach spatial correlations are exploited by modeling the signal covariance as a function of distance in a multi-step collocation procedure. Prior to the collocation, a low-frequency estimate of the gravitational potential is retrieved from the SST data using the *energy conservation approach*. In this step, however, the estimated potential has to be adapted according to the error spectrum of a prior model. This constraint becomes necessary due to unfiltered common mode accelerations.
For the multi-step collocation the following procedure is applied: First, the time-series of gradients is filtered along the orbit with a *Wiener filter* in order to reduce the highly correlated noise of the gradiometer. Second, a spherical grid is interpolated by means of collocation on satellite height. The collocation can also be interpreted as a second, spatial filter stage, because data points close to each other are averaged to a grid point. Note, that gradients in the collocation process are reduced by the SST prior model because collocation is applied to local, overlapping patches of 20° x 20°. Finally, a harmonic analysis by numerical integration is performed to derive the geopotential coefficients. These coefficients are transformed to synthesized observables again, and the space-wise procedure is repeated until convergence. Due to computational reasons, the full covariance matrix is derived by a *Monte Carlo simulation* using only 400 samples.

8.3 Outlier detection methods for GOCE gravity gradients

GOCE gravity gradients, as measured by the satellite's on board gradiometer, are affected by stochastic errors, systematic errors and outliers. The stochastic errors of GOCE gradiometry, the colored noise, can be very well modeled and is taken into account differently in different approaches of gravity field recovery (see section 8.2, and Pail et al. (2011a)). Systematic errors, which can include biases and scale factor errors, are corrected for in an external calibration step (see Bouman et al. (2005)). Outliers are searched for in the so-called gravity field analysis pre-processing step of the HPF. However, remaining undetected outliers can seriously affect the accuracy of the derived gravity field coefficients (see Kern et al. (2005)). Bouman et al. (2005) show that a gravity field solution can be degraded by up to twenty times due to undetected outliers. Hence, for the purpose of gravity field computation from GOCE GG outlier detection algorithms are indispensable.
A variety of methods exist to cope with outliers in GOCE GG. Sound discussions of different outlier detection algorithms for GOCE GG are given, e.g., by Bouman et al. (2005) or Kern

et al. (2005). Here, only methods used or discussed within the thesis and in the TIM gravity recovery approach (see 8.2.2) shall be presented.

8.3.1 Tracelessness condition

The *tracelessness condition* is better known as the Laplace equation, according to which the gravitational potential is a harmonic function outside of the attracting masses (Heiskanen and Moritz (1967)). This physical property of the gravity gradients means, that the sum of the diagonal elements of the gravity tensor (V_{xx},V_{yy},V_{zz}) should be zero. This condition can be expressed for GOCE GG by

$$V_{xx} + V_{yy} + V_{zz} = 0. \tag{29}$$

According to Bouman et al. (2005) the *tracelessness condition* is a sensitive but ambiguous method, because it cannot be discriminated from which gradient component the outlier arises.

8.3.2 Gravity gradient anomalies

Gravity gradient anomalies are derivations of the measured GGs to GGs generated from a global Earth gravity field model along the orbit positions (see Bouman et al. (2005)). Again a threshold can be defined to detect outliers in the epoch-wise gravity gradient anomalies. Alternatively, a w-teststatistic can be introduced as detection criteria (see Bouman (2004)). Generally, also the median value has to be subtracted in order to cope with scale factor errors and biases. In a more advanced approach, the differences can also be weighted with the sum of errors.
An advantage of this method is that all gravity components can be checked individually and point-wise. A drawback of the method is that the gradients derived from the model may be of low accuracy compared to GOCE GG, which makes the method less sensitive (see Bouman et al. (2005)).

8.4 Regularization

Regularization in least squares estimation problems is a method to stabilize the inversion process of an ill-posed normal equation matrix. GOCE normal equations happen to be ill-posed because of various reasons.
In particular, the sun-synchronous orbit of the satellite with an inclination angle of 96.7° leads to a polar observation gap. As the spherical harmonic base functions used to describe the geopotential on Earth are of global support, the matrix of normal equations tends to be ill-posed, leading to a weak determination of the low-order coefficients (see Metzler and Pail (2005)). The effect is a strong oscillation of the geopotential (or other gravity functionals) in the polar areas. It is estimated, that a loss of 13 to 14 significant digits in numerical stability result from the polar gap problem for a spherical harmonic least-squares solution complete up to d/o 250. In contrast, the downward continuation only accounts for a loss of seven significant digits for a satellite's altitude of 250 km. In their analyses of the polar gap issue and its influence on spherical harmonics, Sneeuw and Gelderen (1997) found the zonal and near-zonal coefficients to be affected and distorted. The developed rule of thumb for the spectral region affected by the distortion is given with equation 20 in section 6.3.
Other reasons for ill-posed normal equation matrices may be inhomogeneous data distribution or the introduced stochastic model of the measurements (see Yi (2011)).

Several regularization approaches exist for ill-posed least squares problems. In standard approaches like the *Tikhonov regularization* (of different order) or the *Kaula regularization* usually a diagonal regularization matrix R is added to the normal equation matrix $A^T PA$, in order to stabilize the solving process following the expression

$$\hat{x} = \left(A^T PA + \alpha R \right)^{-1} A^T Pl \tag{30}$$

(Metzler and Pail (2005)). The regularization parameter α controls the impact of the regularization, and its determination is a crucial task in the regularization procedure, as an optimal balance between regularization and data fitting has to be found. Metzler and Pail (2005) provide a list of different methods to find an optimum regularization parameter. The regularization matrix R on the other side enables individual weighting of the parameters.
In the case of Tikhonov (Tikhonov, 1963) (without going into further detail) the regularization matrix is filled on the diagonal with degree n dependent terms following

$$r_{ij} = \delta_{ij}, \tag{31}$$

$$r_{ij} = \delta_{ij} n(n+1) \tag{32}$$

and

$$r_{ij} = \delta_{ij} n^2 (n+1)^2 \tag{33}$$

for Tikhonov of first (31), second (32) and third (33) order (see e.g. Metzler and Pail (2005)). The parameter r_{ij} denotes the element in row i and column j of the R-matrix and δ_{ij} is the Kronecker symbol.

In the case of a Kaula regularization the constraining is based on a degree variance model, and the elements of the regularization matrix correspond to the inverse Kaula rule (see equation 18) following

$$r_{ij} = \delta_{ij} n^4. \tag{34}$$

Instead of a variance model, variances derived from any existing satellite-borne geopotential model can be used to fill the diagonal of the regularization matrix, likewise.
However, a constraining based on the described methods influences the total solution in space domain.

In order to avoid a signal damping two regularization approaches exist which are tailored to GOCE case ill-posed normal equations. The first one is an order dependent Kaula regularization, which is applied only to coefficients affected by the polar gap. The method is basically derived from a combination of equation 34 and equation 20, which defines the maximum order m_{reg} per degree n which is affected by the polar gap. Then, the elements r_{ij} of the regularization matrix R can be written as

$$r_{ij} = \begin{cases} n^4 (m_{reg} - m)^p & \text{if } i = j \text{ and } m \leq m_{reg} \\ 0 & \text{otherwise} \end{cases} \tag{35}$$

(see Metzler and Pail (2005)), where the term $(m_{reg} - m)^p$ represents an order dependent weighting, with an empirically derived value p. The weighting leads to maximum regularization impact in zonal coefficients and decreases the impact continuously with increasing order.

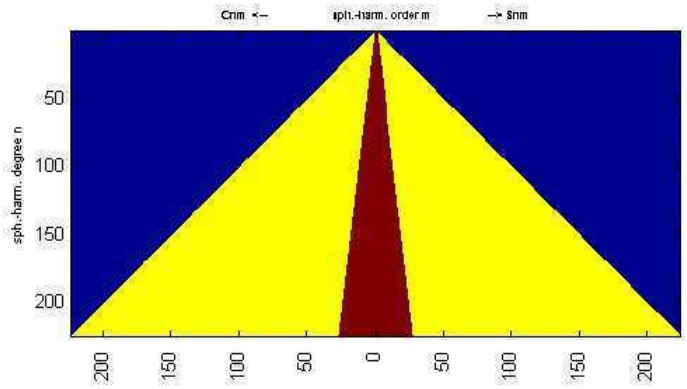

Figure 2: Coefficients of a spherical harmonic analysis which are affected by the order dependent Kaula regularization (in red) as expressed by equation 35, for inclination I=96.7°

Figure 2 shows in red color the spherical harmonic coefficients C_{nm} and S_{nm} (up to d/o 224) which are affected by the order dependent Kaula regularization approach.

The second regularization method which has specifically been designed to stabilize GOCE NEQ is the *Spherical Cap Regularization Approach* (Metzler and Pail (2005)). Without going into any detail, the approach principally is forcing the geopotential at the poles towards a low-frequency gravity signal defined exclusively in the polar region. No external a-priori information needs to be included in this approach, as GOCE observation themselves can be used for a low-degree model, because the missing data in the polar regions does not have a significant effect on a low-resolution GOCE-only solution.

8.5 GOCE time-wise processing at IAPG

Solving the very normal equations which appear in retrieving spherical harmonic coefficients from gravity gradients measured by the GOCE on-board SGG is a computationally costly task. The software for assembling and solving those normal equations developed at the *Institute of Astronomical and Physical Geodesy* (IAPG) at the *Technische Universität München* (TUM) therefore falls back on the *Leibniz Supercomputing Center* (LRZ) in Munich, which provides the relevant infrastructure. The software is very similar to the method used for the generation of TIM gravity models (see section 8.2.2) in the frame of the *High-Level Processing Facility* (HPF), the ESA funded project for scientific processing of GOCE data. Details on HPF's gravity field processing and more information on the software can be found , e.g., in Pail et al. (2005).

The gravitational potential V of the Earth is computed in terms of spherical harmonic coefficients $\bar{C}_{nm}$ and $\bar{S}_{nm}$ as defined in Heiskanen and Moritz (1967) up to a certain maximal degree N_{max} of the series expansion described by equation 1 in section 5. The implemented software is able to solve gravity fields up to degree/order 720, which means a spatial resolution of approximately 30 kilometers. Further, the computation includes the estimation of a full variance-covariance matrix which reflects the true error behavior of the solution.
The software consists of various sub-programs and is conceived in a modular manner that allows the investigation of intermediate results and an adaption to the data input. Figure 3 shows the overall architectural design, main components and comprised programs with their data in-

and outputs for solving the normal equation system. In the diagram data is colored in gray, programs are blue, and processes running on the LRZ environment are orange. The five main components of the software are briefly explained in the following:

goceINPUT.f90
This program reads the official ESA GOCE data products GO_CONS_EGG_NOM_2_, GO_CONS_SST_PRD, and GO_CONS_SST_PRM and writes the values of relevant quantities into specified input files, as they are needed by the program goceNEQ. The period for which data is assembled into files can be defined explicitly. It uses the sub-modules neq_gocevars, neq_globalvars, neq_io and neq_orbit. The first two modules provide all necessary variables, neq_io provides routines for preparing and reading the official GOCE data products. The modul neq_orbit accounts for the synchronization of orbit and gradient data and provides functions for an interpolation of the orbit postions to the gradiometer measurement epochs. The quantities extracted from each product are listed in table 2.

Product name	Product contents
GO_CONS_EGG_NOM_2_	6 gravity gradients (xx-, yy-, zz-, xy-, xz- and yz-component) 4 quaternions (rotation ITRF/GRF) flag
GO_CONS_SST_PRD	reduced-dynamic orbit positions (x-, y-, z-coordinate)
GO_CONS_SST_PRM	4 quaternions (rotation ERF/ ITRF)

Table 2: ESA data products needed for the time-wise processing software at IAPG (serve as input for *goceINPUT.f90*)

startNEQcreation_goce
This script prepares the computation and the assembling of the normal equations before it sends serial jobs (batch-jobs) to the LRZ. It splits the normal equation matrix into a number of computationally feasible parts, so that the whole system can be set-up in independent batch-jobs running the program *goceNEQ.f90*.

goceNEQ.f90
This program assembles the normal equation system and provides a description file (containing the sorting of coefficients), an A^TPA -file (normal equation matrix) and an A^TPl -file (right hand side). As external input an input file containing the gradient observations generated by *goceINPUT.f90*, a filter file and a gap file are needed. The gap file accounts for all the data epochs which shall be excluded due to failure of the measurement system. The filter-file defines an auto-regressive moving-average (ARMA) filter which copes with the colored noise of the gradients and filters the gradients and the columns of the design matrix A over their entire spectra. As the filters are auto-regressive, they need to be fed with a period of data-points before they work correctly. Those periods, where the filter does not work correctly and the corresponding epochs are not taken taken into account for gravity recovery, is called warm-up time. The warm-up time of the filters typically lies between 1500 and 3000 data epochs and can be critical for the quality

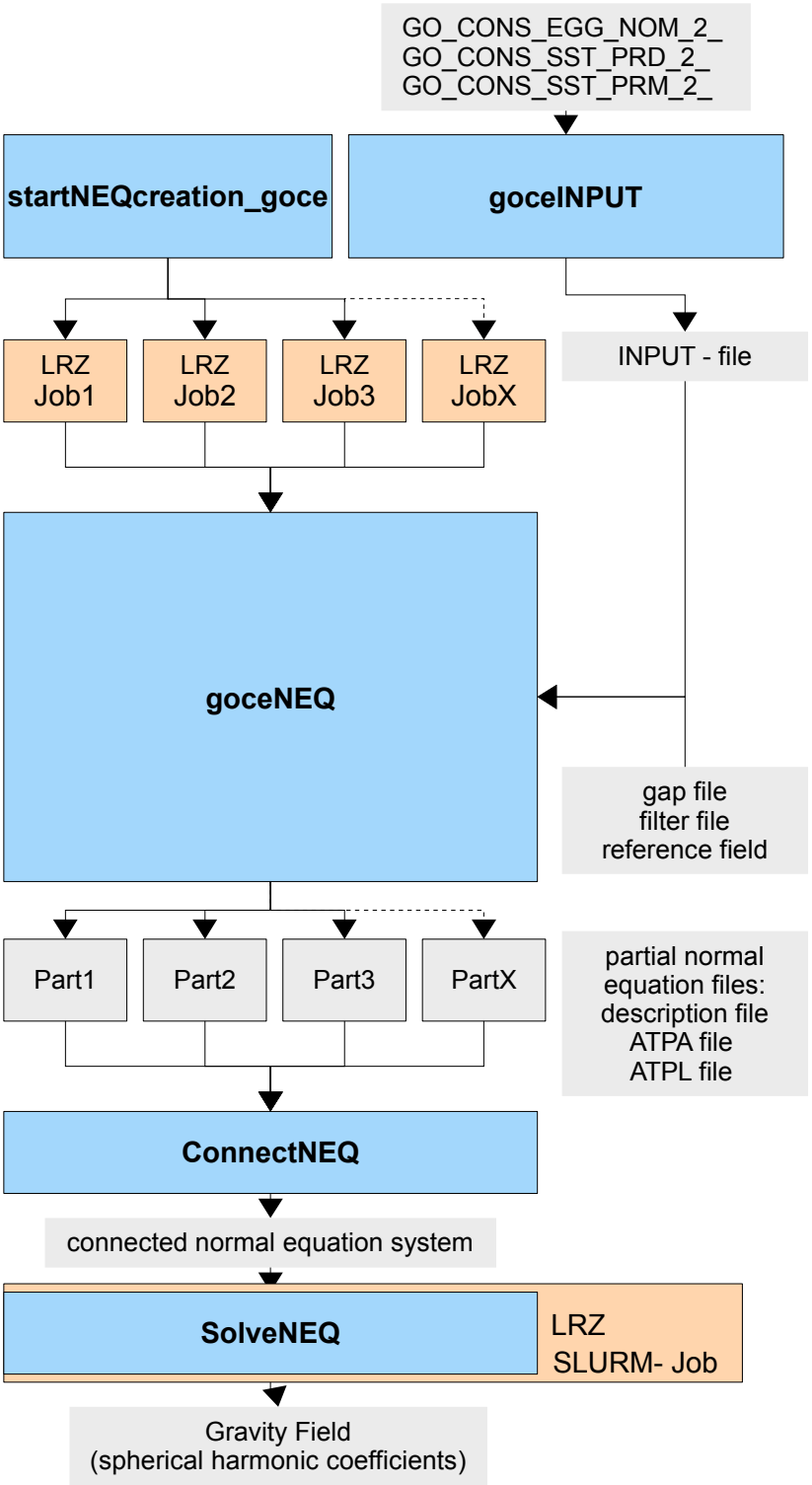

Figure 3: Architectural design and data flow of the time-wise software package at IAPG

for the gravity field as it leads to loss of information. Details on filter design of such filters taking into account the GOCE gradiometer inherited stochastic behavior can be found, e.g., in Stetter (2012). The normal equation system is assembled by serial processing of normal equation parts of computationally feasible size in single batch-jobs as defined in the program *startNEQcreation*.

ConnectNEQ.f90
ConnectNEQ.f90 brings together the individual parts of the normal equation system by assembling the results of the LRZ batch jobs (=normal equation parts) into one normal equation matrix and the right-hand side.

SolveNEQ.f90
In this part of the software, the normal equations are solved on the parallel computing environment of LRZ (SLURM-jobs), as the inversion of the $A^T PA$ matrix is not feasible for a single processor. The outputs are the spherical harmonic coefficients of the gravitational potential of the Earth and their formal errors expressed by the variance-covariance matrix.

9 Variance component estimation

Variance component estimation (VCE) is a method aiming to achieve an optimal combination of different types of satellite data for gravity field determination in terms of a spherical harmonic analysis. In core, weighting factors, so called *variance components*, are estimated for each measurement type before they are applied to the normal equations. If the normal equation systems are ill-conditioned, prior information in terms of regularization can be introduced optimally at the same time. For this thesis, an approach for the combination of satellite gravity gradiometry (SGG) data as measured by GOCE (see section 8) and gravity observations from satellite-to-satellite tracking (SST) as delivered by GRACE (see section 7) is needed. As the SGG observation type suffers from an ill-conditioning of the normal equations due to the polar gap, the inclusion of prior information is necessary. Koch et al. (2002) as well as Brockmann et al. (2010) deliver fast approaches for VCE in case of GOCE SGG and GRACE SST on the basis of normal equations with u unknown parameters of the kind

$$\begin{aligned}&(\omega_{goce}\ A^T PA_{goce} + \omega_{grace}\ A^T PA_{grace} + \omega_{reg}\ P_{reg})\ \beta \\ &= \omega_{goce}\ A^T Pl_{goce} + \omega_{grace}\ A^T Pl_{grace} + \omega_{reg}\ P_{reg}\mu_{reg}\end{aligned} \tag{36}$$

where $A^T PA_i$ denotes the u x u normal equation matrix and $A^T Pl_i$ is the u x 1 right-hand side of the different observation types *i=[goce,grace]*; β is the vector of unknown parameters of size u x 1. The parameter ω_i is the weighting factor of the different observation types, μ_{reg} is the u x 1 vector of prior information (e.g. regularization) and P_{reg} the corresponding regularization matrix of size u x u.

The weighting parameters ω_i with $i \in \{goce, grace, reg\}$ can be retrieved from the variance components σ_i^2 of each observation type as follows:

$$\sigma_i^2 = \frac{1}{\omega_i} = \frac{\Omega_i}{r_i} = \frac{\Omega_i}{n_i - u_i} \tag{37}$$

The partial redundancies of each observation type r_i are the difference of the number of observations n_i and unknowns u_i. The weighted square sum of residuals Ω_i equals

$$\Omega_i = \hat{v_i}^T P_i \hat{v_i} = (A_i \hat{\beta} - l_i)^T P_i (A_i \hat{\beta} - l_i) \tag{38}$$

where A_i is the design matrix of size n x u and l_i is the n x 1 vector of observations. Ω_i can also be estimated using the squared, weighted sum of observations $l^T P l_i$ following the expression

$$\Omega_i = \beta^T \ A_i^T P_i A_i \ \beta - 2 \ \beta^T \ A_i^T P_i l_i + l_i^T P_i l_i \tag{39}$$

for $i = [goce, grace]$. In the case of the prior information, we can write the residuals $\hat{v}_{reg}$ as $\hat{\beta} - \mu_{reg}$ and get

$$\Omega_{reg} = \hat{v}_{reg}^T P_{reg} \hat{v}_{reg}. \tag{40}$$

As shown in Koch and Kusche (2002) the partial redundancies can be estimated through

$$r_i = n_i - trace(\frac{1}{\sigma_i^2} \ A_i^T P_i A_i \ N^{-1}), \quad i \in \{goce, grace\} \tag{41}$$

$$r_{reg} = u - trace(\frac{1}{\sigma_{reg}^2} \ P_{reg} \ N^{-1}) \tag{42}$$

where N denotes the combined normal equation matrix (left hand side of equation 36). With equation 36 to 42 the variance components σ_i^2 for $i \in \{goce, grace, reg\}$ can be computed iteratively. Starting from approximate values one iterates until the variance components converge. It was shown, that not more than five iterations should be necessary (see Koch and Kusche (2002)) to obtain optimal weighting parameters using the above described approach.

10 Least - squares parameter elimination for normal equations

In order to reduce a *Gauss-Markov* model to a number of parameters of interest a parameter elimination can be applied to the normal equations. In this thesis normal equation systems of different size will be combined, and therefore a reduction of the number of parameters is relevant for the bigger system. Further, the parameter elimination greatly reduces computational effort, which generally increases cubical with the number of parameters. The normal equations for a spherical harmonic analyses derived from GOCE SGG have a spherical harmonic degree of more than 60 (up to a maximum of 250 for this observation type, see section 8) and need to be adapted to the spherical harmonic degree of the GRACE SST normal equations. Here, GRACE SST normal equation systems (see section 11.1) of a maximum degree $n_{max,grace} = 60$ will be investigated, which accounts for $(N_{max,grace} + 1)^2 = 61^2 = 3721$ coefficients of a spherical harmonic series expansion.
The general procedure for a parameter elimination of a Gauss-Markov model with n observations and u unknown parameters of kind

$$l + v = A\beta \tag{43}$$

where l denotes the n x 1 observation vector, v is the n x 1 vector of residuals, A is the n x u design matrix and β is the u x 1 vector of unknown parameters, is described, e.g., in Pail (2004). In this approach observations can be correlated and of different accuracy. First of all, the design

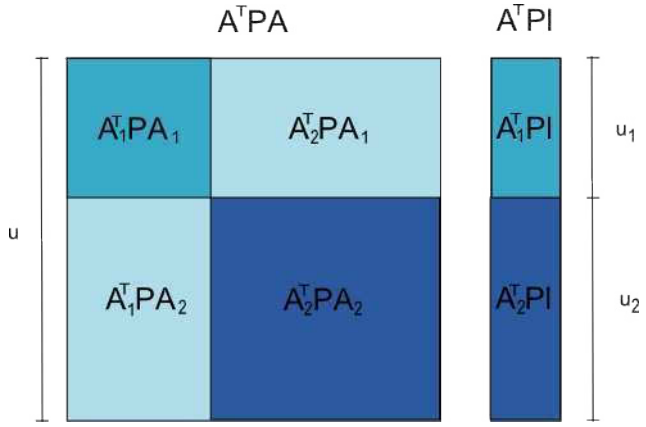

Figure 4: Scheme of normal equation matrix $A^T PA$ and corresponding right-hand side $A^T Pl$ showing the division into parts which is relevant for the parameter elimination procedure

matrix A can be divided into the part A_1 (size n x u_1) containing the remaining parameters β_1 and the part A_2 (size n x u_2) containing the parameters β_2 to be eliminated following

$$A = \{A_1|A_2\} \ , \ \beta = \begin{bmatrix} \beta_1 \\ \beta_2 \end{bmatrix} \tag{44}$$

where u_1 is the number of remaining parameters β_1 and u_2 is the number of parameters β_2 to be eliminated. It is shown that the reduced normal equation matrix of remaining parameters $\bar{A}_i^T P \bar{A}_1$ of size u_1 x u_1 is given by

$$\bar{A}_1^T P \bar{A}_1 = A_1^T PA_1 - A_1^T PA_2 \ (A_2^T PA_2)^{-1} \ A_2^T PA_1 \tag{45}$$

The reduced n_1 x 1 right-hand side $\bar{A}_1^T P\bar{l}$ can be computed using the expression

$$\bar{A}_1^T P\bar{l} = A_1 Pl - A_1^T PA_2 (A_2^T PA_2)^{-1} A_2^T Pl \tag{46}$$

with the reduced vector of observations $\bar{l}$, which follows:

$$\bar{l} = l - A_2 (A_2^T PA_2)^{-1} A_2^T Pl. \tag{47}$$

Figure 4 schematically shows where the relevant parts of the $A^T PA$ and $A^T Pl$ matrix described by equations 45 and 46 are located.

Following equation 45 and 46 the remaining parameters β_1 can be retrieved by solving the reduced normal equations as

$$\beta_1 = (\bar{A}_1^T P \bar{A}_1)^{-1} \ \bar{A}_1^T P\bar{l} \tag{48}$$

Part IV

Estimation and analysis of combined monthly and bi-monthly fields from GOCE and GRACE

11 Description of data

In this thesis GRACE and GOCE satellite data of the year 2010 and of two months in the year 2009 was gathered. Both satellite missions observe the gravity field of the Earth, however, measurement techniques differ as described in chapters 7 and 8. In the case of GOCE, officially released data products of the *European Space Agency* (ESA) and an at IAPG internally produced gradient data set were used. From the provided gravity gradients, orbits, and attitude information, normal equations can be assembled. In the case of GRACE, fully set up normal equations from the *Astronomical Institute* of the *University of Bern* (AIUB) were made available.

11.1 GRACE data

GRACE data utilized for this research was provided by AIUB in terms of fully set up normal equations for every month of the year 2010, and the last two months of the year 2009. Hence, no data screening or editing could be done. Deduced gravity field representations range up to spherical harmonic degree/ order 60. However, coefficients of degree 0 and 1 are not parameterized. Apart from a reduction of tidal effects from tide-models, no other reduction regarding time variable effects has been applied.

The provided files contain the normal equation matrix A^TPA, the right hand side A^TPL and the spherical harmonic coefficients of a 6-year GRACE-only solution (AIUB-6YR). The field described by the AIUB-6YR coefficients was subtracted from the observations before the normal equations were assembled. AIUB-6YR can be regarded as the static part of the Earth's gravity field because it reflects the mean gravity over 6 years. Thus, only a residual part of the gravity field of the Earth, which is assumed to be the time variable effect, is reflected by the values in the A^TPl vector. In order to combine the normal equations with GOCE normal equations, the static field has to be re-introduced into the A^TPl vector as described in section 12.1.

In the appendix, the illustrations 31 to 33 show the given GRACE gravity field solutions complete up to spherical harmonic degree and order 60 that were solved directly from the normal equations. All 11 fields are illustrated in terms of gravity anomalies and show only the residual, time variable part (after removal of the coefficients of a static field). Cleary, the striping aretfacts as well as temporal gravity anomalies in hydrologically active areas (e.g. amazon basin) become visible.

11.2 GOCE data

Data from the GOCE mission utilized for combination with GRACE is mainly taken from officially released data products of ESA's *High-Level Processing Facility* (HPF), which is responsible for the generation of gravity field products and final GOCE orbits from *level-1b* (L1B)

data. L1B means continuously quality-monitored data sets, which have been corrected, internally calibrated and converted to physical meaning by the *Payload Data System* (PDS) and the *Calibration and Monitoring Facility* (CMF) (Koop and Gruber, 2009). The two HPF products which find application in this research are listed below:

GO_CONS_EGG_NOM_2_

GO_CONS_SST_PSO_2_

The *GO_CONS_EGG_NOM___2* product consists of externally calibrated and corrected gravity gradients in the GRF. In order to transform the gradients into the *inertial reference frame* (IRF), 4 attitude quaternions are provided coevally. In addition, all temporal corrections which have been applied to the gradients are given for each of the 6 tensor components. They account for direct tide, Earth tide, ocean tide, pole tide and non-tidal corrections. Further, calibration parameters (scale factors), error estimates for all GG components and flags are given. Flags refer to data epochs expected to be outliers or to periods where data gaps have been filled by interpolation. For synchronization of the observations to the orbit positions the GPS time of each measurement epoch is equally provided.
In the year 2011, the L1B data processing was updated due to the development of an enhanced processing strategy (Stummer et al., 2012). In connection with the new processing strategy, the *GO_CONS_EGG_NOM_2_* product was re-processed regarding the entire mission's lifetime. The changes in the new L1b processor mainly comprise an improved method to reconstruct the angular rates and a new method for the determination of the gradiometer's internal attitude. Further, the new processing strategy enables a combination of all simultaneously available star sensor data and the application of time-variable scaling factors in the calibration procedure. Those changes account for a global and regional improvement of the SGG gravity field solutions (Pail et al., 2012). Spectrally considered, largest improvements can be found at the medium to low frequencies and at the frequencies of the orbit revolution rates (see Stummer et al. (2011, 2012)).

Within the thesis, three different kinds of gradients find application. Gradients from the *old* and the *new* L1b-processor and an *in-house* gradient product, computed at IAPG according to the new L1B processing strategy. In the following the re-processed gradients will be referred to as *new* or *re-processed (repr)*, whilst *in-house* stands for the IAPG gradients. The in-house gradients are only available for November and December 2009, while old and reprocessed gradients are available for the entire mission's lifetime.

The *GO_CONS_SST_PSO* product contains the *Precise Science Orbits* (PSO) which are available in terms of reduced-dynamic orbits (*GO_CONS_SST_PRD*) and kinematic orbits *GO_CONS_SST_PKI*) represented in the *earth-fixed reference frame* (EFRF). Additionally, a rotation matrix in the form of 4 corresponding quaternions for each epoch is given for the transformation of the orbits into the ITRF. The orbits are provided in terms of a times series of 3D-positions and 3D-velocities with a sampling rate of 1 second in the case of PKI orbit, and 10 seconds in the case of PRD orbits. Both refer to GPS time as underlying time system. Within the research, only PRD orbits are used, because a 10 second sampling is enough for the interpolation of the satellites positions to the gradiometer measurement epochs (as described in section 8.5).

More details on the GOCE data products can be found in Koop and Gruber (2009).

11.3 Consistency regarding time variable gravity signals

A combination of two gravitational data sets from different sources requires an adequate calibration, and at the same time an equal treatment of disturbing signals. Consequently, it has to be inspected whether this consistency is given for GRACE SST-ll and GOCE SGG data utilized in this research:

Calibration for GOCE is done internally, in the L1B processing step, and externally to state-of-the-art gravity models. The determined scale factor has already been applied to the GG in the *GO_CONS_EGG_NOM_2_* product (Koop and Gruber, 2009). The utilized GRACE data can be regarded calibrated due to the long lifespan of the mission and experience regarding the processing of its data.
As mentioned in the previous sections 11.1 and 11.2, GRACE and GOCE observations are both corrected for tidal signals, which is assumed to be done in an equivalent way. Additionally, GOCE data has been corrected for non-tidal effects. Those non-tidal effects account for atmospheric, oceanic, hydrological and ice annual mass variations (Koop and Gruber, 2009). In spite of the fact that those non-tidal time variable effects are about 7 orders of magnitude below the measured signal, and thus their contribution to the gravity field solution might be negligible, the corresponding delivered correction from the *GO_CONS_EGG_NOM_2_* product is re-introduced into the GGs. This is done via a simple addition of the equivalent components for each measurement epoch aiming to overcome this remaining inconsistency regarding GRACE (see equation 51 on page 42).

12 Methodology and processing

In this section the overall methodology and individual processing steps are described in order to derive monthly and bi-monthly combined gravity fields from GRACE SST-ll and GOCE SGG. The combination is done on the basis of normal equations from both observation types. Such a combination generally is performed by adding up the involved normal equation matrices and the corresponding right-hand sides, as the problem in the normal equations is given in a linearized form.

Figure 5 shows the overall workflow for the combination of GOCE and GRACE data (green / yellow rectangles) and the processing steps (blue prisms). GRACE normal equations have to pass through a pre-processing step (PP) which consists of a re-ordering of the normal equation parameters and the re-introduction of a previously reduced static gravity field into the normal equations (see section 12.1). To get from GOCE gradients to GOCE SGG normal equations three major processing steps have to be performed (see section 12.2). First, non-tidal signal (NTS) is re-introduced into the corrected (EGG_NOM_2_) gradients (see chapter 12.2.1). Second, outliers in the gradient time-series are detected and flagged in an outlier detection (OD) procedure (see chapter 12.2.2). Third, normal equations are assembled as described in chapter 12.2.3. Since GOCE SGG normal equations are expanded at least to spherical harmonic degree/order 150, they are very memory consuming (around 8.5 GB), and a reduction to spherical harmonic degree/order 60 is performed prior to the combination with GRACE normal equations. A least-squares parameter elimination (PE) procedure provides that the reduction will not lead to spectral leakage effects due to the truncation of the spherical harmonic series at a lower

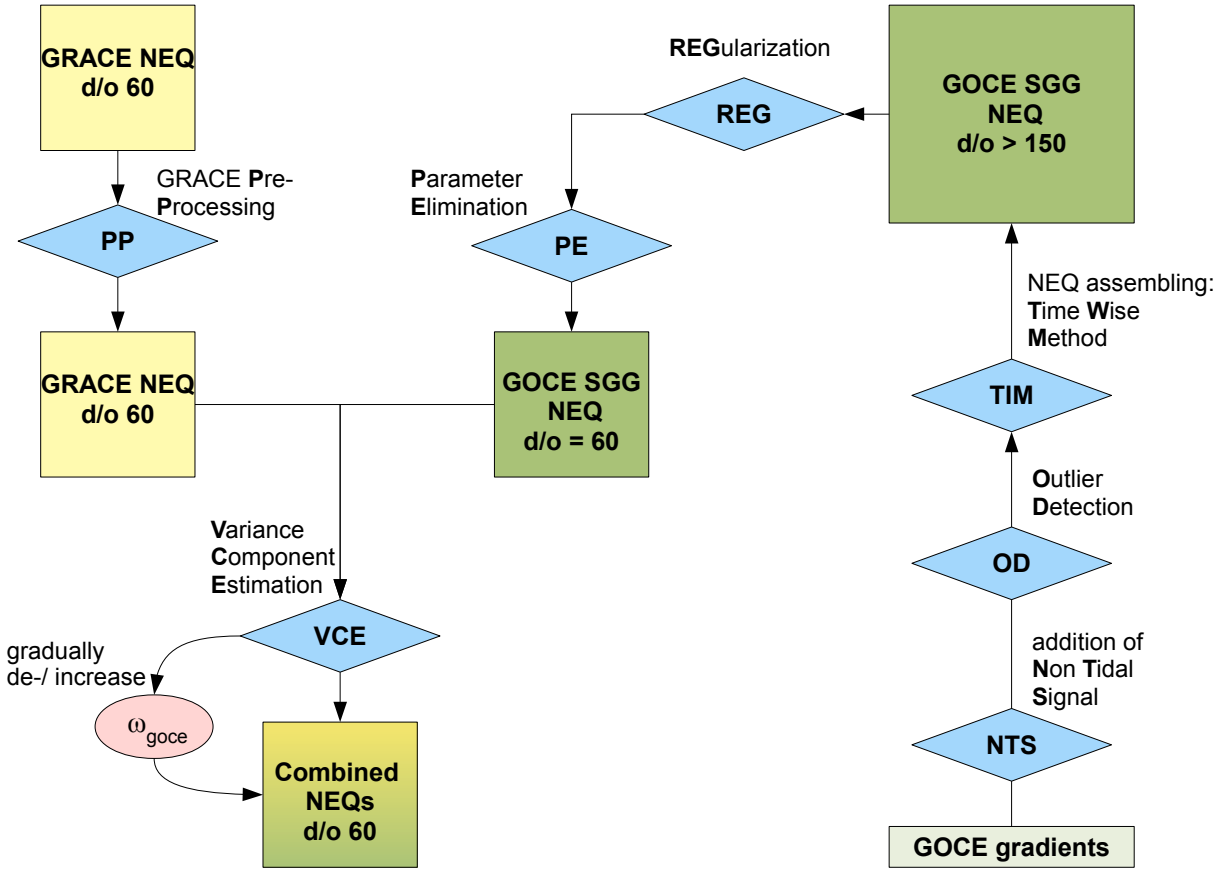

Figure 5: Overall processing scheme for the combination of GRACE SST and GOCE SGG data

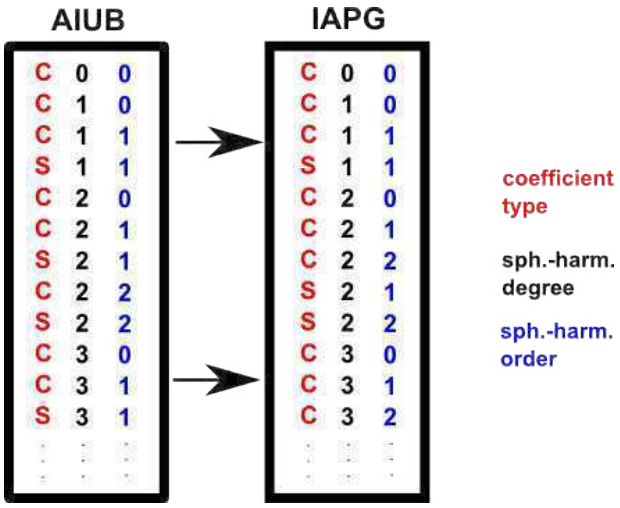

Figure 6: Schematic illustration of the transition from AIUB-like ordering of parameters to IAPG-like ordering

frequency (see chapter 12.2.5). The parameter elimination requires a previous regularization (REG) of the GOCE SGG normal equations, which are ill-conditioned because of orbit induced polar observation gaps (see chapter 12.2.4). Finally, the combination is conducted applying a variance component estimation (VCE), which estimates optimal weights for the combination based on the stochastic models of both normal equations (see section 12.3). Since the error in GRACE is not purely stochastic but as well highly systematic (stripes), the weights derived from a variance component estimation might not reflect the optimum weighting. Therefore, the weight of GOCE normal equations is gradually de- and increased by small values, and the effect is investigated in the combinations. The combined normal equations are in the following analyzed in space and sectral domain regarding their signal and their error behavior (see section 12.4 and 13).

12.1 GRACE data pre-processing

GRACE data as described in section 11.1 has to be subjected to two major processing steps prior to the combination with GOCE. The collating sequence of those two steps is irrelevant :

(1) The parameters of the normal equation matrix $A^T PA$ and the vector $A^T Pl$ from AIUB have to be adapted to the sorting of coefficients in GOCE SGG normal equations which originate from IAPG. Figure 6 schematically shows the transition from Bern-like ordering to IAPG-like ordering. The reordering of IAPG (GOCE SGG) normal equations is likewise possible but computationally more intensive.

(2) The static field AIUB-6YR has to be re-introduced into the normal equations. First of all, the residual field is solved according to the expression

$$\beta_{res} = (A^T PA)^{-1} \cdot A^T Pl \tag{49}$$

where the vector β_{res} represents the spherical harmonic coefficients of the residual field. In the next step, the coefficients β_{AIUB} of the static field AIUB-6YR is added to the residual coefficients

and the *full* $A^T Pl$ vector is retrieved by

$$A^T Pl_{full} = (A^T PA) \cdot (\beta_{res} + \beta_{AIUB}). \tag{50}$$

12.2 GOCE data pre-processing

Following the scheme illustrated in figure 5, five major processing steps can be determined in order to get from GOCE gradient products to normal equations feasible for a combination with GRACE normal equations.

12.2.1 Inclusion of non-tidal time variable signal

As explained in section 11.3, data of the GOCE mission has to be made consistent to GRACE data by re-introducing the provided non-tidal corrections to the GGs, in a first step. Non-tidal corrections (NTC) are re-introduced into the corrected gravity gradients (GG^{cor}) by a component-wise summation for all gravity tensor components following

$$GG_{component} = GG^{cor}_{component} + NTC_{component} \tag{51}$$

where GG represents the gradient containing the non-tidal signal. The NTC can be found in columns 48 to 51 of the official ESA EGG_NOM_2_ products in $\frac{1}{s^2}$.

12.2.2 Outlier detection

In a second step, GOCE gradients are screened for outliers. Erroneous epochs are gapped out in the timeseries. The algorithm for finding and flagging outliers is based on thresholds applied to gradient anomalies, which can be computed with the software tool at the IAPG (see section 8.5). In the study, the gradient anomalies are differences of filtered EGG_NOM_2_ gradients $\frac{\partial^2}{\partial s^2} V^{fil,obs}$ (with non-tidal signal re-introduced) and filtered gradients $\frac{\partial^2}{\partial s^2} V^{fil,model}$ retrieved from the ICGEM [6] listed gravity model *TIM_R3* along the orbit positions. The filter applied to the GGs is an auto-regressive moving-average filter as described in section 8.5, which suppresses the noise in the GGs. The *TIM_R3* gravity model is a GOCE-only solution based on approximately 1 year of data (in a timespan of 1.5 years). The inversely retrieved gradients from this model are assumed to represent the GOCE observations perfectly. Consequently, the expected value for the gradient anomalies $E[\Delta \frac{d^2 V}{ds^2}]$ is zero, following the expression

$$E[\Delta \frac{\partial^2 V}{\partial s^2}] = \frac{\partial^2 V^{fil,obs}}{\partial s^2} - \frac{\partial^2 V^{fil,model}}{\partial s^2} = 0 \tag{52}$$

where the middle part denote the differences between observed and model GGs.

The first step in the outlier detection is a screen for coarse outliers. Coarse outliers are defined on basis of a modified tracelessness condition (see section 8.3) as

$$(\Delta \frac{\partial^2}{\partial s^2} V_{xx})^2 + (\Delta \frac{\partial^2}{\partial s^2} V_{yy})^2 + (\Delta \frac{\partial^2}{\partial s^2} V_{zz})^2 \; > \; 100 \; [mE\ddot{o}tv\ddot{o}s] \tag{53}$$

[6] ICGEM Homepage: http://icgem.gfz-potsdam.de/ICGEM/ICGEM.html (June 2012)

where the left side of the equation is the trace of a gravity tensor consisting of gravity gradient anomalies. Instead of pure GGs, filtered gravity gradient anomalies are used for the trace calculation.
In a second step, each single component (xx, yy, zz and xz) is scanned separately for outliers by applying a threshold directly on the filtered gradient anomalies. The algorithm is partly adapted by the method developed by Weyjong Yi (see Yi (2011)). The threshold is determined individually for each component by a multiple of the standard deviation within the gradient anomaly time-series. For the computation of the standard deviation neglecting the initially detected coarse outliers becomes necessary in order to achieve constant and reasonable values. If an outlier is detected, 40 data epochs before and 300 data epochs after the actual outlier are taken out in order to avoid erroneous signal potentially following the outlier. After major outliers the signal can be found oscillating severely around zero. Figure 7 shows the described behavior in the V_{zz} component of the gradient anomalies in March 2010. In such cases, more than the 300 data points after the outlier were taken out, manually.

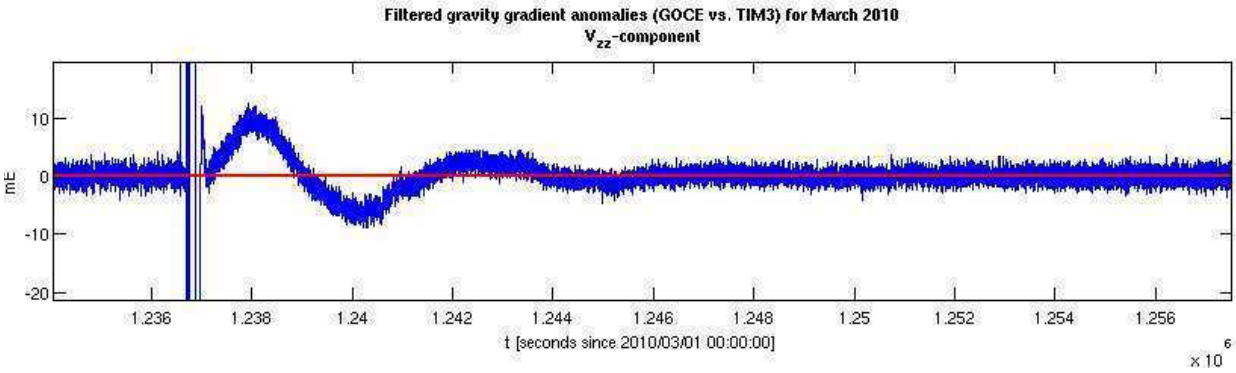

Figure 7: Major outlier in V_{zz} component of gradient anomalies of March (2010)

Figures 8 to 11 exemplary show the results of the outlier detection algorithm for January 2010. The blue time-series shows the gradient anomalies of the component. All values exceeding the red threshold line are considered as outliers. Epochs marked with green balks are previous detected coarse outliers. Used thresholds in all months with available *old* gradient data of the year 2010 are set between 5 - 9.5 mEötvös (see table 3). Those values account for 6.5 to 7.5 times the standard deviation of the components per month.
In the statistics of table 3 the parameter *flagged epochs* refers to all the epochs which were kicked out by (a) initially flagged epochs and (b) gapped epochs , as well as to (c) all epochs which can not be taken into account because of the warm-up period of the filters (see section 8.5). For most months the total amount of flagged epochs ranges between 1 and 6 % of all epochs. March 2010, however, seems to be a bit worse with 14% flagged epochs. Note, that every gapped epoch is followed by a warm-up period of the filter accounting for 1500 epochs in the year 2010, which make up for most flagged epochs. Figure 12 underlines the extent of the filter warm-up time. The upper plot shows the time-series of the filtered trace of the gradient anomalies together with flags and gaps (red balks) and warm-up epochs (green), while the bar diagram shows the contingent of each of the three effects in percent (initially flagged epochs: 0.2% ; gapped epochs: 0.4%; warm-up epochs: 2.05%).
Regarding the new (re-processed) gradients, significantly more outliers were detected by the algorithm. Table 4 gives an overview on the results of the outlier detection for the first 6 months

month	jan	feb	mar	apr	mai	jun	oct	nov	dec
flagged epochs [%]	1.5	4.75	14.69	2.36	6.92	2.66	3.16	0.83	3.6
remaining data [days]	28.87	10.75	20.60	29.29	26.32	29.13	27.12	29.75	28.69
threshold									
V_{xx} [mEötvös]	7.45	6.89	8.23	7.32	7.07	7.08	7.32	7.85	6.64
V_{yy} [mEötvös]	6.15	5.85	6.20	6.08	5.77	5.63	6.48	6.54	5.62
V_{zz} [mEötvös]	6.51	6.08	9.34	6.35	6.12	5.99	6.37	6.38	5.85
V_{xz} [mEötvös]	9.12	8.45	9.06	8.78	8.28	8.32	8.68	9.20	8.16

Table 3: Monthly (2010) outlier statistics for (**old**) GOCE gravity gradients after applying the outlier detection algorithm

month	jan	feb	mar	apr	mai	jun
flagged epochs [%]	21.40	20.43	32.73	44.60	27.09	20.43
remaining data [days]	23.34	8.98	18.47	9.42	17.50	20.69
xz - excluded:						
flagged epochs [%]	15.86	18.31	28.43	37.51	14.03	13.95
remaining data [days]	24.98	9.22	19.65	10.62	20.63	22.37
threshold						
V_{xx} [mEötvös]	8.14	7.73	8.38	7.68	7.41	7.45
V_{yy} [mEötvös]	6.07	6.02	5.97	5.97	5.57	5.51
V_{zz} [mEötvös]	10.71	9.96	9.26	10.08	9.27	9.41
V_{xz} [mEötvös]	12.30	13.16	12.33	12.63	11.41	10.80

Table 4: Monthly (2010) outlier statistics for reprocessed (**new**) GOCE gravity gradients after applying the outlier detection algorithm

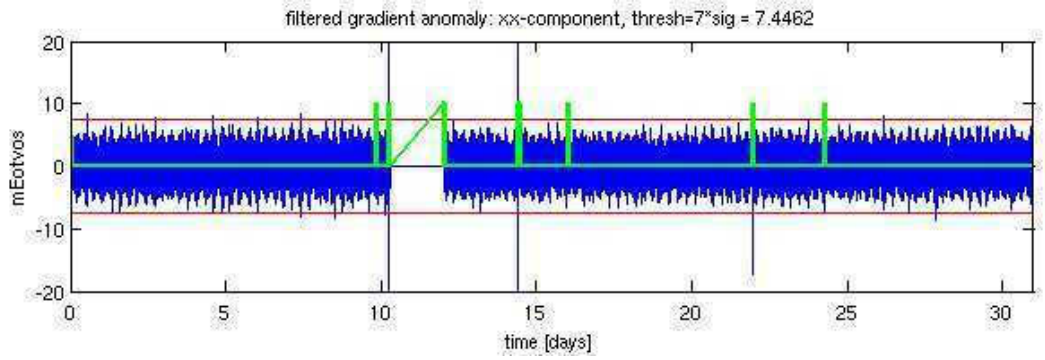

Figure 8: $\Delta\frac{\partial^2}{\partial s^2}V_{xx}$ (January 2010) : Filtered gradient anomalies with respect to TIM3 (with **old** gradients)

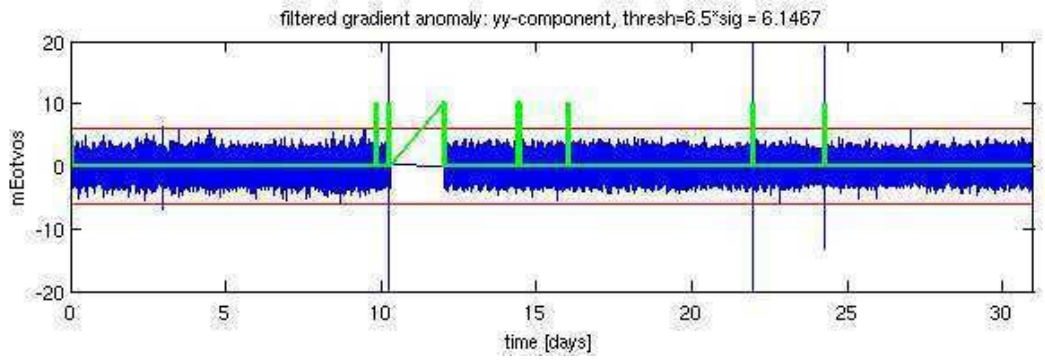

Figure 9: $\Delta\frac{\partial^2}{\partial s^2}V_{yy}$ (January 2010) : Filtered gradient anomalies with respect to TIM3 (with **old** gradients)

in the year 2010. About 20 - 44 % of all data-points in the monthly period have to be taken out (filter warm-up considered). Without evaluating the xz-component, the outliers can be reduced to 15 - 37 %. This shows that the xz-component causes around 25 - 30 % of the total number of flagged epochs and is therefore considered not worth to be evaluated at all in the gravity recovery process, as more valuable information comes from the more important components xx, yy and zz. The thresholds for all components calculated from the standard deviations of the gradient anomalies range from 5 - 13 mEötvös and are generally higher than the thresholds computed for the old gradients (see table 3). In figure 13, exemplary, the time-series of the filtered trace of gradient anomalies of January 2010 (upper plot) shows that the anomalies obviously are worse than those with the old gradients (compare with figure 12). The lower plot shows, that on the one hand significantly more outliers have been detected (around 2%, 2nd red balk). On the other hand, the rise in outliers causes a tremendous rise in the epochs kicked out by the filters, as each gapped epoch is followed by 1500 warm-up points. Similar results were achieved for all the other months when screening for outliers in the new gradients.
This behavior is not fully understood because it is shown e.g. by Stummer et al. (2012, 2011), Pail et al. (2012) that the reprocessing of the gradients should lead to a significant better behavior. Meanwhile there is evidence that the algorithm within the official, new L1B - processor does not work 100 % correct. The issue is currently investigated by ESA and the HPF.

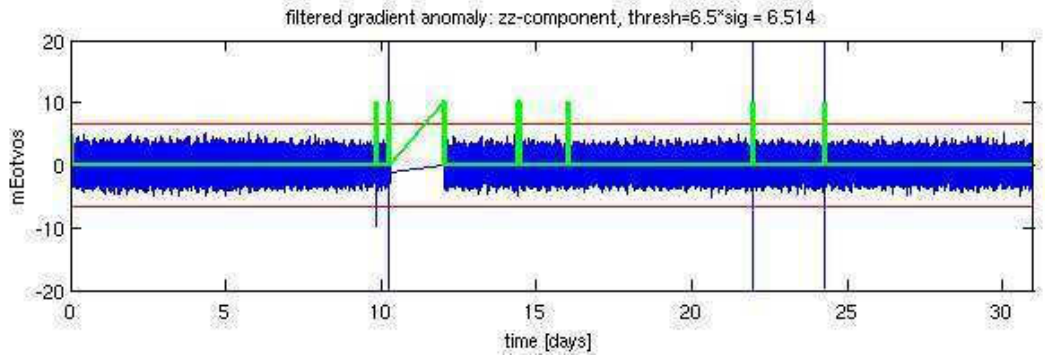

Figure 10: $\Delta\frac{\partial^2}{\partial s^2}V_{zz}$(January 2010) : Filtered gradient anomalies with respect to TIM3 (with **old** gradients)

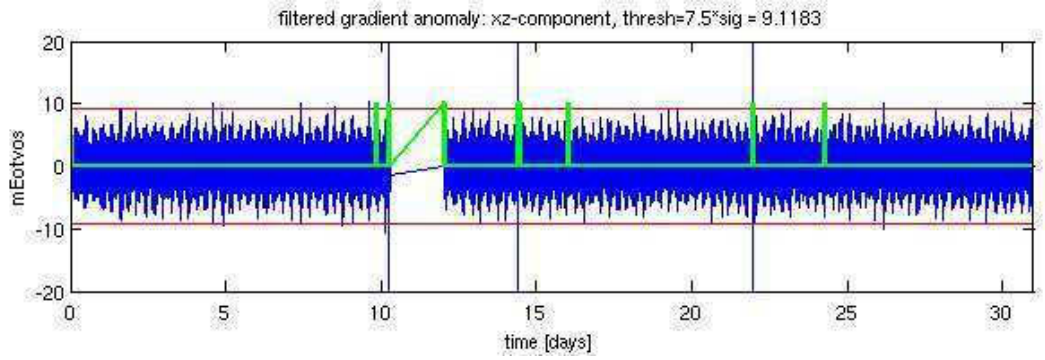

Figure 11: $\Delta\frac{\partial^2}{\partial s^2}V_{xz}$(January 2010) : Filtered gradient anomalies with respect to TIM3 (with **old** gradients)

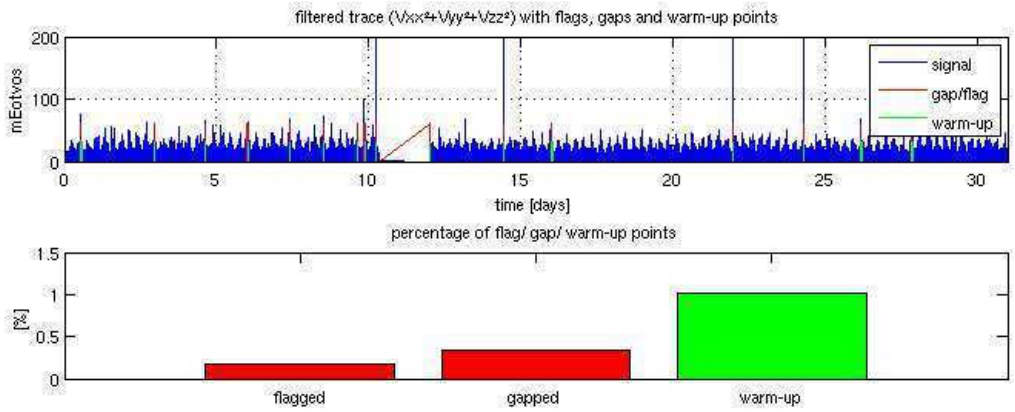

Figure 12: Trace of filtered gradient anomalies and flagged epochs (January 2010) using **old** gradients

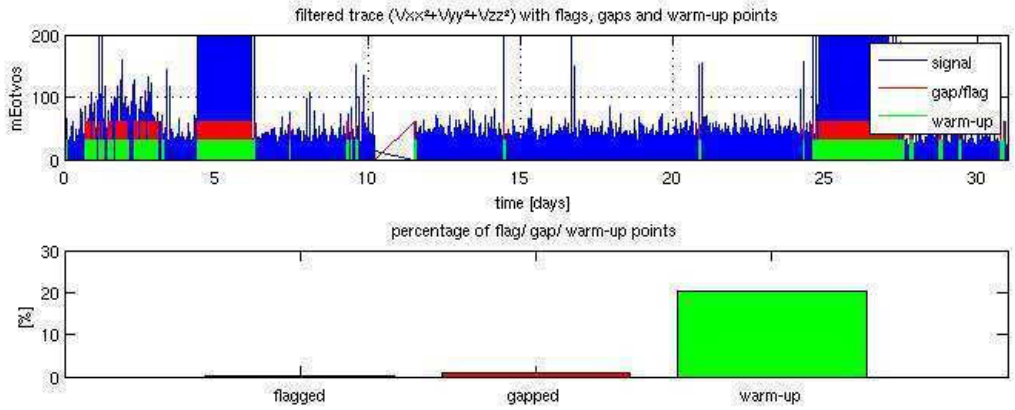

Figure 13: Trace of filtered gradient anomalies and flagged epochs (January 2010) using **new** gradients

In the last step of the outlier detection the normal equations are set up excluding the newly retrieved outliers, and monthly gravity fields are solved for a visualization in space domain (geoid heights and gravity anomalies). In these functionals undetected outliers become visible in terms of regional error structures and aliasing. In the case the outlier detection appears insufficient, data is screening again starting from step two with a reduced threshold. Additionally, the filtered gravity gradient anomalies are specifically scanned for potential erroneous epochs in the erroneous regions, manually.

12.2.3 Assembling of normal equations

The assembling of the normal equations consists of the generation of an $A^T PA$ matrix and an $A^P Tl$ vector according to the time-wise method (see section 8.2.2 and Pail et al. (2010)). The computation is conducted using the above described software at IAPG which requires parallel processing on the linux-cluster environment of LRZ (see section 8.5).
Ideally, intending to get the maximum gravity information, monthly normal equations are assembled to the highest spherical harmonic degree/order which is possible with respect to the available data epochs per month. A rule of thumb used for the definition of the maximum degree N_{max} for a monthly GOCE gravity field solution is chosen by

$$N_{max} = \frac{\alpha}{2} \tag{54}$$

where α denotes the number of revolutions the GOCE satellite passed during one month. Assuming that one day approximately accounts for 16 revolutions, the maximum spherical harmonic d/o can easily be computed using the number of remaining data epochs after outlier detection and the filtering. Referring to table 3 and 4 which list the remaining data epochs for all operational GOCE months of the year 2010 for old and re-processed gradients, the corresponding maximum degrees are listed in table 5 for monthly and in table 6 for bi-monthly solutions. With rising maximum degree the computational effort for assembling and inverting the normal equation matrix increases dramatically as shown in table 7. At a maximum degree of 180 the $A^T PA$ matrix holds approximately 8.5 GB and its assembling on the described environment (see section 8.5) takes around 2 days.

Month	Jan	Feb	Mar	Apr	May	June	Oct	Nov	Dec
old gradients	180	60	150	180	180	180	180	180	180
new gradients	180	60	150	80	160	180	-	-	-

Table 5: Maximum degree of monthly GOCE gravity field solutions for all operational GOCE months of the year 2010

Month	Nov + Dec (2009)	May + June (2010)
old gradients	224	180
new gradients	-	180
in-house	224	-

Table 6: Maximum degree of bi-monthly GOCE gravity field solutions for all operational GOCE months of 2009 and 2010

12.2.4 Regularization and solving GOCE SGG NEQs

In order to solve the monthly GOCE normal equations a constraining becomes necessary, because the normal equations are strongly ill-posed mainly due to the polar gap (see section 8.4). Constraining or regularization is a delicate topic because it means inclusion of external information which later makes it difficult to distinguish between the impact of real GOCE information and other information, when it comes to analyzing combined GOCE-GRACE solutions. Actually, a regularization is not necessary for a combination of GOCE NEQs with GRACE NEQs, because the GRACE NEQs are generally not ill-posed. However, the combination with GRACE is conducted with GOCE NEQ systems of degree/order 60 due to computational reasons. This requires an adequate parameter elimination of the GOCE NEQs which is not possible without regularization when all the information of the high degrees shall be maintained (see section 12.2.5).

The regularization applied to GOCE NEQs is an order dependent *Kaula regularization* (see 8.4) of selected groups of coefficients in the A^TPA matrix, which are affected by the polar gap. This constraining enables the inversion of the A^TPA matrix following equation 30 (section 8.4), and thus gravity coefficients can generally be retrieved from monthly pure GOCE SGG NEQs. The regularization parameter for monthly solutions is set to 10 ($\alpha = 10$), which is an empirically defined value.

The regularization also makes an inspection of monthly GOCE solutions possible prior to the combination with GRACE. The inspection of the monthly fields e.g. in terms of gravity anomalies is needed for the iterative outlier procedure (see step 2 in section 12.2). During the iterative outlier detection it becomes obvious, that monthly GOCE-only solutions are very sensitive to gapping. Generating a clean solution up to the above defined maximum degrees (see table 5) is difficult, as taking out a few hundred more data epochs in the outlier gapping procedure can lead to an unstable NEQ system. For example, it was tried to remove remaining outlier structures in the monthly solution of November 2010 by taking out 241 more epochs (out of a total of 2.6 million observations). The consequence was that the system became unsolvable. In October 480 additional outliers (out of 2.4 million observations) led to the same effect. Therefore, some monthly fields regionally show minor or big error structures which could not be removed even by

N_{max}	Memory [MB]
60	110.8
100	832.5
120	1714.9
150	4159.1
180	8586.3
224	20141.0

Table 7: Memory demand for the normal equation matrix at different maximum degrees in mega byte

iterative outlier detection (see section 13.3), others remain unsolvable. Table gives an overview on all monthly available and successfully solvable monthly gravity field solutions with old, new and in-house gradients. An x denotes a solvable solution and when data sets were not available or used, corresponding fields in the table are marked with *n.a.* (not available). Bi-monthly solutions could be retrieved for November and December of the year 2009 and for May and June of the year 2010.

Year Month	09 Nov	09 Dec	10 Jan	10 Feb	10 Mar	10 Apr	10 May	10 June	10 Oct	10 Nov	10 Dec
old	x	x	x	-	x	-	x	x	x	x	x
new	-	-	x	-	-	-	-	x	n.a.	n.a.	n.a.
in-house	x	x	n.a.	n.a.	n.a.	n.a.	n.a.	n.a.	n.a.	n.a.	n.a.

Table 8: Solvable monthly GOCE SGG solutions (x) for different gradient data sets

12.2.5 Parameter elimination

In the last step before the combination with GRACE, GOCE SGG normal equations are reduced to GRACE NEQ size (spherical harmonic degree/order 60) by means of a parameter elimination following the procedure described in section 10. The reduction is not a crucial prerequisite for a combination with GRACE, but it was necessary regarding the time frame of this research as the parameter elimination greatly reduces computational effort and NEQs become invertible on an usual PC. GOCE normal equations are assembled up to maximum possible degree regarding the available observations per month, which is a necessary prerequisite in order to avoid spectral leakage problems in the gravity field solutions. The parameter elimination introduces the information of the higher-order parameters, which shall be reduced, into the lower-order parameters, without information loss.

The result of the parameter elimination is shown exemplary for the month January (2010) for a GOCE SGG solution initially assembled up to d/o 180 in figure 14. One can see the degree error median w.r.t the GOCO02S signal of the not-reduced solution (d/o 180) in red and the reduced solution (d/o 60) in blue. As indicated by the dashed-magenta line, which shows the median of the coefficient differences of the two solutions, the differences are far below the differences to GOCO02S. This result is a proof for the validity of the parameter elimination process,

as the reduced solution basically shows the identical behavior concerning EGM2008.

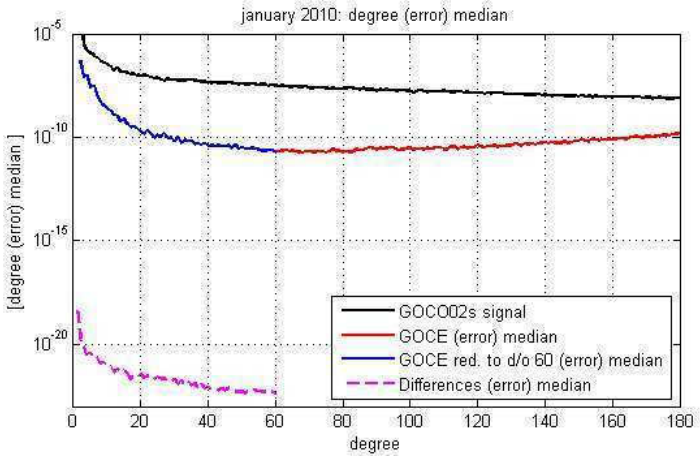

Figure 14: Degree error median (w.r.t. GOCO02S) of the GOCE SGG solution of January 2010 complete up to d/o 180 (red) and its reduced equivalent, with parameters > d/o 60 eliminated (blue); the dashed line (magenta) indicates the median of the coefficient differences

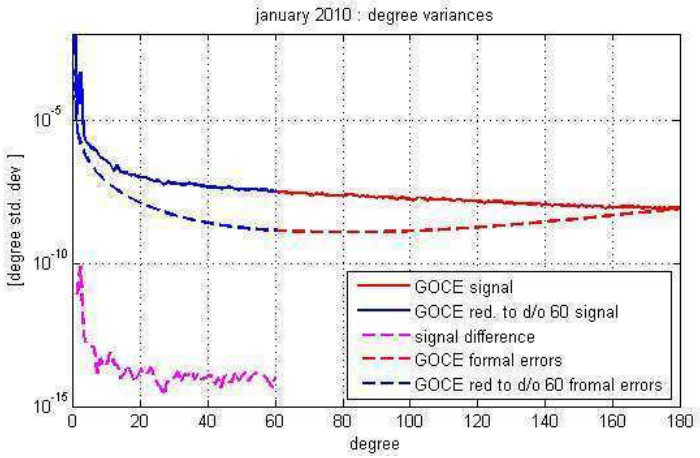

Figure 15: Degree (error) variances of the GOCE SGG solution of January 2010 complete up to d/o 180 (red) and its reduced equivalent, with parameters > d/o 60 eliminated (blue); the dashed line (magenta) indicates the differences between the signal variances; the dashed blue and red line indicate the error degree variances of both solutions

In the same way the degree variances in figure 15 validate the parameter elimination process. It displays the signal variances and the variances of the formal error of the GOCE SGG January 2010 solution, complete up to d/o 180 (solid red line), and of its equivalent reduced to d/o 60 (solid blue line). The difference (dashed magenta line) is 5 orders of magnitude below the signal. The formal errors (blue and red dashed lines) also show identical behavior.

12.3 Optimal combination of GOCE and GRACE on basis of normal equations

The optimal combination between the GOCE SGG normal equations and the GRACE SST-ll normal equations is done by means of a variance component estimation as described in section 9. The variance component estimation is the final step to derive combined normal equations after successful pre-processing of GRACE and GOCE normal equations (see figure 5). Formula 36 on page 34 simplifies to

$$\begin{aligned}(\omega_{goce}\ A^T P A_{goce} + \omega_{grace}\ A^T P A_{grace})\ \beta \\ = \omega_{goce}\ A^T P l_{goce} + \omega_{grace}\ A^T P l_{grace}\end{aligned} \tag{55}$$

because the regularization is already applied to the ill-posed GOCE SGG normal equations prior to the parameter elimination. Hence, two weight factors ω_{goce} and ω_{grace} are estimated.

Since the $l^T P l_{grace}$ value as received from AIUB does only contain the observations that reflect the residual part of the field (the static field AIUB-6YR has been subtracted), the full value has to be restored. This can be done using the coefficients β_{AIUB} of the 6 year static GRACE solution following the expression

$$l^T P l_{full} = l^T P l_{res} + \beta_{AIUB}\ (A^T P A_{grace})\ \beta_{AIUB}. \tag{56}$$

The variance component estimation is an iterative process, where the estimated weights are continually improved regarding the combined solution. Initial values for both variance components σ_{goce} and σ_{grace} are set to 1. First, normal equations are combined using the initial weights. Afterwards, the combined system is inverted and new weights are estimated based on the retrieved parameters. Then the new weights are used for combination and the system is inverted again. This is done until the solution converges and the estimated variances are close to 1 again.
It could be shown that the process works correctly as not more than 5 iterations are necessary for a perfect convergence of the variances. Tables 12 and 13 on page 88 show the variances after each iteration step for old and re-processed gradients, respectively. The convergence of the variance component estimation expressed by $\frac{\sigma^2_{grace}}{\sigma^2_{goce}}$ for all monthly solutions is also shown in figure 16. The combined solution hardly changes already after the third iteration.

Looking at the final relative weights of GOCE SGG and GRACE normal equations in the combinations, one can see directly the minor impact of GOCE gradiometry in the solutions. The GOCE SGG normal equations are down-weighted relatively to GRACE normal equations by factors ranging from 0.0003 to 0.1 (see last columns of appended tables 12 and 13 on page 88. Those values are corrected for an initial a-priori scaling difference of 5.00E-12 between both types of normal equations. The down-weighting generally appears correct, as formal errors of the gradiometer in the spectral domain up to spherical harmonic d/o 60 exceed formal errors of the GRACE observation type, and we expect GOCE only to contribute marginally to the total solution. However, a variance component estimation only accounts for weighting according to the stochastic error models of the involved normal equations. GRACE is suffering from severe stripes in its monthly and bi-monthly gravity field estimates (see section 7) which are highly systematic and are not totally expressed within the formal errors. Thus, the variance component estimation might not lead to an optimally combined solution taking into account the real GRACE error. Nevertheless, it can be assumed that the variances from the estimation

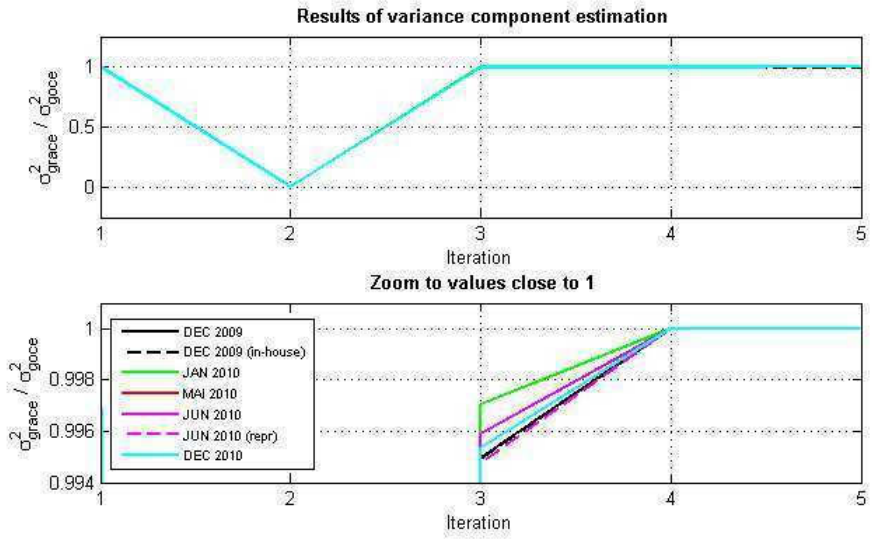

Figure 16: Convergence of variance component estimation for all monthly solutions

process are a good starting point. In the following, therefore, not only combinations with weights originating directly from the variance component estimation, but also combinations with gradually increased or decreased relative weights are investigated.

12.4 Quality evaluation methods for gravity field estimates

The aim of the thesis is to determine whether GOCE gradients can contribute positively to GRACE monthly and bi-monthly solutions. The investigations shall specifically indicate whether the striping in the combined solutions can be reduced. Therefore a method is needed which is able to express the quality of the combined gravity field and the severeness of the stripes.
Generally, the analyses of gravity field estimates can be done in spatial domain through functionals, and in spectral domain, by directly investigating the coefficients. The most common methods for a spatial analyses are given in section 5. They allow the visualization of the gravity field in terms of different gravity functionals, such as geoid heights, gravity anomalies, and equivalent water heights. All of the three functionals express the gravity in the estimated solution w.r.t a static reference. Geoid heights show the deviations from the normal potential in terms of meters geoid height, while gravity anomalies show the deviation to the normal acceleration in $\frac{m}{s^2}$ (see section 5.1). Equivalent water heights express the deviations to a static gravity model in terms of meters water column (see section 5.2).
In spectral domain degree variances allow an investigation of the signal (energy) content and the error regarding a static reference per degree of the spherical-harmonic series (see section 6). In the same way the degree median and the degree standard deviations are tools to express the deviation to a static reference field per degree (see section 6.2 and 6.3).
All methods listed above, generally can express the quality and the deviation from a static reference field, but they do not solely express the extend of the striping. The normal potential and the static reference field which serve as a reference for the methods do not account for the temporal gravity changes of the investigated month. Therefore, temporal gravity variations may be interpreted as part of the striping error in those methods.

In order to avoid misinterpretation due to time variable gravity signal, a method is introduced here, where the temporal signal is eliminated prior to the investigation of the striping error. The temporal gravity signal for this approach is approximated by lowpass-filtering of the GRACE field to be investigated. The result of the filtering is a smoothed solution, that does not contain stripes any more. The filtered field then serves as reference for comparisons, as it reflects the gravity signal of the month better than a static reference field.
Figure 17 shows (a) an unfiltered monthly GRACE solution, (b) the same monthly GRACE solution, filtered by an isotropic Gaussian filter with a radius of 500km, and (c) the difference between both - the filtered and the unfiltered - solutions. In the sub-figure (c) only the stripes remain, while all temporal large-scale gravity signal is not contained. Excluding the time variable monthly signal enables an inter-monthly comparison of the stripes in GRACE solutions.

For the quantification of the extent of the striping error in a monthly GRACE or combined GRACE-GOCE solution a global *root mean square error* (RMSE) value is introduced. Considering a global grid containing the errors $\sigma_{r,c}$ of a gravity field solution in equivalent water heights, the RMSE is expressed as

$$RMSE = \sqrt{\left(\frac{\sum_{r=0}^{R} \sum_{c=0}^{C} \omega(\phi_r) \sigma_{r,c}^2}{\sum_{r=0}^{R} \sum_{c=0}^{C} \omega(\phi_r)} \right)} \tag{57}$$

where r is the current row and c is the current column of a grid with the size R x C. The errors $\sigma_{r,c}$ (=striping error) of a gravity field solution can be obtained by subtracting a smoothed solution, as described above (see also subplot (c) in figure 17). The parameter $\omega(\phi_r)$ denotes a weighting function of the kind

$$\omega(\phi_r) = cos(\phi_r) \tag{58}$$

where ϕ_r is the geographic latitude which corresponds to the current row r of the grid point. The weighting is introduced because of the meridian convergence. Error values at higher latitudes are down-weighted in the total RMSE according to the smaller area comprised by the corresponding grid point.

13 Results

In this section, first, GRACE SST-ll (only) solutions and GOCE SSG (only) solutions are evaluated regarding their quality. This is necessary to better understand the behavior and the contribution of GOCE in joint GRACE - GOCE gravity solutions. The combined solutions are investigated on monthly (see section 13.3.1) and bi-monthly (see section 13.3.2) basis, afterwards. All investigations, however, are restricted to months where solvable GOCE SGG normal equations could be assembled (see table 8 on page 49).

13.1 GRACE SST-ll gravity field solutions

The monthly GRACE gravity field solutions obtained from AIUB are visualized in space domain in figures 31, 32 and 33 on page 81. The striping errors in the gravity anomalies reflect the typical error type (see section 7.3). The months November and December 2009, and May and June 2010, seem to be affected more severely than the other months regarding the density and amplitude of the stripes. In the months October and November 2010 the striping errors seem to be most

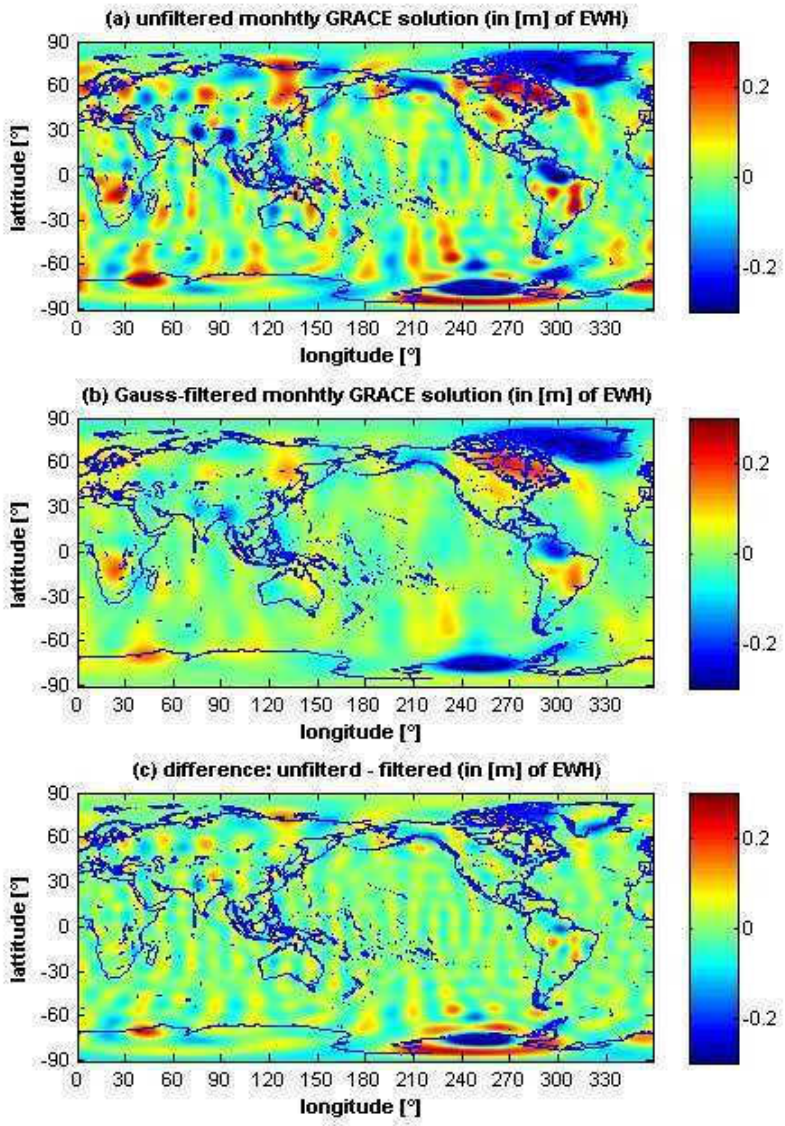

Figure 17: GRACE monthly solution: Equivalent water heights evaluated up to spherical harmonic d/o 30 with C_{20} excluded in meters; (a): unfiltered solution; (b): filtered solution; (c): difference of solutions

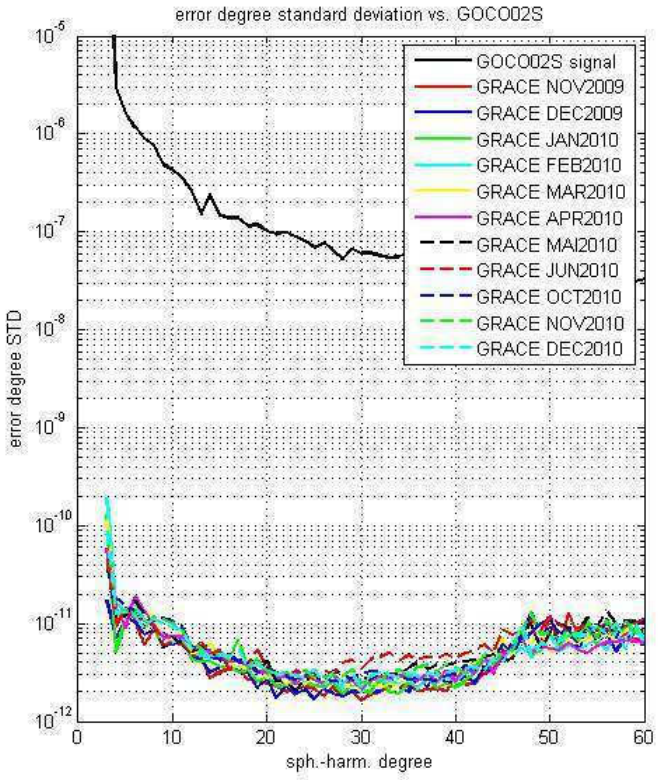

Figure 18: Degree standard deviation of monthly GRACE solutions w.r.t. GOCO02S

dominant around +30°and -30°latitude.

From the degree standard deviations with respect to the reference model GOCO02S in figure 18 it becomes obvious that all solutions loose quality significantly from degree 40 onwards. This is where the striping error becomes more severe. Between degree 20 and 40 the coefficients show the smallest deviations to the reference model. In this spectral range, the striping error is not so severe and time variable signal can be determined. In the degrees below 20, the relatively higher deviations mainly originate from the time variable signal which can be measured there (and not striping error). The large standard deviation for the C_{20} coefficient shows that the oblateness of the Earth is determined weakly in GRACE fields from AIUB, generally. The month June 2010 shows poor accuracy, as its standard deviations exceed the others between degree 30 and 45.

The two bi-monthly GRACE solutions investigated in this thesis are shown in figure 34 on page 83 in terms of gravity anomalies. They were obtained by addition of normal equations of the two consecutive months. Their standard deviations with respect to GOCO02S in figure 19 proove that the November+December solution is better regarding the May+June solution. Between d/o 12 to 40 the bi-monthly solution of 2009 shows less deviations to the static reference than the 2010 solution, which may be due to time variable effects. From degree 40 onwards, however, the 2009 solution outperforms the other. This is also reflected in the gravity anomalies (figure 34) where the May+June 2010 solution shows a more severe striping error.

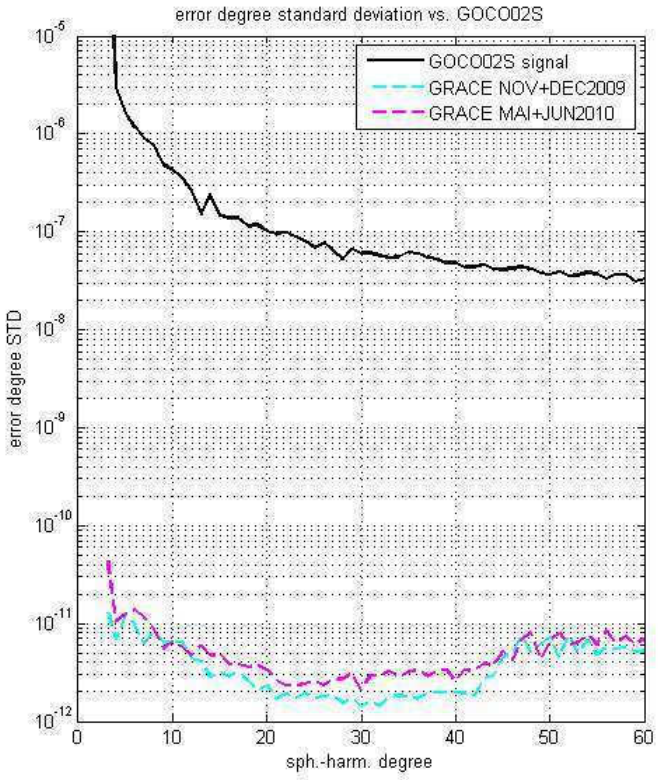

Figure 19: Degree standard deviation of bi-monthly GRACE solutions regrading GOCO02S

The characteristics of the single GRACE solutions of figure 18 and 19 is also reflected in the values of the global RMSE, which can be obtained using the procedure described in section 12.4. Table 9 shows the RMSE values (in cm of EWH) of GRACE solutions which were used for combinations, when evaluated at different degrees. The month June, followed by the month May, show the highest RMSE values over all degrees and the highest average. Those are the months (as identified above) which suffer most from the striping error. December 2009 and January 2010 happen to be the months with lowest RMSE values, which is consistent to their characteristics in the degree standard deviations of figure 18. The RMSE value of the two bi-monthly solutions is significantly lower than that of their corresponding monthly solutions. The November+December period behaves better than the May+June period, below d/o 50. This indicates that the striping error is reduced in accumulated GRACE solutions.

To get the full picture of the quality of the GRACE solutions the formal errors are given degree-wise in figure 20. It shows that the coefficients at low degrees and orders can be better determined (apart from C_{20}) and that the error is rising towards the higher degrees. The months November and December of the year 2009 show very similar characteristics that differ from the rest of the months. Until d/o 12 they exceed the error level of the other months (as well as for d/o 16). Between d/o 12 and 45 they are within the accuracy of the other months and loose quality again from d/o 45 onwards. The special behavior of the error in both months may be due to a different orbit configuration. GRACE flew a 7-day sub-cycle in November and December of the year 2009, which might slightly decrease the quality within both months (Pail et al., 2011b).

Year	2009	2010	2010	2010	2010	2009	2010
Month	Dec	Jan	May	Jun	Dec	Nov+Dec	May+Jun
d/o 30	4.02	4.46	5.64	7.03	5.71	3.49	5.28
d/o 35	6.00	6.15	8.45	11.01	7.94	4.74	7.89
d/o 40	8.49	8.17	11.98	15.12	10.70	6.46	11.98
d/o 45	13.70	14.68	16.52	23.00	15.59	11.40	14.91
d/o 50	28.87	23.09	29.70	37.01	24.86	21.11	24.87
d/o 55	38.03	35.27	44.82	47.20	35.59	28.65	33.55
d/o 60	53.23	45.64	56.16	58.92	46.13	38.54	41.32
Average	**21.76**	**19.64**	**24.75**	**28.47**	**20.93**	**16.34**	**19.97**

Table 9: Global RMSE values [cm EWH] of selected monthly and bi-monthly GRACE-only solutions at different degrees

However, the weak performance does neither not show up in the degree standard deviations, nor in the error degree medians (w.r.t. GOCO02S). Interestingly the weak performance of the months June and May 2010, which has been observed in the standard deviations (see figure 19), is reflected in the formal errors, as the solutions show higher errors compared the others in the mid-wavelengths.

13.2 GOCE SGG gravity field solutions

Appended figures 35 to 41 (on pages 83 to 86) show gravity anomalies of GOCE-only solutions with old gradients regarding the reference model GOCO02S (visualizations exclude coefficients below d/o 20) together with corresponding coefficient differences to GOCO02S. All monthly solutions clearly show the polar gap effect in both types of visualization. Gravity anomalies in areas north of +80°and south of -80°latitude show relatively big differences (<-1 $\frac{m}{s^2}$ / >+1 $\frac{m}{s^2}$) to GOCO02S. In the same way the coefficient differences indicate the polar gap problem, as near-zonal coefficients are badly determined (orange / red ridge in the middle of the triangles). In the triangles one can also see the slightly worse determination of very low frequencies (below degree 20), which is inherent due to the gradiometer's specifications (see section 8). Those badly determined coefficients are excluded from the gravity anomaly visualizations.
The GOCE-only solutions of the months March, October and November with old gradients, however, show regional error structures of erroneous observations, that could not be gapped out (see section 12.2.4). The coefficients from these months generally show a worse performance in high degrees and in the near-zonal area. The March solution additionally suffers from a problem affecting the near-sectorial coefficients, leading to symmetric error structures in the geoid. These errors make the usage of those months for GOCE-GRACE combinations questionable.
An investigation of the long wavelength parts show north-south arranged large-scale error structures in the geoid representations of all months, as shown in figure 21.
The figure exemplary shows the geoid differences of the June 2010 GOCE-only solution to GOCO02S in the Australia/Oceania region, only considering selected coefficient groups. In the upper left image the geoid differences of the coefficients are starting from d/o 30, in the other images the starting degree is continually augmented by 5. In solutions starting above degree 40 the north-south error structures vanish. This large scale errors of a magnitude of up to 40 cm indicate that no improvement of GRACE solutions is to be expected due to GOCE SGG

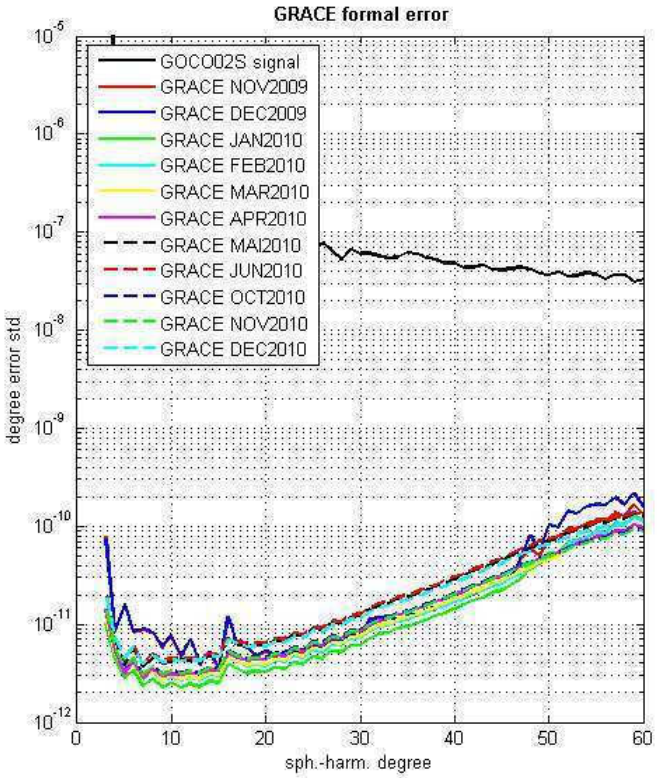

Figure 20: Formal errors of investigated monthly GRACE solutions

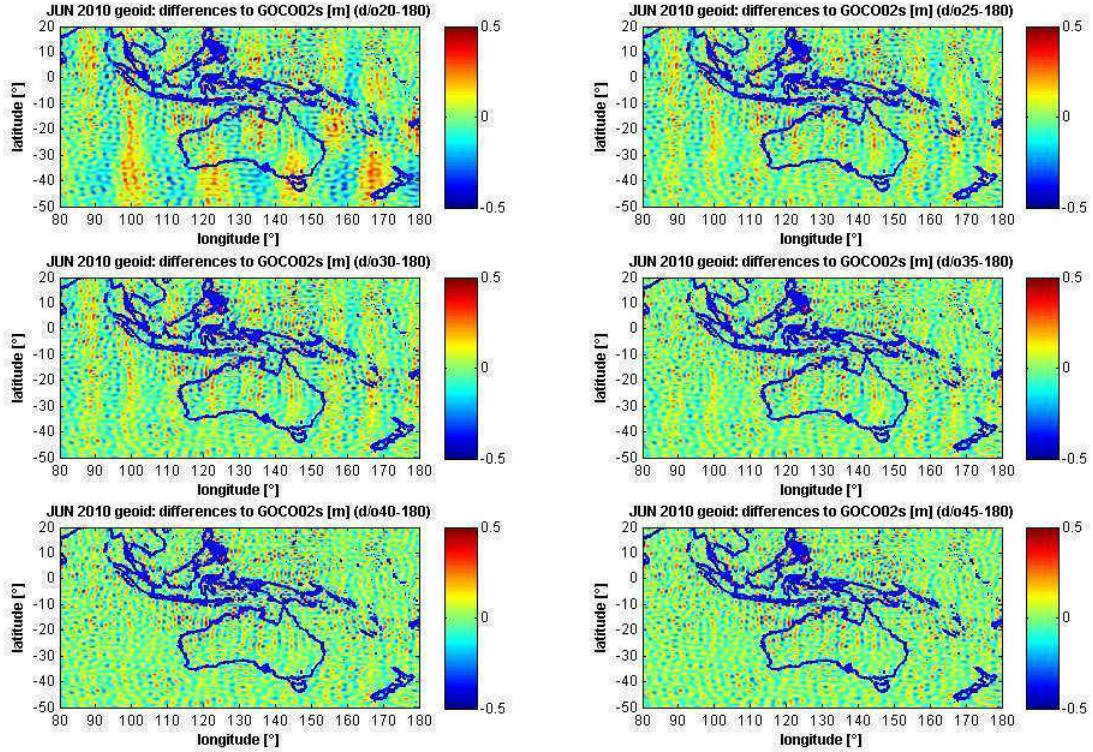

Figure 21: GOCE SGG geoid differences over Australia to GOCO02s for June 2010 in dependence of different coefficient groups (in meters)

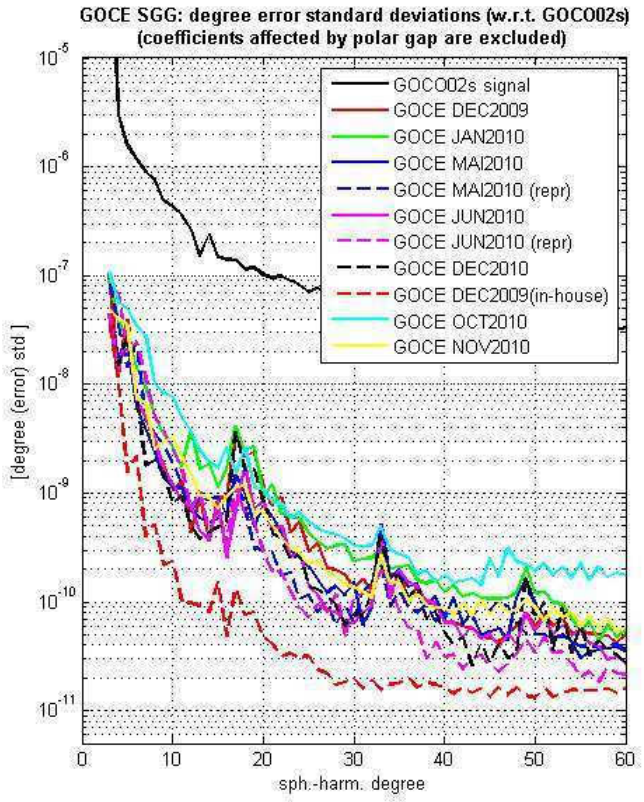

Figure 22: Degree standard deviations w.r.t GOCO02S of all monthly obtained GOCE SGG solutions excluding the polar gap

observations in the degrees/orders lower than 40.

In a joint spectral analysis the qualitative characteristics of the solutions and the differences between the different used gradient products (old, new, in-house) in the obtained GOCE-only SGG solution become visible. Figure 22 shows the degree standard deviations with respect to GOCO02S of all monthly GOCE SGG solutions excluding coefficient groups affected by the polar observation gap. Four conclusions can be drawn from the illustration:

(1) The solutions based on old gradients show dominant peaks with high deviations from the reference model which occur at multiples of the orbit frequency (16, 32, ...) of GOCE satellite. (2) The GOCE SGG solution of December 2009 (red dashed line) based on in-house gradients outperforms the other solutions regarding the entire observed spectrum, by far. (3) The monthly solutions based on new (re-processed) gradients do not show the extent of improvement which can be observed with the in-house gradients (which are as well generated with the new processing strategy). However, the solutions with reprocessed gradients still perform better than their monthly equivalents based on old gradients over big parts of the spectrum (especially for June). Most probably, the impact of the new processing strategy does not show to advantage due to a significant larger number of flagged observations in the outlier detection procedure (see table 4 in section 12.2.2). (4) The monthly solution of October 2010 (cyan solid line) shows the biggest deviations to GOCO02S. This finding is consistent to the gravity anomalies of that month (see

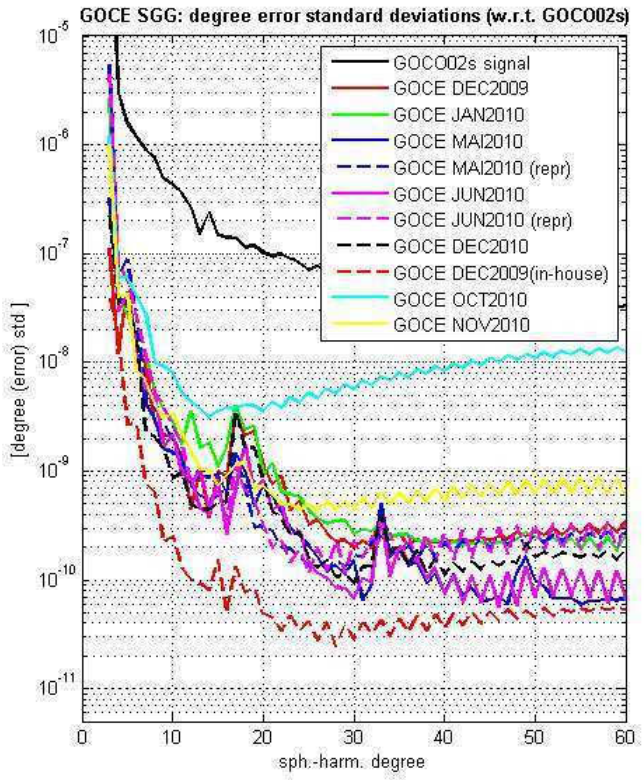

Figure 23: Degree standard deviations w.r.t GOCO02S of all monthly obtained GOCE SGG solutions

figure 39 on page 85), which show large error structures.

Conclusions (3) and (4) have to be modified when looking at the standard deviations without excluding coefficients affected by the polar gap (see figure 23):
(3) The monthly SGG solutions based on reprocessed gradients perform better than the corresponding solutions with old gradients over big parts of the spectrum, only, if coefficients affected by the polar gap are not considered. Probably, the polar gap issue is more severe in solutions based on reprocessed gradients due to less observations. (4) October and November 2010 are affected most by the polar gap issue, starting already at d/o 16 and d/o 25, respectively.

13.3 Combined gravity field solutions from GRACE and GOCE

In this section the investigated monthly combined gravity field solutions from GRACE SST-ll and GOCE SGG data are presented. Each combination has been performed (1) with weighting factors obtained by the variance component estimation (see section 12.3), and (2) with weights differing from the variance component estimation by up to 2 orders of magnitude. The test of different weights is necessary to cope with the fact, that the VCE only accounts for the stochastic error models of both involved normal equations (see section 12.3). It is checked whether better or worse results are achieved when continually augmenting or decreasing the relative weight (until the best result is found). The best result is defined in terms of the lowest global RMSE

value (eq. 57 on page 53) with respects to a smoothed GRACE-only solution (of the month to be investigated).
Generally, all combined solutions are compared to the corresponding GRACE-only solutions. A combined solution is considered improved (= less affected by the striping error) when the RMSE is smaller than the value of the GRACE-only solution. To validated the RMSE the solutions and their (coefficient) differences are also visualized spatially in terms of EWH. Additionally, the degree (error) median with respect to GOCO02S serves as third analysis method.

13.3.1 Monthly combined solutions

Table 10 shows the seven monthly combinations which have finally been conducted on the basis of the best available GOCE SGG gravity solutions. No combinations have been analyzed for the months March, October and November 2010 because of the poor quality of their SGG solutions (see section 13.2).

Month	gradient data set	$N_{max,GOCE}$
December 2009	old	180
	in-house	180
January 2010	old	180
May 2010	old	180
June 2010	old	180
	new	180
December 2010	old	180

Table 10: Monthly combined GRACE + GOCE SGG solutions, used gradient data sets and maximum degrees

Combined solutions of December 2009
In December 2009 combinations could be achieved using the old and the in-house SGG gradient data set. Appended tables 14 and 15 on page 90 show the results of the RMSE values (in terms of EWH) for all checked weights at different maximum degrees. The column at the very right gives the best achieved RMS improvement [in %] of the combined solution regarding the GRACE-only solution per degree for all weights. The values indicate that, at best, an improvement of 1% (at d/o 45) can be achieved with in-house gradients, and 0.6% with old gradients (at d/o 45). However, at all other degrees GOCE SGG data seems to corrupt the GRACE solution in combined solutions at the investigated weights, as the RMSE exceeds the one of the GRACE-only solution. The tables also show that continually down-weighting GOCE SGG normal equations reduces the RMSE values.

Combined solution of January 2010
In January 2010 the combinations on the basis of the old gradients indicate that there is hardly any improvement due to GOCE SGG data. Looking at the best achieved RMSE improvements (right column of table 16 on page 92) one finds that they are below 1 % for all degrees. The weights for which the best results are achieved are close to the weights estimated by the vari-

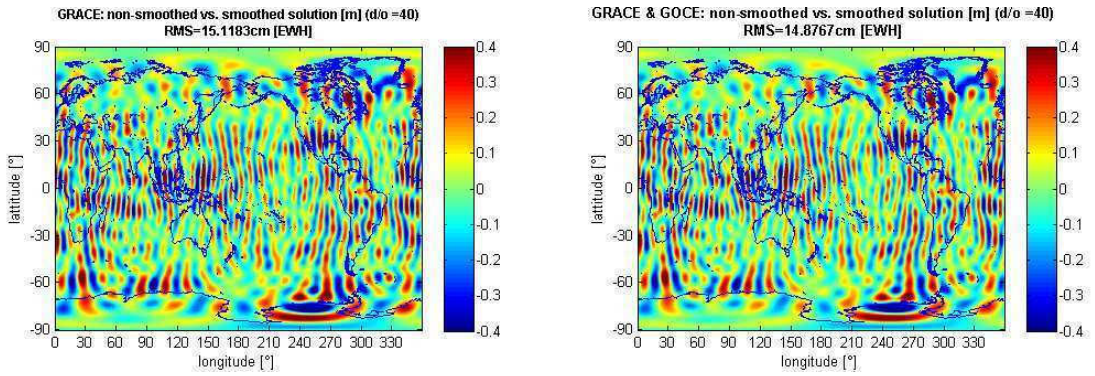

Figure 24: Comparison of a GRACE-only with the combined GRACE + GOCE SGG (new gradients) solution in terms of EWH [m] (at d/o **40**); a smoothed GRACE-only solution with filter radius r=500km has been subtracted from the solutions

ance component estimation (bold letters) for degrees 30 to 45. At higher degrees the GOCE SGG data seems to corrupt the combined solutions more severely, and the variance component estimation gives too much emphasis to GOCE SGG normal equations.

Combined solution of May 2010

Table 17 (right column) shows that old GOCE SGG gradients can, at best, improve the solution by less than 1 % in terms of the global RMSE value. The highest improvements can be achieved in high degrees (> d/o 50). The relative weights at which those values could be achieved indicate that GOCE SGG normal equations gained a too high weight in the variance component estimation.

Combined solutions of June 2010

For the month June 2010 combined solutions of GRACE with GOCE SGG solutions on the basis of old and of new (re-processed) gradients could be investigated. The results of the RMSE calculation in the combinations at different degrees and for different weights are shown in table 18 for old and in table 19 for new gradients (page 94). The weights from the variance component estimation (in bold letters) seem to reflect the optimum weighting between GOCE and GRACE normal equations quite well, especially for combinations including new gradients, looking at the computed RMSE values.

With old gradients improvement can be achieved above d/o 30, with a maximum of nearly 2% at d/o 45. With new gradients the RMSE improvement starts at d/o 30 with little improvement of almost 1% and reaches highest values between d/o 45 and d/o 60. Here, the RMSE value could be reduced by 4.5 - 7% due to a combination with GOCE SGG data. Figure 24 show the GRACE-only solution on the left and the combined GOCE+GRACE SGG solution (using the weights which showed best results) on the right in terms of equivalent water heights evaluated at to d/o 40. In this images the influence of SGG data is hardly visible. The differences of both solutions in figure 25 highlight the structure and the regional occurrence of the improvement. Figures 26 and 27 show the solutions and their differences evaluated at d/o 50.

The differences for d/o 40 show that the improvement really turns out to be in the structure of stripes. However, the grade of stripe reduction differs regionally (with maximum in the

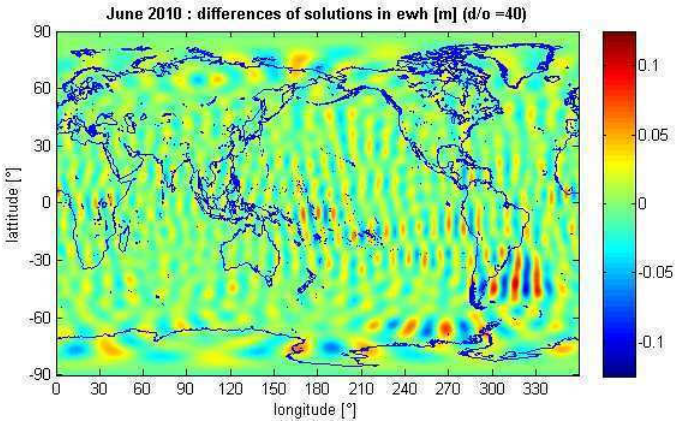

Figure 25: Difference of the GRACE-only and the combined GRACE + GOCE SGG (new gradients) solution in terms of EWH [m] (at d/o **40**)

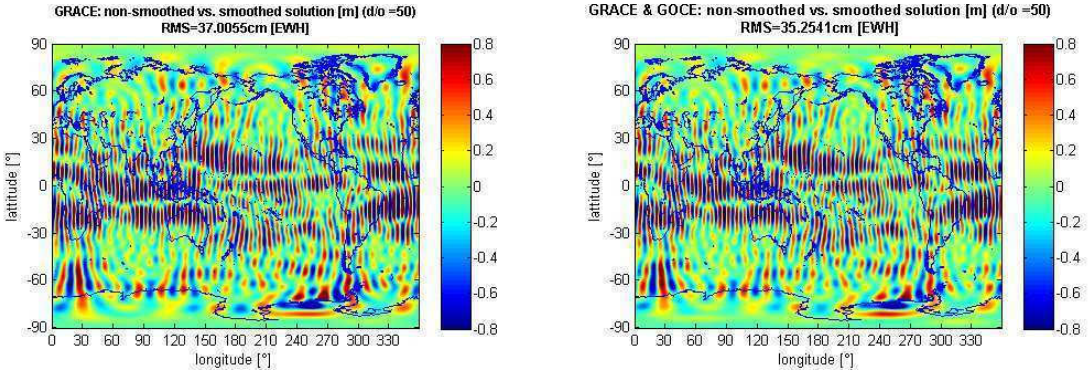

Figure 26: Comparison of a GRACE-only with the combined GRACE + GOCE SGG (new gradients) solution in terms of EWH [m] (at d/o **50**); a smoothed GRACE-only solution with filter radius r=500km has been subtracted from the solutions

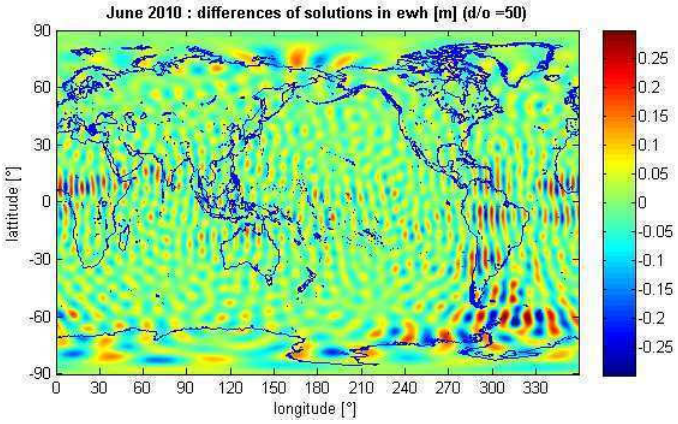

Figure 27: Difference of the GRACE-only and the combined GRACE + GOCE SGG (new gradients) solution in terms of EWH [m] (at d/o **50**)

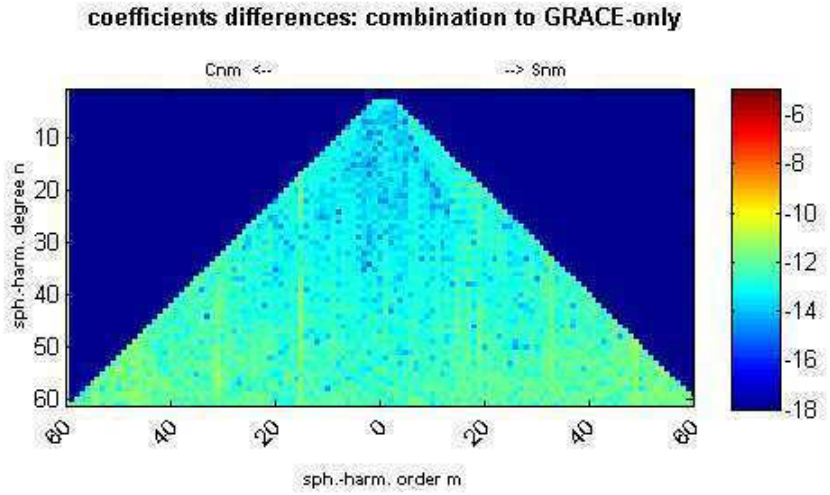

Figure 28: Coefficient differences between the GRACE-only and the combined GRACE + GOCE SGG (**old** gradients) solution

south-east of South America), and they hardly reach more than ± 5 *cm* amplitude. Considering the amplitude of the striping error in GRACE-only solutions at this degree (which is about ± 30 *cm*), this improvement appears rather low. Note that in the area of largest differences (South-America) the differences show stripes, where in the GRACE-only solution there are no stripes. Hence, this structure comes from the GOCE SGG solution and might be erroneous signal degrading the solution, rather than improving it. Looking at the differences of the GRACE-only and the GOCE SGG solution at d/o 50, one sees stripes over parts of Africa and South America. Those are areas, where the inclusion of GOCE SGG data leads to a reduction of the striping error. The oceans and other continents are covered by a more or less isotropic structure. There, GOCE SGG data does not lead to a positive impact but rather seems to distort the solution. This shows that the impact of GOCE SGG data is hardly at the edge to be degrading the solutions in large areas. The suspicion that there is also bad influence of GOCE SGG errors is substantiated also in the coefficient differences between the combined and the GRACE-only solution in figure 28 (with old gradients). The coefficient differences show that the SGG inherit spectral bands at the orders 16 and 32 that are related to the orbit repeat frequency alias into the solution. This is a clear sign for degradation regarding the pure GRACE solution. The spectral bands vanish when looking at differences to GRACE-only coefficients regarding a combined solution using new gradients in figure 29.

Combined solution of December 2010

The RMSE values for GRACE-only and for the combined GRACE + GOCE SGG (old gradients) solution of December 2010 are listed in appended table 20 on page 96. Best combinations - meaning the lowest RMSE values - can be achieved using the weights directly obtained by the variance component estimation for d/o 30 to d/o 45. Here including GOCE SGG leads to an improvements below 1% of the RMSE with respect to the pure GRACE-only solution. Above d/o 45 the weights from the variance component estimation are very close to the weights which bring the lowest RMSE value. In that spectral domain the combination gains by increasing the weight for GOCE normal equations. In that context the RMSE can be reduced by a maximum

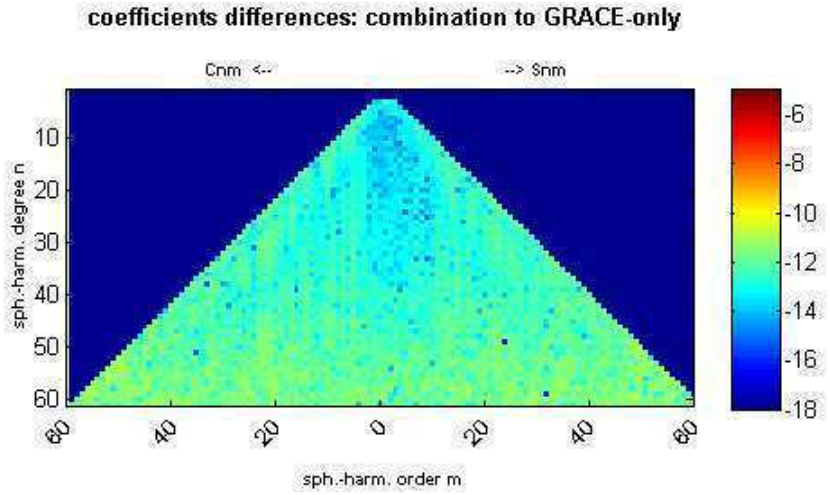

Figure 29: Coefficient differences between the GRACE-only and the combined GRACE + GOCE SGG (**new** gradients) solution

of 1.3%.

13.3.2 Bi-monthly combined solutions

Table 11 lists the four investigated bi-monthly gravity field combinations. In the following each of the combinations is analyzed.

Period	gradient data set	$N_{max,GOCE}$
November + December 2009	old	224
	in-house	224
May + June 2010	old	180
	new	180

Table 11: Bi-monthly combined GRACE + GOCE SGG solutions, used gradient data sets and maximum degrees

Combined solutions of November and December 2009
For the bi-monthly period November to December 2009 combinations with the old and the in-house gradients could be achieved. Appended tables 21 and 22 on page 97 show the obtained RMSE values (in terms of EWH) for all checked weights at different maximum degrees. The column at the very right gives the highest achieved RMS improvement [in %] of the combined solution with respect to the GRACE-only solution per degree for all weights. The combinations show that, independently of the used gradient data sets, the RMSE improvement does not exceed 2.4%. At most degrees the RMSE could be reduced by around 1% due to the impact of GOCE SGG data. At higher degrees (> d/o 40) the in-house gradient solutions seems to perform

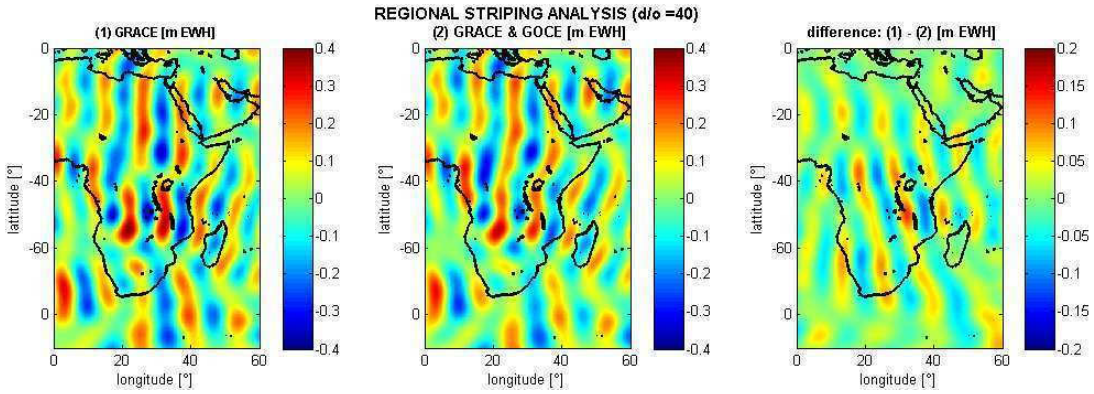

Figure 30: Differences between the GRACE-only and the combined GRACE + GOCE SGG (**new** gradients) solution of May and June 2010 at d/o 40

better than the one based on old gradients, but the contrary at lower degrees. Generally, the weights from the variance component estimation (in bold numbers) do not reflect the optimal combination, as GOCE normal equations tend to be down-weighted too much.

Combined solutions of May and June 2010

Regarding the combined solution for the period May and June 2010, significant differences between the combinations using old and new gradients can be observed. Appended tables 23 and 24 on page 99 show the RMSE values obtained by the solutions based on different weights at different degrees. While the maximum improvements of the RMSE at different degrees stays below 1 % using old gradients for the combination, the improvement is between 2 and 3 % for new gradients. However, in both cases the weights from the variance component estimation (in bold letters) are not consistent to the optimal weighting considering the (lowest) RMSE values per degree.

A lower RMSE value in the combination, however, does not necessarily mean a reduction of the stripes. In figure 30 the striping error in the GRACE-only and its alleged reduction in the combined solution is explored over a region covering the African continent. The image on the left shows the differences of the GRACE-only gravity solution to a smoothed GRACE-only solution in terms of meters EWH. In the middle the differences of the combined solution to the same smoothed GRACE-only solution are plotted. In some regions the striping error seems to be reduced, in others the striping seems to be more severe. The differences of the GRACE-only to the combined solution indicate that the impact of GOCE does not only affect or reduce the stripes, respectively. The right image shows that the differences between both solutions show a northwest-southeast structure and do not follow the north-south aligned structure of the stripes in the GRACE-only solution.

Part V
Conclusion

In this part of the thesis the results are summarized and the findings are formulated. Within the thesis in total seven combinations of GRACE SST and GOCE SGG normal equations on monthly basis and four on bi-monthly basis, all complete up to degree and order 60 of the spherical harmonic series, have been performed. GRACE SST normal equations could be acquired from the *Astronomical Institute at the University Bern* (AIUB). GOCE SGG normal equations were assembled using the software at the *Institute for Astronomical and Physical Geodesy* (IAPG), which is following the GOCE time-wise processing strategy (TIM). Computations were performed on the environment of the *Leibnitz Rechenzentrum* (LRZ) in Munich. For this purpose an outlier detection algorithm for GOCE gradients has been designed and implemented. In this context it could be studied up to which extent it is possible to derive monthly gravity field estimates only from GOCE gradiometer measurements. The combination of GOCE SGG and GRACE SST normal equations was conducted by means of variance covariance estimation. Further, it was systematically analyzed whether altering the weights from the variance component process can improve the impact of GOCE SGG in the combination. This allowed an evaluation of the performance of the variance component estimation. In order to investigate and evaluate the quality of the retrieved combinations, especially the extent of the stripes, a method based on the calculation of a global RMSE value has been implemented. The evaluation of the combinations was further based on the comparison to pure GRACE-only solutions in order to determine benefits evolving from GOCE SGG observations.
The joint analysis of all gathered monthly and bi-monhtly GRACE-ll and GOCE SGG gravity field solutions and their combinations could be summarized in 6 key conclusions:

- **Assembling of monthly and bi - monthly GOCE SGG normal equations**
  Using old gradients (EGG_NOM_2_ products before re-processing), seven out of the nine operational months in the year 2010 were solvable. Among those only two (June and December) show no erroneous structure at all in their gravity anomaly representations. Three months (January, May, November) show minor error structures, two months (March, October) show large errors. These errors could not be removed in the outlier detection procedure, as taking out more outliers led to an ill-conditioning of the whole system. Hence, retrieving gravity field estimates from GOCE gradiometer observations on monthly basis using the time-wise method is a difficult task. Stable systems with a resolution of <135 km half-wavelength (spherical-harmonic d/o >150) are only possible if enough observations are available during the month. The month February 2010 simply does not have sufficient observations (8 days) to deliver a solution. For the month April no usable gravity field solution could be computed although the amount of remaining observations after the outlier procedure (29 days) lies in the order of months where solutions could be achieved. The reason for this remains unclear.
  With the new gradients (re-processed EGG_NOM_2_ products according the new processing strategy) even less solutions were invertible. The new gradients are found to suffer occasionally from a problem in the xx- , zz- and xz- tensor components that leads to high values (>10 mEötvös) in filtered gravity gradient anomalies with respect to GOCO02S. Consequently, in the first half of 2010 solely solutions for the months January, May and June could be retrieved. The reason for this is that in comparison to old gradients far more outliers were detected. Due to the outliers and the filtering procedure, which is

inherent to the TIM method and leads to additional data loss due to the warm-up periods of the filters, up to 20% less observations were used for the gravity field estimation, than with old gradients. It has to be mentioned, that a more advanced outlier strategy (e.g. interpolating over small outliers) could downsize the problem that is related to the data loss during the warm-up periods. Because of the data loss, however, the benefits of the new processing strategy do not show advantage in all coefficients of the retrieved solutions (January, May, June). Near-zonal coefficients seem to be of poorer accuracy in the case of the new gradients. In contrast coefficients outside of the polar-gap affected wedge show a lower standard deviation than those derived from old gradients. The in-house data set, which comprises gradients originating from the new processing strategy, delivers the best gravity field estimates from GOCE SGG observations, because the amount of outliers is not augmented compared to old EGG_NOM gradients.
Regarding their quality and accuracy all GOCE SGG monthly and bi-monthly gravity field estimates are found to be far below their corresponding GRACE gravity field estimates up to d/o 60, which is consistent to the formal errors of both measurement types. This could be, e.g., proven by the degree standard deviations w.r.t GOCO02S. Apart from the in-house gradients, the best monthly GOCE SGG solutions show almost twice (1.5 for in-house) the error level of the worst GRACE monthly solution at d/o 60 in terms of degree standard deviations even when excluding the coefficients affected by the polar gap. Additionally, monthly GOCE SGG solutions are found to suffer from large scale north-south arranged error structures (with amplitude of $\pm 40cm$ geoid height) below degree and order 40. From this perspective, improvement of GRACE solutions in this spectral domain does not seem feasible.

- **Quality of monthly and bi-monthly GRACE SST-ll gravity field estimates**
  The analysis of 11 monthly and bi-monthly GRACE SST-ll solutions in the years 2009 and 2010 show that they differ regarding the severeness of the striping error which is inherent to the GRACE satellite-to-satellite along-track measurement system. Generally the striping error is less severe in bi-monthly solutions. This can be found by analyzing the global RMSE at different degrees. The average RMSE values over all degrees show that the striping is reduced by 26 up to 47 % for Mai and June, respectively, (and 31% for December 2009) regarding their bi-monthly equivalent.
  The 7-day sub-cycle of GRACE satellite in the months November and December 2009 does not degrade the quality of the gravity field estimate between d/o 12 and 45 according to a spectral analysis in terms of degree standard deviations and degree medians with respect to GOCO02S. However, the formal errors retrieved for both months in the estimation process indicates that the gravity field estimates loose quality regarding the other months below d/o 12 and from d/o 45 onwards. The months June and May are affected most by the erroneous striping pattern, given by their high RMSE and degree standard deviations.

- **Contributions of GOCE SGG observations to monthly and bi-monhtly GRACE gravity field estimates**
  GOCE SGG observations are found to contribute positively to monthly as well as to bi-monthly GRACE SST-ll gravity field solutions only marginally (if at all). A systematic analysis of 7 monthly and 4 bi-monthly combined GRACE SST - GOCE SGG gravity field estimates at different weightsshows that the reduction of the stripes hardly exceeds 1% in terms of a global RMSE evaluated at different degrees. An improvement in terms of a reduced RMSE value of maximum 2 - 7 % could only be observed for the monthly

solutions June 2010 with new gradients (1 - 2% with old gradients). This result is plausible as the GRACE solution of June is of poorest quality (compared to the other observed solutions), and a positive impact of GOCE gradiometer data in that month seems most likely. However, a spatial analysis shows that the reduced RMSE value in the combination is not directly linked to a reduction of the stripes. Wide areas seem to be distorted anisotropically, and the reduction of the stripes seems to be rather coincident. Further in an area south-east of South America stripes seem to be introduced into the solution by the gradiometer data.
The new reprocessing strategy is not showing advantage significantly in the combined solutions, even in combinations with the in-house gradients, which are found to deliver best GOCE SGG gravity estimates.

- **Analysis of water mass storage changes from combined GOCE SGG and GRACE SST-ll fields**
  Due to the fact that there is hardly any reduction of GRACE error evolving from a combination with GOCE SGG data, additional benefits cannot be expected for the regional analysis of water storage changes.

- **Assessment of the extent of the striping error**
  The extent of the striping error can be well assessed and quantified with the developed RMSE method. This was shown in the joint analysis of the GRACE-only solutions in terms of their degree standard deviations with respect to GOCO02S and their gravity anomaly representations. All three methods show consistency regarding the quality of the observed GRACE months.
  However, it turned out that little RMSE changes (<5%) do not necessarily mean a reduction of the striping error. In those cases a separate inspection of the striping error in spatial domain is suggested.

- **Evaluation of the variance component estimation**
  The variance component estimation is found to not necessarily giving the optimum weighting factors for a combination of GRACE SST-ll and GOCE SSG monthly and bi-monthly normal equations. In some cases the global RMSE values indicate that the (striping) error in combined gravity field solutions is lower when using weights which slightly differing from those of the variance component estimation. This may be due to the fact that a variance component estimation only takes into account the stochastic error behavior of both measurement types. The error which is inherent to the GRACE monthly and bi-monthly estimates in contrast comprises highly systematic (stripes) parts. In the same way GOCE SGG solutions up to d/o 180 suffer of an (less severe) systematic error due to truncation of the series expansion and the resulting underparametrization of the gravity signal.

Part VI

Outlook

In contrast to the finding, that it is not worth to combine GOCE gradiometer information, solely, with GRACE monthly and bi-monthly gravity field estimates, there are benefits when GOCE SST-hl observations are used at the same time. During the research it could be shown in tests with a bi-monthly GRACE solution (November + December 2009) that the inclusion of GOCE SGG together with GOCE SST-hl leads to a significant reduction of the stripes. The results of the tests validate the findings of the study by Pail et al. (2011b), and indicate that there might be a significant reduction of the stripes even above d/o 45. This reinforces the suspicion that GOCE satellite can serve as a valuable additional information source, in order to improve the knowledge about changes in the Earth's gravity field.
However, there are many remaining questions, especially regarding the benefits of such a combination. Today, it has been shown that there are positive contributions of GOCE in a bi-monthly combination, but there has been no systematic study examining whether similar results can be achieved for other bi-monthly periods and for monthly periods. In their investigations Pail et al. (2011b) mention that it is possible to find the same results in monthly combinations but deliver no analysis. More on monthly combinations will be found in the proceedings of the 2012 IAG Symposium in Venice (Springer), which will be published soon.
An analysis of the benefits of the combination with both GOCE observation types for one of the most prominent GRACE applications, the determination of terrestrial water storage changes (TWSC), is missing as well. For example it would be interesting to investigate whether smoothing and filtering procedures can be reduced to some extent due to the observed stabilization by GOCE observations, and whether, in consequence, hydrological signals (or other geophysical signals) can be better separated out.

Part VII

Annex

Acknowledgments

I want to thank my supervisor Prof. Roland Pail for the advise and continuous support throughout the thesis. My thanks are as well dedicated to the staff-members at IAPG who contributed to this work in terms of literature and advice on the Linux-Cluster. Especially I acknowledge the help of Thomas Fecher who helped me a lot to get familiar with the IAPG gravity processing software.

The author further acknowledges the European Space Agency for the provision of the GOCE data. Almost all of the computations were performed at the Leibniz-Rechenzentrum (LRZ) of the Bavarian Academy of Sciences.

Abbreviations

AIUB - Astronomical Institute, University Bern

CHAMP - Challenging Microsatellite Payload

CMF - Calibration and Monitoring Facility

DIR - Direct Method

DLR - Deutsches Zentrum für Luft und Raumfahrt

ECMWF - European Center for Medium Range Weather Forecast

EFRF - Earth Fixed Reference Frame

ESA - European Space Agency

EWH - Equivalent Water Heights

GFZ - Deutsches GeoForschungsZentrum

GG - Gravity Gradient

GLDAS - Global Land Data Assimilation Center

GOCE - Gravity field and steady-state Ocean Circulation Explorer

GPS - Global Positioning System

GRACE - Gravity Recovery and Climate Experiment

GRF - Gradiometer Reference Frame

HPF - High-level Processing Facility

IAG - International Association of Geodesy

IAPG - Institute for Astronomical and Physical Geodesy

ICGEM - International Center for Global Earth Models

IERS - International Earth Rotation Service

IRF - Inertial Reference Frame

ITRF - International Reference Frame

JPL - Jet Propulsion Laboratory

LaD - Land Dynamics Model

LAGEOS - Laser Geodynamic Satellite

LRZ - Leibniz Rechenzentrum (Leibniz Supercomputing Centre)

NASA - National Aeronautics and Space Administration

OMCT - Ocean Model for Circulation and Tides

PDS - Payload Data System

RMSE - Root Mean Square Error

PSO - Precise Science Orbit

SGG - Satellite Gravity Gradiometer

SLR - Satellite Laser Ranging

SPW - Space-Wise Method

SST - Satellite-to-Satellite Tracking

SST-hl - Satellite-to-Satellite Tracking in high-low mode

SST-ll - Satellite-to-Satellite Tracking in low-low mode

TIM - Time-Wise Method

TUM - Technische Universität München

TWSC - Terrestrial Water Storage Changes

VCE - Variance Component Estimation

WGHM - Water Gap Hydrology Model

References

J. Bouman. Quick-look outlier detection for GOCE gravity gradients. Technical report, SRON National Institute for Space Research, 2004.

J. Bouman, M. Kern, R. Koop, R. Pail, R. Haagmans, and T. Preimesberger. Comparison of outlier detection algorithms for GOCE gravity gradients. In C. Jekeli, L. Bastos, and J. Fernandes, editors, *Gravity, Geoid and Space Missions (GGSM 2004), IAG Symposia*, volume 129, pages 83–88. Springer, 01 2005. ISBN 978-3-540-26930-4. doi: 10.1007/3-540-26932-0_15.

S. Bruinsma, J. Marty, G. Balmino, R. Biancale, C. Förste, O. Abrikosov, and H. Neumayer. GOCE gravity field recovery by means of the direct numerical method. In H. Lacoste-Francis, editor, *Proceedings of the ESA living planet symposium*. ESA Publication SP-686, 2010.

J. Chen, C. Wilson, B. Tapley, and S. Grand. GRACE detects coseismic and postseismic deformation from the sumatra-andaman earthquake. *Geophysical Research Letters*, 34, 2007.

ESA. Gravity field and steady-state ocean circulation mission. Report for the mission selection of the four candiate earth explorer missions, ESA, 1999.

F. Flechtner. AOD1B product description document for releases 01 and 04. Technical report, GeoForschungsZentrum Potsdam, 2007.

T. Gruber. Globale Schwerefeldmodellierung und Anwendungen, Aktuelle Satellitenmissionen, 2011. Skriptum.

T. Gruber and F. Flechtner. Vereinfachte Darstellung der GRACE Datananalyse. Technical report, DFG Schwerpunktprogramm 1257, 2007.

T. Gruber, R. Rummel, O. Abrikosov, and R. van Hees. GOCE Level 2 product data handbook. Technical Report GO-MA-HPF-GS-0110, EGG-C, 2009. V4.1.

T. Gruber, P. N. A. M. Visser, C. Ackermann, and M. Hosse. Validation of GOCE gravity field models by means of orbit residuals and geoid comparisons. *Journal of Geodesy*, 85(11): 845–860, 10 2011. ISSN 0949-7714. doi: 10.1007/s00190-011-0486-7. Special issue: "GOCE - The Gravity and Steady-state Ocean Circulation Explorer".

A. Güntner. Improvement of Global Hydrological Models Using GRACE Data. *Surveys in Geophysics*, 29:375–397, October 2008. doi: 10.1007/s10712-008-9038-y.

S.C. Han, C.K. Shum, M. Bevis, C. Ji, and Y. Kuo. Crustal dilattation observed by GRACE after the 2004 sumatra-andaman earthquake. *Science*, 313:658–662, 2006.

W.A. Heiskanen and H. Moritz. *Physical Geodesy*. WH Freeman Comp, 1967.

B. Hofmann-Wellenhof and H. Moritz. *Physical Geodesy*. Springer Wien New York, 2nd edition, 2006.

A. Jäggi, G. Beutler, L. Prange, and R. Dach. Assessment of GPS-only observables for gravity field recovery from grace. In M.G. Sideris, editor, *Observing our Changing Earth*, pages 113–120. Springer, Heidelberg, 2009.

A. Jäggi, G. Beutler, and L. Mervart. GRACE Gravity field determination using the celestial mechanics approach - first results. *Gravity, Geoid and Earth Observations, IAG Symposia*, 135:177–184, 2010.

C. Jekeli. Alternative methods to smooth the earth's gravity field. Technical report, Department of Geod. Science and Surveilling, Ohio State University, 1981.

M. Kern, T. Preimesberger, M. Allesch, R. Pail, J. Bouman, and R. Koop. Outlier detection algorithms and their performance in GOCE gravity field processing. *Journal of Geodesy*, 78: 509–519, 2005. ISSN 0949-7714. URL `http://dx.doi.org/10.1007/s00190-004-0419-9`. 10.1007/s00190-004-0419-9.

K.-R. Koch and J. Kusche. Regularization of geopotential determination from satellite data by variance components. *Journal of Geodesy*, 76:259–268, 2002.

R. Koop and Th. Gruber. Product specification for level-2 products and auxiliary data products. Technical Report GP-ID-HPF-GS-0041, EGG-C, 2009. V6.1.

T. Mayer-Gürr and E. Kurtenbach. ITG-Grace2010 Gravity Field Model. Technical report, www.igg.uni-bonn.de/apmg/index.php?id=itg-grace2010, 2010.

B. Metzler and R. Pail. GOCE data processing: the spherical cap regularization approach. *Studia Geophysica et Geodaetica*, 49(4):441–462, 01 2005. ISSN 0039-3169. doi: 10.1007/s11200-005-0021-5.

F. Migliaccio, M. Reguzzoni, F. Sanso, C. Tscherning, and M. Veicherts. GOCE data analysis: the space-wise method approach and the first space-wise gravity field model. In *Proc. of the ESA Living Planet Symposium, Bergen (Norway)*, 2010.

R. Pail. Parameterschätzung, 2004. Skriptum.

R. Pail, W.-D. Schuh, and M. Wermuth. GOCE gravity field processing. *Gravity, Geoid and Space Missions, IAG Symposia*, 129:36–41, 2005.

R. Pail, H. Goiginger, R. Mayrhofer, W.-D. Schuh, J.-M. Brockmann, I. Krasbutter, E. H¨ ock, and T. Fecher. GOCE gravity field model derived from orbit and gradiometry data applying the time-wise method. *Proc. ESA Living Planet Symposium*, 28. June - 2. July, 2010.

R. Pail, S. Bruinsma, F. Migliaccio, C. Förste, H. Goiginger, W.-D. Schuh, E. Höck, M. Reguzzoni, J. M. Brockmann, O. Abrikosov, M. Veicherts, T. Fecher, R. Mayrhofer, I. Krasbutter, F. Sanso, and C. C. Tscherning. First GOCE gravity field models derived by three different approaches. *Journal of Geodesy*, 85(11):819–843, 10 2011a. ISSN 0949-7714. doi: 10.1007/s00190-011-0467-x. Special issue: "GOCE - The Gravity and Steady-state Ocean Circulation Explorer".

R. Pail, T. Fecher, A. Jäggi, and H. Goiginger. Can GOCE help to improve temporal gravity field estimates? In L. Ouwehand, editor, *Proceedings of the 4th International GOCE User Workshop*. ESA Publication SP-696, 2011b.

R. Pail, T. Fecher, and M. Rexer. Impact of GOCE L1b data reprocessing on GOCE-only and combined gravity field models. In *Studia Geophysica & Geodaetica*. tbd, 2012.

T. Peters. *Modellierung zeitlicher Schwerevariationen und ihre Erfassung mit Methoden der Satellitengravimetrie*. PhD thesis, Technische Universität München, 2007.

T. Peters, J. Müller, and N. Sneeuw. Temporal variations in the earth's gravity field. *Deutsche Geodätische Kommission*, A118:133–140, 2001.

G. Petit and B. Luzum, editors. *IERS Conventions (2010)*, number 36 in IERS Technical Note, 2010. IERS Conventions Centre, Verlag des Bundesamtes für Kartographie und Geodäsie, Frankfurt am Main.

L. Prange. *Global Gravity Field Determination Using the GPS Measurements Made Onboard the Low Earth Orbiting Satellite CHAMP*. PhD thesis, ETH Zürich, 2010.

C. Reiberger, H. Jochmann, J. Wünsch, S. Pretrovic, P. Schwintzer, F. Barthelmes, K.-H. Neumayer, R. König, C. Förste, G. Balmino, R. Biancale, J.-M. Lemione, S. Loyer, and F. Perosanz. Earth gravity field and seasonal variability from CHAMP. In C. Reiberger, editor, *Earth Observation from CHAMP: Results from Three Years in Orbit*, pages 25–30. Springer, Berlin, Heidelberg, 2005.

N. Sneeuw. *A semi-analytical approach to gravity field analysis from satellite observations*. PhD thesis, TU Munich, DGK, 2000. DKG C 521.

N. Sneeuw and M. Gelderen. The polar gap. in: Geodetic boundary value problems in view of the one centimeter geoid. *Lecture Notes in Earth Science*, 65:559–568, 1997.

N. Sneeuw, C. Gerlach, L. Földvary, T. Gruber, T. Peters, R. Rummel, and D. Svehla. One year of time-variable CHAMP-only gravity field models using kinematic orbits. In F. Sanso, editor, *A Window on the Future of Geodesy, IAG Symposia*, volume 128, pages 288–293. Springer, 06 2005. ISBN 978-3-540-24055-6. doi: 10.1007/3-540-27432-4_49.

M. Stetter. Stochastische Modellierung von GOCE Gradiometriebeobachtungen mittels digitaler Filter. Master's thesis, Techische Universität München, 2012.

C. Stummer, R. Pail, and T. Fecher. Alternative method for angular rate determination within the GOCE gradiometer processing. *Journal of Geodesy*, Vol. 85 (9):585–596, 2011.

C. Stummer, C. Siemes, R. Pail, B. Frommknecht, and R. Floberghagen. Upgrade of the GOCE level 1b gradiometer processor. *Advances in Space Research*, 49 (4):739–752, 2012.

A.N. Tikhonov. On the solution of ill-posed problems and the morthod of regularization. *Doklay Akademii Nauk SSSR*, 151:501–504, 1963.

W. Torge. *Geodäsie*. Walter de Gruyter, Berlin, 2003.

J. Wahr. Time-variable gravity from satellites. *Treatise on Geophysics*, 3:213–237, 2007.

J. Wahr and Molenaar M. Time variability of the earth's gravity field: Hydrological and oceanic effects and their possible detection using GRACE. *Journal of Geophysical Research*, 103 (B12): 30205 – 30229, 1998.

S. Werth, A. Güntner, R. Schmidt, and J. Kusche. Evaluation of GRACE filter tools from a hydrological perspective. *Geophysical Journal International*, 179/3:1499 – 1515, 2009.

W. Yi. *The Earth's gravity field from GOCE*. PhD thesis, Technische Universität München, 2011.

List of Figures

1 Scheme of GOCE gradiometer with 6 accelerometers and the axes defined in the Gradiometer Reference Frame . . . 26
2 Sph.h. coefficients affected by the order dependent Kaula regularization . . . 31
3 Architectural design and data flow of the time-wise software package at IAPG . . 33
4 Schematic illustration of the parameter elimination procedure . . . 36
5 Overall processing scheme for the combination of GRACE and GOCE data . . . 40
6 Schematic illustration for re-ordering of GRACE least-square parameters . . . 41
7 Major outlier in V_{zz} component of gradient anomalies of March (2010) . . . 43
8 Filtered gradient anomalies with **old** gradients: $\Delta\frac{\partial^2}{\partial s^2}V_{xx}$ . . . 45
9 Filtered gradient anomalies with **old** gradients: $\Delta\frac{\partial^2}{\partial s^2}V_{yy}$ . . . 45
10 Filtered gradient anomalies with **old** gradients: $\Delta\frac{\partial^2}{\partial s^2}V_{zz}$ . . . 46
11 Filtered gradient anomalies with **old** gradients:$\Delta\frac{\partial^2}{\partial s^2}V_{xz}$ . . . 46
12 Trace of filtered gradient anomalies for **old** gradients . . . 46
13 Trace of filtered gradient anomalies for **new** gradients . . . 47
14 Parameter elimination: degree error median of full and eliminated solution (January 2010) . . . 50
15 Parameter elimination: degree (error) variances of full and eliminated solution (January 2010) . . . 50
16 Convergence of variance component estimation for all monthly solutions . . . 52
17 Equivalent water heights of GRACE monthly solution (filtered, unfiltered, differenced) . . . 54
18 Degree standard deviation of monthly GRACE solutions . . . 55
19 Degree standard deviation of bi-monthly GRACE solutions regrading GOCO02S 56
20 Formal errors of investigated monthly GRACE solutions . . . 58
21 GOCE SGG geoid differences over Australia to GOCO02s for June 2010 . . . 59
22 Degree standard deviations of monthly GOCE SGG solutions (polar gab excluded) 60
23 Degree standard deviations of monthly GOCE SGG solutions . . . 61
24 Comparison of a GRACE-only with the combined (new gradients) solution in terms of EWH at d/o 40 . . . 63
25 Difference of the GRACE-only and the combined (new gradients) solution in terms of EWH at d/o 40 . . . 64
26 Comparison of a GRACE-only with the combined (new gradients) solution in terms of EWH at d/o 50 . . . 64
27 Difference of the GRACE-only and the combined (new gradients) solution in terms of EWH at d/o 50 . . . 64
28 Coefficient differences between the GRACE-only and the combined GRACE + GOCE SGG (**old** gradients) solution . . . 65
29 Coefficient differences between the GRACE-only and the combined GRACE + GOCE SGG (**new** gradients) solution . . . 66
30 Differences between the GRACE-only and the combined GRACE + GOCE SGG (**new** gradients) solution of May and June 2010 at d/o 40 . . . 67
31 GRACE gravity anomalies November and December 2009 in $[\frac{m}{s2}]$ . . . 81
32 GRACE gravity anomalies January to June 2010 in $[\frac{m}{s2}]$ . . . 82
33 GRACE gravity anomalies October to December 2010 in $[\frac{m}{s2}]$ . . . 82

34 GRACE (bi-monthly) gravity anomalies November+December 2009 and May+June 2010 in $[\frac{m}{s2}]$ 83
35 January 2010 - GOCE SGG-only gravity anomaly differences and coefficient differences to GOCO02s 83
36 March 2010 - GOCE SGG-only gravity anomaly differences and coefficient differences to GOCO02s 84
37 May 2010 - GOCE SGG-only gravity anomaly differences and coefficient differences to GOCO02s 84
38 June 2010 - GOCE SGG-only gravity anomaly differences and coefficient differences to GOCO02s 85
39 October 2010 - GOCE SGG-only gravity anomaly differences and coefficient differences to GOCO02s 85
40 November 2010 - GOCE SGG-only gravity anomaly differences and coefficient differences to GOCO02s 86
41 December 2010 - GOCE SGG-only gravity anomaly differences and coefficient differences to GOCO02s 86

List of Tables

1 Temporal gravity variations and their characteristics (Peters, 2007) (modified) . 13
2 ESA data products needed by the time-wise processing software at IAPG 32
3 Monthly (2010) outlier statistics for (**old**) GOCE gravity gradients 44
4 Monthly (2010) outlier statistics for reprocessed (**new**) GOCE gravity gradients 44
5 Maximum degree of monthly GOCE gravity field estimates for 2010 48
6 Maximum degree of bi-monthly GOCE gravity field estimates of 2009 and 2010 . 48
7 Memory demand for the normal equation matrix at different degrees 49
8 Solvable monthly GOCE SGG solutions (x) for different gradient data sets 49
9 Global RMSE values (cm EWH) of selected monthly and bi-monthly GRACE-only solutions 57
10 Monthly combined GRACE + GOCE SGG solutions 62
11 Bi-monthly combined GRACE + GOCE SGG solutions 66
12 Results of the variance component estimation with *old* gradients 88
13 Results of the variance component estimation with *new* gradients 89
14 December 2009: RMSE for combined gravity field solution 90
15 December 2009 (in-house): RMSE for combined gravity field solution 91
16 January 2010: RMSE for combined gravity field solution 92
17 May 2010: RMSE for combined gravity field solution 93
18 June 2010: RMSE for combined gravity field solution 94
19 June 2010 (repr): RMSE for combined gravity field solution 95
20 December 2010: RMSE for combined gravity field solution 96
21 November+ December 2009: RMSE for combined gravity field solution 97
22 November+ December 2009 (in-house): RMSE for combined gravity field solution 98
23 May + June 2010: RMSE for combined gravity field solution 99
24 May + June 2010 (repr): RMSE for combined gravity field solution 100

Appended Figures

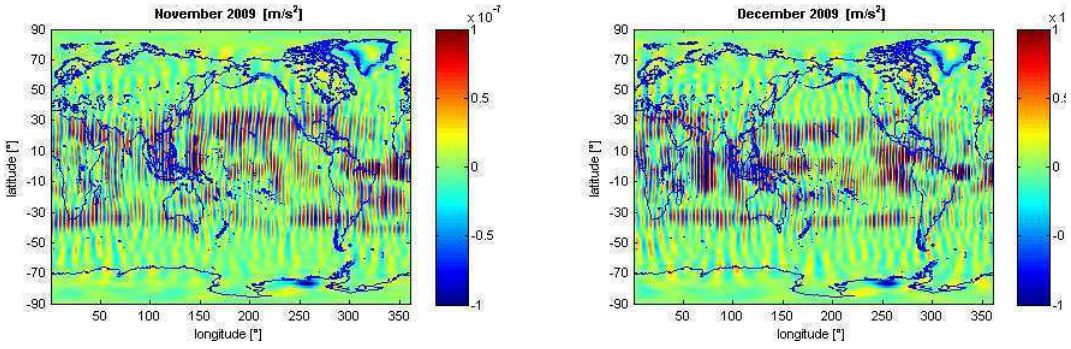

Figure 31: GRACE gravity anomalies November and December 2009 in $[\frac{m}{s2}]$

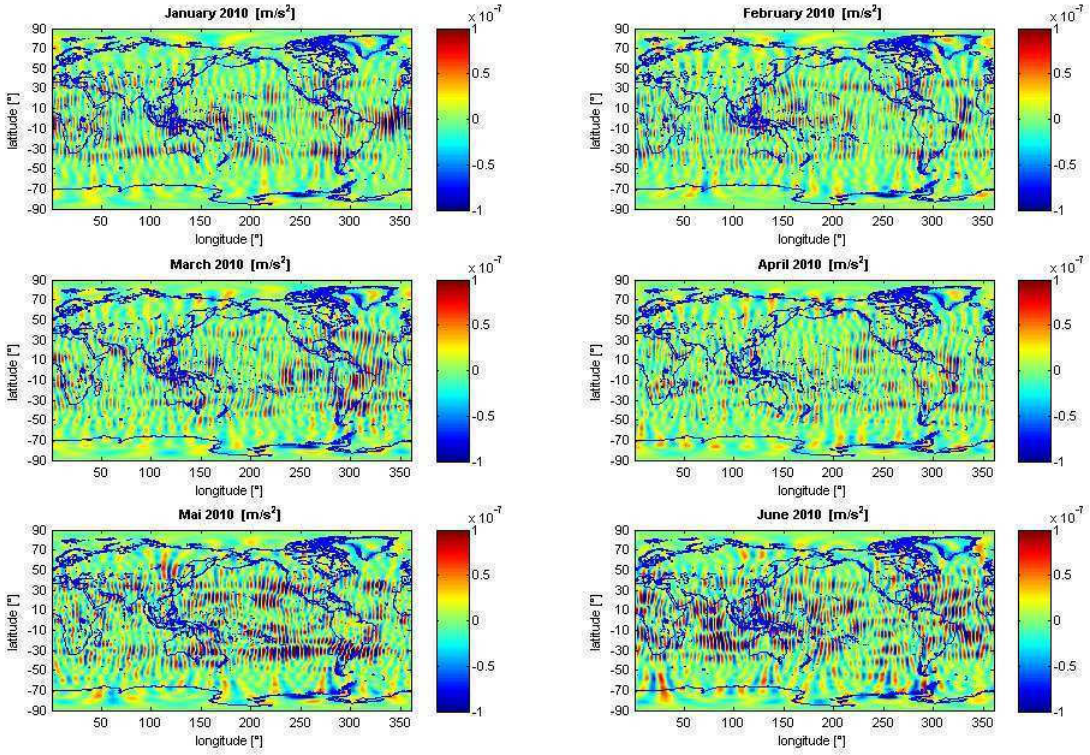

Figure 32: GRACE gravity anomalies January to June 2010 in $[\frac{m}{s2}]$

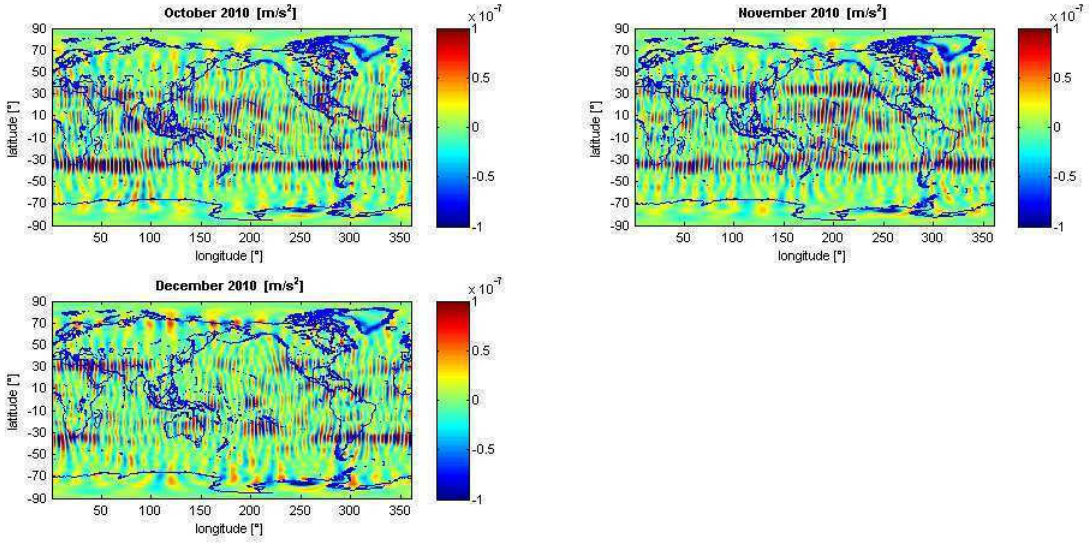

Figure 33: GRACE gravity anomalies October to December 2010 in $[\frac{m}{s2}]$

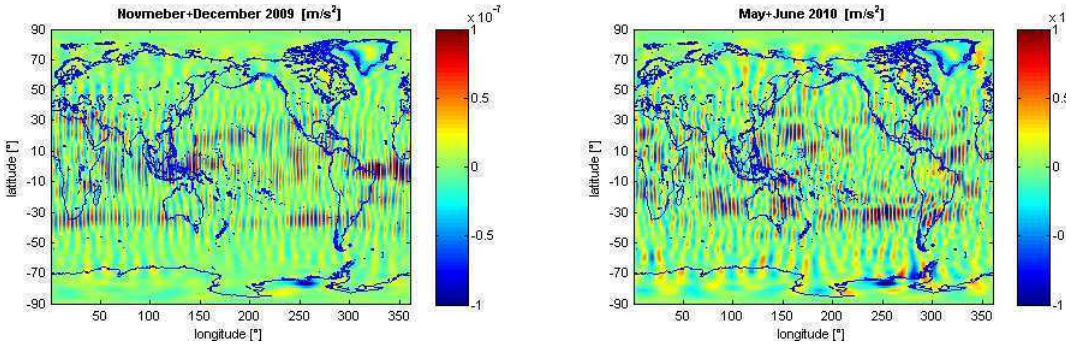

Figure 34: GRACE (bi-monthly) gravity anomalies November+December 2009 and May+June 2010 in $[\frac{m}{s2}]$

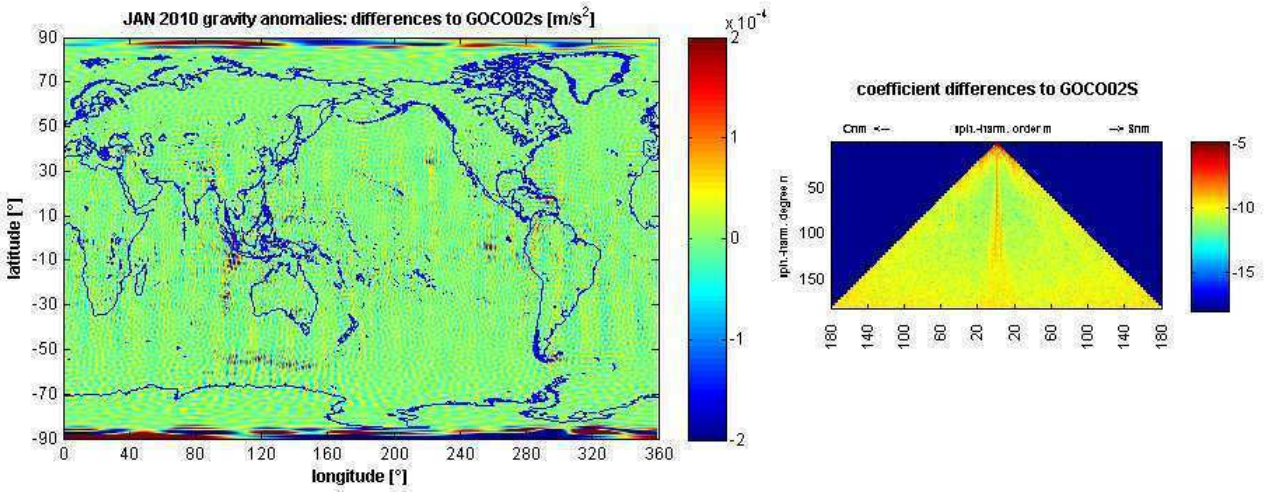

Figure 35: January 2010
GOCE SGG-only gravity anomaly differences and coefficient differences to GOCO02s (coefficients below spherical harmonic degree 20 are excluded from the visualization)

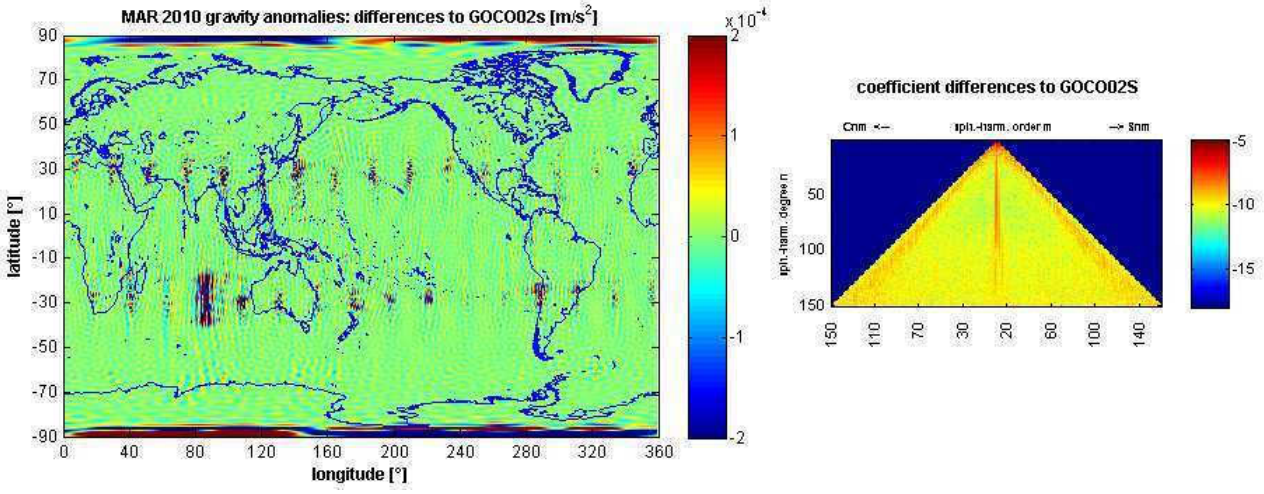

Figure 36: March 2010
GOCE SGG-only gravity anomaly differences and coefficient differences to GOCO02s (coefficients below spherical harmonic degree 20 are excluded from the visualization)

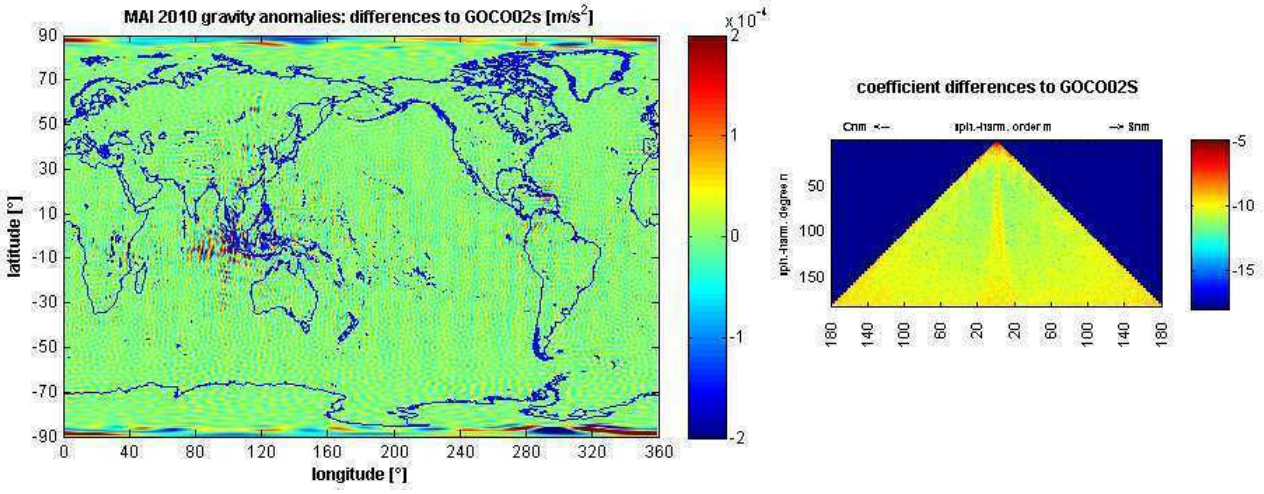

Figure 37: May 2010
GOCE SGG-only gravity anomaly differences and coefficient differences to GOCO02s (coefficients below spherical harmonic degree 20 are excluded from the visualization)

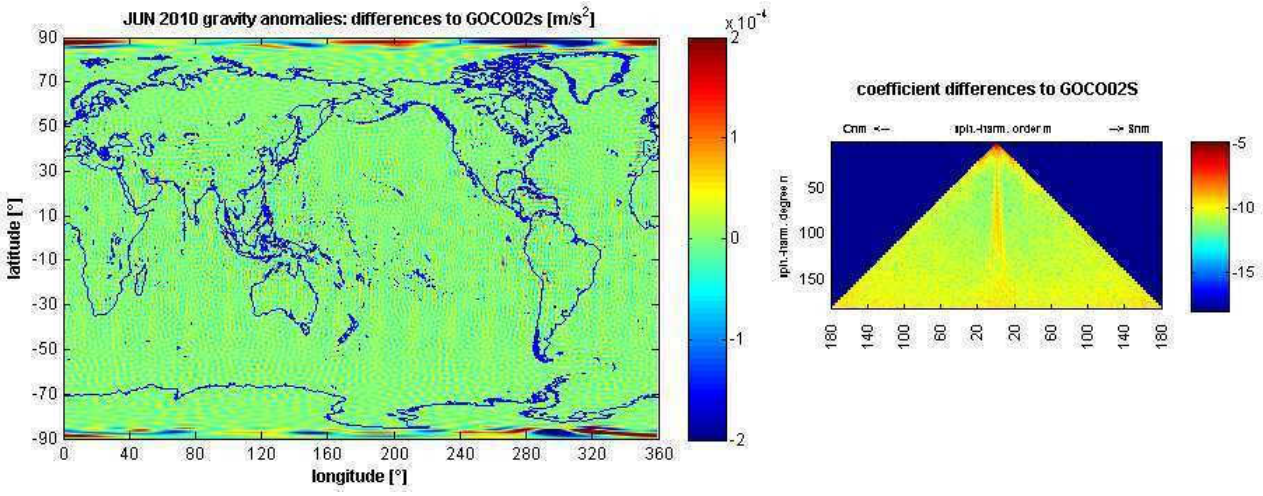

Figure 38: June 2010
GOCE SGG-only gravity anomaly differences and coefficient differences to GOCO02s (coefficients below spherical harmonic degree 20 are excluded from the visualization)

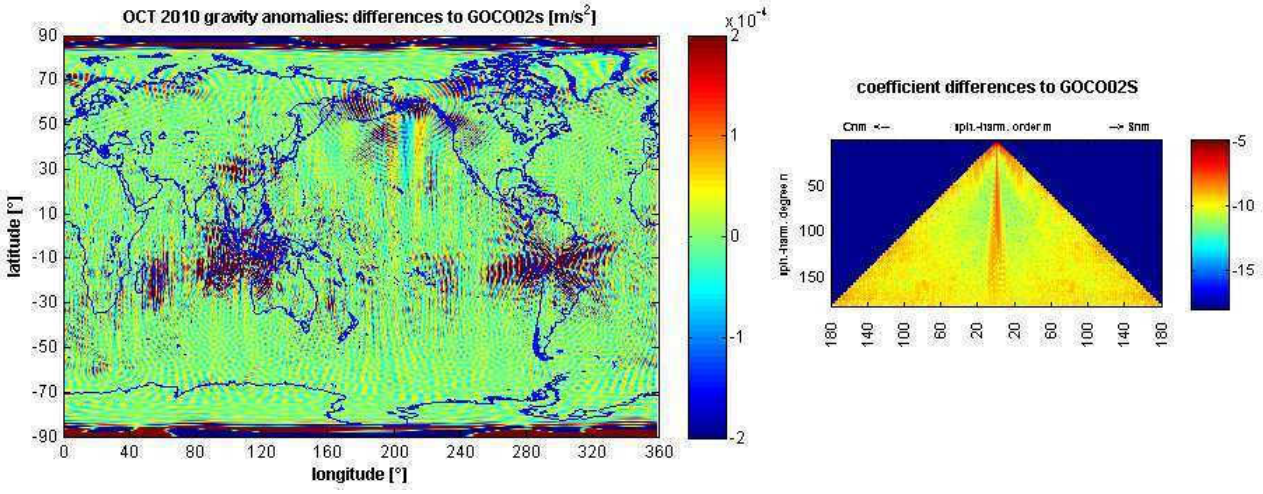

Figure 39: October 2010
GOCE SGG-only gravity anomaly differences and coefficient differences to GOCO02s (coefficients below spherical harmonic degree 20 are excluded from the visualization)

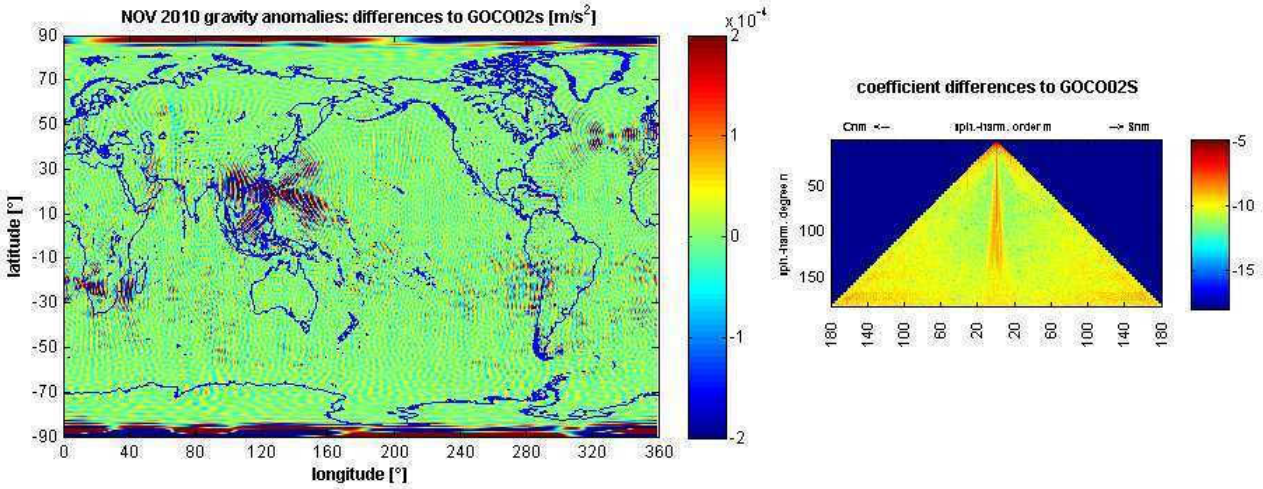

Figure 40: November 2010
GOCE SGG-only gravity anomaly differences and coefficient differences to GOCO02s (coefficients below spherical harmonic degree 20 are excluded from the visualization)

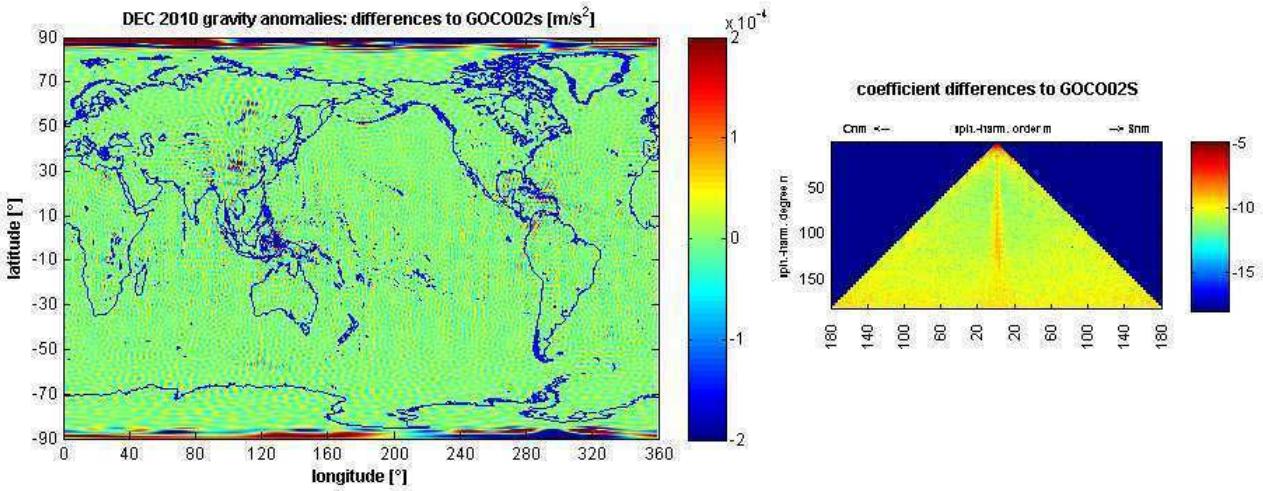

Figure 41: December 2010
GOCE SGG-only gravity anomaly differences and coefficient differences to GOCO02s (coefficients below spherical harmonic degree 20 are excluded from the visualization)

Appended Tables

Table 12: Results of the variance component estimation for every iteration and final weight factors for all monthly and bi-monthly combinations with *old* gradients (corrected for initial scaling difference of 5.00E-012)

	Iteration	1	2	3	4	5	Final Weight Factor (1/σ^2)
DEC_2009	GRACE: σ^2	1.000000000000000	0.021745596435324	1.003672531562230	0.999999981965954	1.000000000000090	45,818054588898
	GOCE:σ^2	1.000000000000000	26.559299498324500	0.998608858759751	1.000000006644310	0.999999999999968	0,037704046849
	($\sigma_{GRACE}^2 / \sigma_{GOCE}^2$)	1.000000000000000	0.000818756399682	0.994954855649385	0.999999975321644	1.000000000000120	**0,000822908069**
JAN_2010	GRACE: σ^2	1.000000000000000	0.021049170643614	1.001523057219580	0.999999609667400	1.000000000074090	47,435581454804
	GOCE:σ^2	1.000000000000000	0.197032050914544	0.998577558547815	1.000000168120710	0.999999999968088	5,082545173223
	($\sigma_{GRACE}^2 / \sigma_{GOCE}^2$)	1.000000000000000	0.106831201045273	0.997058980668960	0.999999441546784	1.000000000106000	**0,107146260620**
MAI_2010	GRACE: σ^2	1.000000000000000	0.021950282521916	1.002537815651100	0.999999424365063	1.000000000114770	45,442202469215
	GOCE:σ^2	1.000000000000000	0.563019685771650	0.998465086630489	1.000000234637260	0.999999999953219	1,778866819952
	($\sigma_{GRACE}^2 / \sigma_{GOCE}^2$)	1.000000000000000	0.038986705219430	0.995937580650795	0.999999189727993	1.000000000161550	**0,039145699885**
JUN_2010	GRACE: σ^2	1.000000000000000	0.022474252899928	1.002718449111730	0.999999033139315	1.000000000302570	44,374773621992
	GOCE:σ^2	1.000000000000000	0.563019685771650	0.998627933916078	1.000000310527000	0.999999999902823	1,778576603422
	($\sigma_{GRACE}^2 / \sigma_{GOCE}^2$)	1.000000000000000	0.039917348305727	0.995920574514934	0.999998722612712	1.000000000399750	**0,040080803985**
DEC_2010	GRACE: σ^2	1.000000000000000	0.022347708542404	1.003181647542420	0.999999871587543	1.000000000004640	44,605404144345
	GOCE:σ^2	1.000000000000000	5.584799077496500	0.998511664315751	1.000000039632860	0.999999999998569	0,179324358950
	($\sigma_{GRACE}^2 / \sigma_{GOCE}^2$)	1.000000000000000	0.004001524178811	0.995344827890234	0.999999831954690	1.000000000006070	**0,004020238408**
NOV DEC 2009	GRACE: σ^2	1.000000000000000	0.021641940122337	1.000840251670920	0.999999999453701	1.000000000000000	46,167785727943
	GOCE:σ^2	1.000000000000000	66.980037477493000	0.999288551081795	1.000000000210240	1.000000000000000	0,014940450811
	($\sigma_{GRACE}^2 / \sigma_{GOCE}^2$)	1.000000000000000	0.000323110301776	0.998449602135271	0.999999999243461	1.000000000000000	**0,000323612029**
MAI JUN 2010	GRACE: σ^2	1.000000000000000	0.022191001685428	1.000753832558870	0.999999921145330	1.000000000005670	45,029369481883
	GOCE:σ^2	1.000000000000000	0.924987195569115	0.999256946943371	1.000000028635360	0.999999999997942	1,081899924382
	($\sigma_{GRACE}^2 / \sigma_{GOCE}^2$)	1.000000000000000	0.023990604185363	0.998504241935630	0.999999892509973	1.000000000007730	**0,024026539497**

Table 13: Results of the variance component estimation for every iteration and final weight factors for all monthly and bi-monthly combinations with *new* gradients (corrected for initial scaling difference of 5.00E-012)

	Iteration	1	2	3	4	5	Final Weight Factor (1/σ^2)
DEC_2009 (in-house)	**GRACE: σ^2**	1.000000000000000	0.021745588158521	1.003672881592480	0.999999981708266	0.999999999999966	45,818056060952
	GOCE:σ^2	1.000000000000000	25.74901376557250	0.998582259111675	1.000000006868170	1.000000000000090	0,038891576818
	(σ_{GRACE}^2 / σ_{GOCE}^2)	1.000000000000000	0.000844521205996	0.994928006351305	0.999999974840096	0.999999999999876	**0,000848826427**
JUN_2010 (repr)	**GRACE: σ^2**	1.000000000000000	0.022455504731089	1.003549589268270	0.999998737623265	1.000000000425550	44,375053474536
	GOCE:σ^2	1.000000000000000	0.19195606119201	0.998284428560075	1.000000507659790	0.999999999828866	5,218475546446
	(σ_{GRACE}^2 / σ_{GOCE}^2)	1.000000000000000	0.116982525019758	0.994753462345559	0.999998229964374	1.000000000596680	0,117599307220
NOV DEC 2009 (in-house)	**GRACE: σ^2**	1.000000000000000	0.021622801820126	1.001725816010460	0.999999998461149	1.000000000000000	46,167798564666
	GOCE:σ^2	1.000000000000000	67.96535781583300	0.999278200535239	1.000000000600920	0.999999999999999	0,014724005764
	(σ_{GRACE}^2 / σ_{GOCE}^2)	1.000000000000000	0.000318144456456	0.997556601381235	0.999999997860229	1.000000000000000	**0,000318923714**
MAI JUN 2010 (repr)	**GRACE: σ^2**	1.000000000000000	0.022179916226760	1.001309291525300	0.999999997150220	1.000000000000010	45,026879863442
	GOCE:σ^2	1.000000000000000	22.18971847201500	0.999046937491816	1.000000001292410	0.999999999999997	0,045108908059
	(σ_{GRACE}^2 / σ_{GOCE}^2)	1.000000000000000	0.000999558252834	0.997740604174323	0.999999995857810	1.000000000000010	**0,001001821761**

December 2009	Relative weight of NEQ (σ_{GRACE}^2 / σ_{GOCE}^2)	RMS in [m] equivalent water height		RMS [mm]	RMS Improvement
		GRACE only	GRACE + SGG	Difference	[%]
d/o 30	**4,1145403473717E-015**	0.04018	0.04028	-0.102	
	1,00E-014	0.04018	0.04020	-0.022	**-0,0545720116**
	5,00E-014	0.04018	0.04048	-0.302	
	8,00E-014	0.04018	0.04338	-3.195	
	1,00E-013	0.04018	0.04701	-6.830	
	2,00E-013	0.04018	0.04844	-8.259	
	3,00E-013	0.04018	0.04996	-9.778	
	5,00E-013	0.04018	0.06842	-28.236	
	8,00E-013	0.04018	0.08963	-49.451	
	1,20E-012	0.04018	0.13376	-93.573	
d/o 35	**4,1145403473717E-015**	0.05995	0.06015	-0.199	
	1,00E-014	0.05995	0.05999	-0.042	**-0,0702299235**
	5,00E-014	0.05995	0.06055	-0.602	
	8,00E-014	0.05995	0.06656	-6.613	
	1,00E-013	0.05995	0.07399	-14.042	
	2,00E-013	0.05995	0.07686	-16.913	
	3,00E-013	0.05995	0.07989	-19.940	
	5,00E-013	0.05995	0.11509	-55.142	
	8,00E-013	0.05995	0.15353	-93.578	
	1,20E-012	0.05995	0.23014	-170.189	
d/o40	**4,1145403473717E-015**	0.08491	0.08495	-0.048	
	1,00E-014	0.08491	0.08491	-0.003	**-0,0038323994**
	5,00E-014	0.08491	0.08518	-0.275	
	8,00E-014	0.08491	0.09122	-6.316	
	1,00E-013	0.08491	0.09992	-15.017	
	2,00E-013	0.08491	0.10341	-18.504	
	3,00E-013	0.08491	0.10713	-22.223	
	5,00E-013	0.08491	0.15188	-66.973	
	8,00E-013	0.08491	0.20159	-116.680	
	1,20E-012	0.08491	0.30035	-215.447	
d/o45	**4,1145403473717E-015**	0.13696	0.13654	0.423	
	1,00E-014	0.13696	0.13685	0.111	
	5,00E-014	0.13696	0.13609	0.866	**0,6324467248**
	8,00E-014	0.13696	0.13794	-0.984	
	1,00E-013	0.13696	0.14431	-7.351	
	2,00E-013	0.13696	0.14723	-10.266	
	3,00E-013	0.13696	0.15048	-13.523	
	5,00E-013	0.13696	0.19577	-58.811	
	8,00E-013	0.13696	0.25157	-114.609	
	1,20E-012	0.13696	0.36687	-229.908	
d/o50	**4,1145403473717E-015**	0.28866	0.29007	-1.402	
	1,00E-014	0.28866	0.28898	-0.320	**-0,1110229995**
	5,00E-014	0.28866	0.29243	-3.768	
	8,00E-014	0.28866	0.31662	-27.958	
	1,00E-013	0.28866	0.34038	-51.719	
	2,00E-013	0.28866	0.34889	-60.229	
	3,00E-013	0.28866	0.35760	-68.939	
	5,00E-013	0.28866	0.44901	-160.349	
	8,00E-013	0.28866	0.53900	-250.336	
	1,20E-012	0.28866	0.70266	-414.000	
d/o55	**4,1145403473717E-015**	0.38031	0.38275	-2.441	
	1,00E-014	0.38031	0.38082	-0.511	**-0,1342347317**
	5,00E-014	0.38031	0.38768	-7.370	
	8,00E-014	0.38031	0.44844	-68.126	
	1,00E-013	0.38031	0.50638	-126.069	
	2,00E-013	0.38031	0.52606	-145.750	
	3,00E-013	0.38031	0.54565	-165.339	
	5,00E-013	0.38031	0.72577	-345.461	
	8,00E-013	0.38031	0.87466	-494.345	
	1,20E-012	0.38031	1.10903	-728.723	
d/o60	**4,1145403473717E-015**	0.53230	0.53755	-5.248	
	1,00E-014	0.53230	0.53347	-1.171	**-0,2199634582**
	5,00E-014	0.53230	0.54684	-14.538	
	8,00E-014	0.53230	0.64070	-108.399	
	1,00E-013	0.53230	0.72205	-189.755	
	2,00E-013	0.53230	0.74895	-216.648	
	3,00E-013	0.53230	0.77545	-243.148	
	5,00E-013	0.53230	1.01067	-478.373	
	8,00E-013	0.53230	1.19706	-664.764	
	1,20E-012	0.53230	1.47893	-946.634	

Table 14: December 2009: RMSE for combined gravity field solution for different relative weights of GRACE SST-ll and GOCE SGG normal equations at different d/o of the spherical harmonic expansion

December 2009 (in-house)	Relative weight of NEQ (σ_{GRACE}^2 / σ_{GOCE}^2)	RMS in [m] equivalent water height		RMS [mm]	RMS Improvement
		GRACE only	GRACE + SGG	Difference	[%]
	4,2441321350E-015	0.04018	0.04021	-0,0317989232	
	1,00E-017	0.04018	0.04018	-6,0973917505E-005	**-0,0001517425**
	1,00E-016	0.04018	0.04018	-0,0006127076	
	1,00E-015	0.04018	0.04019	-0,0064237714	
	1,00E-014	0.04018	0.04028	-0,0938471272	
	5,00E-014	0.04018	0.04130	-1,1139148237	
	8,00E-014	0.04018	0.04270	-2,5173647285	
	9,00E-014	0.04018	0.04328	-3,0967543119	
	1,00E-013	0.04018	0.04391	-3,7282314587	
	2,00E-013	0.04018	0.05258	-12,3964643169	
d/o 35	**4,2441321350E-015**	0.05995	0.06003	-0,0743639164	
	1,00E-017	0.05995	0.05995	-0,0001291678	**-0,0002154567**
	1,00E-016	0.05995	0.05995	-0,0013014964	
	1,00E-015	0.05995	0.05996	-0,0139960914	
	1,00E-014	0.05995	0.06019	-0,2372927665	
	5,00E-014	0.05995	0.06317	-3,2241155962	
	8,00E-014	0.05995	0.06726	-7,3140750257	
	9,00E-014	0.05995	0.06892	-8,9663357243	
	1,00E-013	0.05995	0.07069	-10,743161581	
	2,00E-013	0.05995	0.09318	-33,2290454368	
d/o40	**4,2441321350E-015**	0.08491	0.08484	0,0643316519	
	1,00E-017	0.08491	0.08490	0,0002126898	
	1,00E-016	0.08491	0.08490	0,0021138866	
	1,00E-015	0.08491	0.08489	0,0198381904	
	1,00E-014	0.08491	0.08484	0,068905239	**0,0811555132**
	5,00E-014	0.08491	0.08732	-2,414106735	
	8,00E-014	0.08491	0.09176	-6,8542672788	
	9,00E-014	0.08491	0.09365	-8,7485917541	
	1,00E-013	0.08491	0.09573	-10,8242366405	
	2,00E-013	0.08491	0.12349	-38,5871946048	
d/o45	**4,2441321350E-015**	0.13696	0.13654	0,4174351591	
	1,00E-017	0.13696	0.13696	0,0010486356	
	1,00E-016	0.13696	0.13695	0,0104725253	
	1,00E-015	0.13696	0.13686	0,103342261	
	1,00E-014	0.13696	0.13607	0,8950802478	
	5,00E-014	0.13696	0.13552	1,4378227211	**1,0498059506**
	8,00E-014	0.13696	0.13814	-1,1763564841	
	9,00E-014	0.13696	0.13953	-2,5717476988	
	1,00E-013	0.13696	0.14117	-4,208650817	
	2,00E-013	0.13696	0.16790	-30,9343549584	
d/o50	**4,2441321350E-015**	0.28866	0.28966	-1,0007946481	
	1,00E-017	0.28866	0.28867	-0,0021649548	**-0,0007499909**
	1,00E-016	0.28866	0.28869	-0,0216919344	
	1,00E-015	0.28866	0.28889	-0,2211242198	
	1,00E-014	0.28866	0.29127	-2,6014135415	
	5,00E-014	0.28866	0.30785	-19,1877019733	
	8,00E-014	0.28866	0.32404	-35,3773012531	
	9,00E-014	0.28866	0.32984	-41,1762650351	
	1,00E-013	0.28866	0.33578	-47,1178201175	
	2,00E-013	0.28866	0.39898	-110,3110696264	
d/o55	**4,2441321350E-015**	0.38031	0.38408	-3,7660574535	
	1,00E-017	0.38031	0.38032	-0,0075980855	**-0,0019978595**
	1,00E-016	0.38031	0.38039	-0,0762641031	
	1,00E-015	0.38031	0.38110	-0,7906705799	
	1,00E-014	0.38031	0.39074	-10,4281404651	
	5,00E-014	0.38031	0.46470	-84,385090963	
	8,00E-014	0.38031	0.53002	-149,7131298405	
	9,00E-014	0.38031	0.55156	-171,252173004	
	1,00E-013	0.38031	0.57273	-192,4221805645	
	2,00E-013	0.38031	0.75743	-377,121475513	
d/o60	**4,2441321350E-015**	0.53230	0.53825	-5,9543329571	
	1,00E-017	0.53230	0.53231	-0,0126813749	**-0,0023823853**
	1,00E-016	0.53230	0.53242	-0,1271147448	
	1,00E-015	0.53230	0.53360	-1,3008942368	
	1,00E-014	0.53230	0.54795	-15,6526702759	
	5,00E-014	0.53230	0.64280	-110,5051669608	
	8,00E-014	0.53230	0.72228	-189,9857918857	
	9,00E-014	0.53230	0.74820	-215,9003948086	
	1,00E-013	0.53230	0.77358	-241,2787557534	
	2,00E-013	0.53230	0.99244	-460,1418418256	

Table 15: December 2009 (in-house): RMSE for combined gravity field solution for different relative weights of GRACE SST-ll and GOCE SGG normal equations at different d/o of the spherical harmonic expansion

January 2009	Relative weight of NEQ	RMS in [cm] equivalent water height		RMS [mm]	RMS Improvement
	(σ_{GRACE}^2 / σ_{GOCE}^2)	GRACE only	GRACE + SGG	Difference	[%]
d/o 30	**5,3573130310051E-013**	4.46010	4.51370	-0.536	
	5,00E-014	4.46010	4.45400	0.061	
	8,00E-014	4.46010	4.45170	0.084	
	9,00E-014	4.46010	4.45110	0.090	
	1,00E-013	4.46010	4.45070	0.094	
	2,00E-013	4.46010	4.45040	0.097	0,2174839129
	3,00E-013	4.46010	4.46210	-0.020	
	5,00E-013	4.46010	4.50380	-0.437	
	8,00E-013	4.46010	4.60400	-1.439	
	1,20E-012	4.46010	4.78380	-3.237	
d/o 35	**5,3573130310051E-013**	6.14960	6.20780	-0.582	
	5,00E-014	6.14960	6.13660	0.130	
	8,00E-014	6.14960	6.13100	0.186	
	9,00E-014	6.14960	6.12950	0.201	
	1,00E-013	6.14960	6.12810	0.215	
	2,00E-013	6.14960	6.12690	0.227	0,3691296995
	3,00E-013	6.14960	6.13360	0.160	
	5,00E-013	6.14960	6.19250	-0.429	
	8,00E-013	6.14960	6.35840	-2.088	
	1,20E-012	6.14960	6.68420	-5.346	
d/o40	**5,3573130310051E-013**	8.17120	8.38470	-2.135	
	5,00E-014	8.17120	8.15010	0.211	
	8,00E-014	8.17120	8.14210	0.291	
	9,00E-014	8.17120	8.14020	0.310	
	1,00E-013	8.17120	8.13870	0.325	
	2,00E-013	8.17120	8.13750	0.337	0,4124241238
	3,00E-013	8.17120	8.18040	-0.092	
	5,00E-013	8.17120	8.34430	-1.731	
	8,00E-013	8.17120	8.77150	-6.003	
	1,20E-012	8.17120	9.58350	-14.123	
d/o45	**5,3573130310051E-013**	14.68290	14.86580	-1.829	
	5,00E-014	14.68290	14.64920	0.337	
	8,00E-014	14.68290	14.61970	0.632	
	9,00E-014	14.68290	14.61430	0.686	
	1,00E-013	14.68290	14.60940	0.735	
	2,00E-013	14.68290	14.60510	0.778	
	3,00E-013	14.68290	14.60230	0.806	0,5489378801
	5,00E-013	14.68290	14.81630	-1.334	
	8,00E-013	14.68290	15.39400	-7.111	
	1,20E-012	14.68290	16.56010	-18.772	
d/o50	**5,3573130310051E-013**	23.09110	24.33950	-12.484	
	5,00E-014	23.09110	23.05650	0.346	
	8,00E-014	23.09110	23.05330	0.378	0,163699434
	9,00E-014	23.09110	23.05500	0.361	
	1,00E-013	23.09110	23.05820	0.329	
	2,00E-013	23.09110	23.06270	0.284	
	3,00E-013	23.09110	23.39210	-3.010	
	5,00E-013	23.09110	24.16380	-10.727	
	8,00E-013	23.09110	25.91490	-28.238	
	1,20E-012	23.09110	28.93360	-58.425	
d/o55	**5,3573130310051E-013**	35.27320	38.30780	-30.346	
	5,00E-014	35.27320	35.27650	-0.033	-0,0093555447
	8,00E-014	35.27320	35.31450	-0.413	
	9,00E-014	35.27320	35.33290	-0.597	
	1,00E-013	35.27320	35.35400	-0.808	
	2,00E-013	35.27320	35.37780	-1.046	
	3,00E-013	35.27320	36.28130	-10.081	
	5,00E-013	35.27320	37.95160	-26.784	
	8,00E-013	35.27320	41.31990	-60.467	
	1,20E-012	35.27320	46.62530	-113.521	
d/o60	**5,3573130310051E-013**	45.64440	50.16490	-45.205	
	5,00E-014	45.64440	45.52380	1.206	0,2642164209
	8,00E-014	45.64440	45.52570	1.187	
	9,00E-014	45.64440	45.53780	1.066	
	1,00E-013	45.64440	45.55500	0.894	
	2,00E-013	45.64440	45.57870	0.657	
	3,00E-013	45.64440	46.89660	-12.522	
	5,00E-013	45.64440	49.58890	-39.445	
	8,00E-013	45.64440	54.97300	-93.286	
	1,20E-012	45.64440	63.12490	-174.805	

Table 16: January 2010: RMSE for combined gravity field solution for different relative weights of GRACE SST-ll and GOCE SGG normal equations at different d/o of the spherical harmonic expansion

May 2010	Relative weight of NEQ (σ_{GRACE}^2 / σ_{GOCE}^2)	RMS in [cm] equivalent water height		RMS [mm]	RMS Improvement
		GRACE only	GRACE + SGG	Difference	[%]
d/o 30	**1,9572849942E-013**	5.63670	5.69860	-0.619	
	5,00E-014	5.63670	5.60350	0.332	
	8,00E-014	5.63670	5.60090	0.358	**0,6351233878**
	9,00E-014	5.63670	5.60280	0.339	
	1,00E-013	5.63670	5.60600	0.307	
	2,00E-013	5.63670	5.61050	0.262	
	3,00E-013	5.63670	5.91030	-2.736	
	5,00E-013	5.63670	6.55410	-9.174	
	8,00E-013	5.63670	0.87347	47.6323	
	1,20E-012	5.63670	9.29200	-36.553	
d/o 35	**1,9572849942E-013**	8.44700	8.96020	-5.132	
	5,00E-014	8.44700	8.44070	0.063	**0,0745826921**
	8,00E-014	8.44700	8.48640	-0.394	
	9,00E-014	8.44700	8.50940	-0.624	
	1,00E-013	8.44700	8.53600	-0.89	
	2,00E-013	8.44700	8.56630	-1.193	
	3,00E-013	8.44700	9.70060	-12.536	
	5,00E-013	8.44700	11.61040	-31.634	
	8,00E-013	8.44700	14.98330	-65.363	
	1,20E-012	8.44700	19.65560	-112.086	
d/o40	**1,9572849942E-013**	11.98420	13.10680	-11.226	
	5,00E-014	11.98420	12.01490	-0.307	**-0,2561706247**
	8,00E-014	11.98420	12.12780	-1.436	
	9,00E-014	11.98420	12.17990	-1.957	
	1,00E-013	11.98420	12.23890	-2.547	
	2,00E-013	11.98420	12.20460	-2.204	
	3,00E-013	11.98420	14.51810	-25.339	
	5,00E-013	11.98420	17.92660	-59.424	
	8,00E-013	11.98420	23.56090	-115.767	
	1,20E-012	11.98420	30.94940	-189.652	
d/o45	**1,9572849942E-013**	16.51620	18.15070	-16.345	
	5,00E-014	16.51620	16.59370	-0.775	**-0,469236265**
	8,00E-014	16.51620	16.76690	-2.507	
	9,00E-014	16.51620	16.84390	-3.277	
	1,00E-013	16.51620	16.93000	-4.138	
	2,00E-013	16.51620	17.02490	-5.087	
	3,00E-013	16.51620	20.08000	-35.638	
	5,00E-013	16.51620	24.65380	-81.376	
	8,00E-013	16.51620	32.10320	-155.87	
	1,20E-012	16.51620	41.74600	-252.298	
d/o50	**1,9572849942E-013**	29.70370	31.41730	-17.136	
	5,00E-014	29.70370	29.51880	1.849	**0,6224813744**
	8,00E-014	29.70370	29.64190	0.618	
	9,00E-014	29.70370	29.71830	-0.146	
	1,00E-013	29.70370	29.81120	-1.075	
	2,00E-013	29.70370	29.92010	-2.164	
	3,00E-013	29.70370	34.22950	-45.258	
	5,00E-013	29.70370	41.09100	-113.873	
	8,00E-013	29.70370	52.17990	-224.762	
	1,20E-012	29.70370	66.11760	-364.139	
d/o55	**1,9572849942E-013**	44.81620	46.68910	-18.729	
	5,00E-014	44.81620	44.48130	3.349	**0,7472744231**
	8,00E-014	44.81620	44.58950	2.267	
	9,00E-014	44.81620	44.67160	1.446	
	1,00E-013	44.81620	44.77530	0.409	
	2,00E-013	44.81620	44.89960	-0.834	
	3,00E-013	44.81620	50.12510	-53.089	
	5,00E-013	44.81620	58.54470	-137.285	
	8,00E-013	44.81620	72.05020	-272.34	
	1,20E-012	44.81620	88.71020	-438.94	
d/o60	**1,9572849942E-013**	56.16440	59.56530	-34.009	
	5,00E-014	56.16440	55.75820	4.062	**0,7232339347**
	8,00E-014	56.16440	56.01240	1.52	
	9,00E-014	56.16440	56.16970	-0.053	
	1,00E-013	56.16440	56.36040	-1.96	
	2,00E-013	56.16440	56.58290	-4.185	
	3,00E-013	56.16440	64.92500	-87.606	
	5,00E-013	56.16440	77.23570	-210.713	
	8,00E-013	56.16440	95.71050	-395.461	
	1,20E-012	56.16440	117.22200	-610.576	

Table 17: May 2010: RMSE for combined gravity field solution for different relative weights of GRACE SST-ll and GOCE SGG normal equations at different d/o of the spherical harmonic expansion

June 2010	Relative weight of NEQ (σ_{GRACE}^2 / σ_{GOCE}^2)	RMS in [cm] equivalent water height		RMS [mm]	RMS Improvement
		GRACE only	GRACE + SGG	Difference	[%]
d/o 30	**2,9956050246E-013**	7.02840	7.09070	-0.623	
	5,00E-014	7.02840	7.02970	-0.013	**-0,0184963861**
	8,00E-014	7.02840	7.03270	-0.043	
	9,00E-014	7.02840	7.03410	-0.057	
	1,00E-013	7.02840	7.03560	-0.072	
	2,00E-013	7.02840	7.05800	-0.296	
	3,00E-013	7.02840	7.09090	-0.625	
	5,00E-013	7.02840	7.17780	-1.494	
	8,00E-013	7.02840	7.34110	-3.127	
	1,20E-012	7.02840	7.59410	-5.657	
d/o 35	**2,9956050246E-013**	11.01360	11.00770	0.059	
	5,00E-014	11.01360	10.99230	0.213	
	8,00E-014	11.01360	10.98420	0.294	
	9,00E-014	11.01360	10.98220	0.314	
	1,00E-013	11.01360	10.98050	0.331	
	2,00E-013	11.01360	10.98080	0.328	**0,2978136123**
	3,00E-013	11.01360	11.00790	0.057	
	5,00E-013	11.01360	11.12550	-1.119	
	8,00E-013	11.01360	11.42160	-4.080	
	1,20E-012	11.01360	11.97380	-9.602	
d/o40	**2,9956050246E-013**	15.11830	15.12290	-0.046	
	5,00E-014	15.11830	15.06850	0.498	
	8,00E-014	15.11830	15.05000	0.683	
	9,00E-014	15.11830	15.04560	0.727	
	1,00E-013	15.11830	15.04200	0.763	**0,5046863735**
	2,00E-013	15.11830	15.04920	0.691	
	3,00E-013	15.11830	15.12340	-0.051	
	5,00E-013	15.11830	15.42780	-3.095	
	8,00E-013	15.11830	16.15940	-10.411	
	1,20E-012	15.11830	17.44640	-23.281	
d/o45	**2,9956050246E-013**	22.99940	22.56170	4.377	
	5,00E-014	22.99940	22.83060	1.688	
	8,00E-014	22.99940	22.75070	2.487	
	9,00E-014	22.99940	22.72740	2.720	
	1,00E-013	22.99940	22.70560	2.938	
	2,00E-013	22.99940	22.56940	4.300	
	3,00E-013	22.99940	22.56190	4.375	**1,9022235363**
	5,00E-013	22.99940	22.84930	1.501	
	8,00E-013	22.99940	23.81210	-8.127	
	1,20E-012	22.99940	25.67890	-26.795	
d/o50	**2,9956050246E-013**	37.00550	37.58340	-5.779	
	5,00E-014	37.00550	36.91550	0.900	
	8,00E-014	37.00550	36.90420	1.013	**0,2737430922**
	9,00E-014	37.00550	36.90700	0.985	
	1,00E-013	37.00550	36.91290	0.926	
	2,00E-013	37.00550	37.12950	-1.240	
	3,00E-013	37.00550	37.58580	-5.803	
	5,00E-013	37.00550	39.01130	-20.058	
	8,00E-013	37.00550	41.90640	-49.009	
	1,20E-012	37.00550	46.33360	-93.281	
d/o55	**2,9956050246E-013**	47.19888	48.37870	-11.798	
	5,00E-014	47.19888	47.01650	1.824	
	8,00E-014	47.19888	46.99660	2.023	**0,4285694915**
	9,00E-014	47.19888	47.00036	1.985	
	1,00E-013	47.19888	47.01710	1.818	
	2,00E-013	47.19888	47.46870	-2.698	
	3,00E-013	47.19888	48.38350	-11.846	
	5,00E-013	47.19888	51.10530	-39.064	
	8,00E-013	47.19888	56.25620	-90.573	
	1,20E-012	47.19888	63.52650	-163.276	
d/o60	**2,9956050246E-013**	58.92120	59.70150	-7.803	
	5,00E-014	58.92120	58.41590	5.053	
	8,00E-014	58.92120	58.26680	6.544	
	9,00E-014	58.92120	58.24030	6.809	
	1,00E-013	58.92120	58.22470	6.965	**1,1820872623**
	2,00E-013	58.92120	58.59440	3.268	
	3,00E-013	58.92120	59.70760	-7.864	
	5,00E-013	58.92120	63.26770	-43.465	
	8,00E-013	58.92120	70.00240	-110.812	
	1,20E-012	58.92120	79.21810	-202.969	

Table 18: June 2010: RMSE for combined gravity field solution for different relative weights of GRACE SST-ll and GOCE SGG normal equations at different d/o of the spherical harmonic expansion

June 2010 (repr)	Relative weight of NEQ (σ_{GRACE}^2 / σ_{GOCE}^2)	RMS in [m] equivalent water height		RMS [mm]	RMS Improvement
		GRACE only	GRACE + SGG	Difference	[%]
d/o 30	**5,8799653610E-013**	0.07028	0.06961	0,670780376	
	5,00E-014	0.07028	0.07016	0,1199295187	
	8,00E-014	0.07028	0.07010	0,1844198648	
	9,00E-014	0.07028	0.07008	0,2047476296	
	1,00E-013	0.07028	0.07006	0,2245102387	
	2,00E-013	0.07028	0.06989	0,3933351437	
	3,00E-013	0.07028	0.06977	0,5160151491	
	5,00E-013	0.07028	0.06963	0,6502817178	**0,9252229493**
	1,00E-012	0.07028	0.06975	0,5349733942	
	5,00E-012	0.07028	0.07797	-7,6885361115	
d/o 35	**5,8799653610E-013**	0.11014	0.11003	0,1081669719	
	5,00E-014	0.11014	0.11002	0,1161145128	
	8,00E-014	0.11014	0.10996	0,1736801899	
	9,00E-014	0.11014	0.10994	0,1909538116	
	1,00E-013	0.11014	0.10993	0,2072962797	
	2,00E-013	0.11014	0.10981	0,3226339209	
	3,00E-013	0.11014	0.10978	0,3591557491	**0,3261031001**
	5,00E-013	0.11014	0.10990	0,2344302932	
	1,00E-012	0.11014	0.11107	-0,9387530131	
	5,00E-012	0.11014	0.13728	-27,1457405996	
d/o40	**5,8799653610E-013**	0.15118	0.14862	2,5587288015	**1,6924716821**
	5,00E-014	0.15118	0.15079	0,3929663913	
	8,00E-014	0.15118	0.15057	0,609462441	
	9,00E-014	0.15118	0.15050	0,6785569855	
	1,00E-013	0.15118	0.15044	0,7461530757	
	2,00E-013	0.15118	0.14984	1,3441072929	
	3,00E-013	0.15118	0.14937	1,812461307	
	5,00E-013	0.15118	0.14877	2,416044316	
	1,00E-012	0.15118	0.14877	2,4165341221	**1,5984169827**
	5,00E-012	0.15118	0.18067	-29,4891213091	
d/o45	**5,8799653610E-013**	0.22999	0.22038	9,6115612622	
	5,00E-014	0.22999	0.22889	1,1029646327	
	8,00E-014	0.22999	0.22826	1,7341806978	
	9,00E-014	0.22999	0.22805	1,9396888087	
	1,00E-013	0.22999	0.22785	2,1427992372	
	2,00E-013	0.22999	0.22595	4,0481456202	
	3,00E-013	0.22999	0.22425	5,7419562285	
	5,00E-013	0.22999	0.22142	8,5741630735	
	1,00E-012	0.22999	0.21694	13,0542401912	**5,6759153768**
	5,00E-012	0.22999	0.24059	-10,596645313	
d/o50	**5,8799653610E-013**	0.37006	0.35054	19,5169231484	
	5,00E-014	0.37006	0.36775	2,3084325717	
	8,00E-014	0.37006	0.36643	3,6251425112	
	9,00E-014	0.37006	0.36600	4,0530363115	
	1,00E-013	0.37006	0.36558	4,4755259634	
	2,00E-013	0.37006	0.36164	8,415535729	
	3,00E-013	0.37006	0.35818	11,8731453204	
	5,00E-013	0.37006	0.35254	17,513926376	
	1,00E-012	0.37006	0.34436	25,6917658469	**6,9426810042**
	5,00E-012	0.37006	0.39310	-23,046548741	
d/o55	**5,8799653610E-013**	0.47199	0.44880	23,1842879857	
	5,00E-014	0.47199	0.46849	3,5032155972	
	8,00E-014	0.47199	0.46655	5,4379901538	
	9,00E-014	0.47199	0.46593	6,0561334937	
	1,00E-013	0.47199	0.46533	6,6611728169	
	2,00E-013	0.47199	0.45996	12,026483975	
	3,00E-013	0.47199	0.45574	16,2505782646	
	5,00E-013	0.47199	0.45020	21,7926740861	
	1,00E-012	0.47199	0.44871	23,2783026062	**4,9319664191**
	5,00E-012	0.47199	0.58356	-111,5707793821	
d/o60	**5,8799653610E-013**	0.58921	0.56112	28,0960386553	**4,7684064019**
	5,00E-014	0.58921	0.58394	5,2750647863	
	8,00E-014	0.58921	0.58111	8,1065307221	
	9,00E-014	0.58921	0.58021	8,9975296907	
	1,00E-013	0.58921	0.57935	9,8628500845	
	2,00E-013	0.58921	0.57202	17,1939295308	
	3,00E-013	0.58921	0.56683	22,3813589787	
	5,00E-013	0.58921	0.56163	27,5773455015	**4,6803747835**
	1,00E-012	0.58921	0.56852	20,6918255948	
	5,00E-012	0.58921	0.77467	-185,4540964225	

Table 19: June 2010 (repr): RMSE for combined gravity field solution for different relative weights of GRACE SST-ll and GOCE SGG normal equations at different d/o of the spherical harmonic expansion

December 2010	Relative weight of NEQ ($\sigma_{GRACE}^2 / \sigma_{GOCE}^2$)	RMS in [m] equivalent water height		RMS [mm]	RMS Improvement
		GRACE only	GRACE + SGG	Difference	[%]
d/o 30	**2,0101192041E-014**	0.05709	0.05705	0.047	**0,0822117913**
	1,00E-016	0.05709	0.05709	0.000	
	1,00E-015	0.05709	0.05709	0.004	
	5,00E-015	0.05709	0.05708	0.018	
	1,00E-014	0.05709	0.05706	0.032	
	5,00E-014	0.05709	0.05710	-0.003	
	1,00E-013	0.05709	0.05746	-0.367	
	5,00E-013	0.05709	0.06793	-10.837	
	1,00E-012	0.05709	0.08931	-32.220	
	5,00E-012	0.05709	0.29242	-235.323	
d/o 35	**2,0101192041E-014**	0.07945	0.07913	0.319	**0,4013251522**
	1,00E-016	0.07945	0.07944	0.002	
	1,00E-015	0.07945	0.07942	0.023	
	5,00E-015	0.07945	0.07934	0.106	
	1,00E-014	0.07945	0.07925	0.194	
	5,00E-014	0.07945	0.07917	0.281	
	1,00E-013	0.07945	0.08048	-1.037	
	5,00E-013	0.07945	0.12216	-42.715	
	1,00E-012	0.07945	0.19194	-112.498	
	5,00E-012	0.07945	0.63579	-556.343	
d/o40	**2,0101192041E-014**	0.10702	0.10675	0.267	**0,249696591**
	1,00E-016	0.10702	0.10701	0.003	
	1,00E-015	0.10702	0.10699	0.025	
	5,00E-015	0.10702	0.10690	0.113	
	1,00E-014	0.10702	0.10682	0.195	
	5,00E-014	0.10702	0.10724	-0.222	
	1,00E-013	0.10702	0.11018	-3.162	
	5,00E-013	0.10702	0.17990	-72.880	
	1,00E-012	0.10702	0.28501	-177.994	
	5,00E-012	0.10702	0.88811	-781.098	
d/o45	**2,0101192041E-014**	0.15594	0.15578	0.165	**0,1056874204**
	1,00E-016	0.15594	0.15594	0.002	
	1,00E-015	0.15594	0.15592	0.024	
	5,00E-015	0.15594	0.15584	0.103	
	1,00E-014	0.15594	0.15578	0.164	
	5,00E-014	0.15594	0.15670	-0.760	
	1,00E-013	0.15594	0.16102	-5.072	
	5,00E-013	0.15594	0.25480	-98.854	
	1,00E-012	0.15594	0.39393	-237.985	
	5,00E-012	0.15594	1.15469	-998.750	
d/o50	**2,0101192041E-014**	0.24858	0.24681	1.770	
	1,00E-016	0.24858	0.24857	0.011	
	1,00E-015	0.24858	0.24846	0.113	
	5,00E-015	0.24858	0.24804	0.539	
	1,00E-014	0.24858	0.24757	1.012	
	5,00E-014	0.24858	0.24603	2.545	**1,0238640255**
	1,00E-013	0.24858	0.24914	-0.557	
	5,00E-013	0.24858	0.36834	-119.767	
	1,00E-012	0.24858	0.54855	-299.972	
	5,00E-012	0.24858	1.42487	-1176.296	
d/o55	**2,0101192041E-014**	0.35585	0.35285	3.002	
	1,00E-016	0.35585	0.35583	0.019	
	1,00E-015	0.35585	0.35567	0.187	
	5,00E-015	0.35585	0.35496	0.893	
	1,00E-014	0.35585	0.35416	1.688	
	5,00E-014	0.35585	0.35112	4.729	**1,3288079774**
	1,00E-013	0.35585	0.35459	1.258	
	5,00E-013	0.35585	0.50933	-153.479	
	1,00E-012	0.35585	0.73222	-376.369	
	5,00E-012	0.35585	1.71101	-1355.156	
d/o60	**2,0101192041E-014**	0.46125	0.45871	2.545	
	1,00E-016	0.46125	0.46123	0.018	
	1,00E-015	0.46125	0.46108	0.177	
	5,00E-015	0.46125	0.46042	0.833	
	1,00E-014	0.46125	0.45972	1.531	
	5,00E-014	0.46125	0.45858	2.671	**0,5790301227**
	1,00E-013	0.46125	0.46649	-5.239	
	5,00E-013	0.46125	0.66800	-206.752	
	1,00E-012	0.46125	0.92639	-465.144	
	5,00E-012	0.46125	1.96342	-1502.172	

Table 20: December 2010: RMSE for combined gravity field solution for different relative weights of GRACE SST-ll and GOCE SGG normal equations at different d/o of the spherical harmonic expansion

November / December 2009	Relative weight of NEQ (σ_{GRACE}^2 / σ_{GOCE}^2)	RMS in [m] equivalent water height		RMS [mm]	RMS Improvement
		GRACE only	GRACE + SGG	Difference	[%]
d/o 30	**1,6180601447E-015**	0.03489	0.03489	0,0026422262	
	1,00E-016	0.03489	0.03489	0,0001637929	
	1,00E-015	0.03489	0.03489	0,0016349813	
	5,00E-015	0.03489	0.03488	0,008109614	
	1,00E-014	0.03489	0.03487	0,0160569374	
	5,00E-014	0.03489	0.03482	0,0739742175	
	1,00E-013	0.03489	0.03476	0,1330159603	
	5,00E-013	0.03489	0.03470	0,1911464175	**0,5478444441**
	1,00E-012	0.03489	0.03532	-0,4293948364	
	5,00E-012	0.03489	0.04915	-14,2638481667	
d/o 35	**1,6180601447E-015**	0.04735	0.04735	0,0022863303	
	1,00E-016	0.04735	0.04735	0,0001425858	
	1,00E-015	0.04735	0.04735	0,0014182371	
	5,00E-015	0.04735	0.04734	0,0069221834	
	1,00E-014	0.04735	0.04734	0,0134234654	
	5,00E-014	0.04735	0.04730	0,0505938644	
	1,00E-013	0.04735	0.04729	0,0613689826	**0,129607043**
	5,00E-013	0.04735	0.04839	-1,0419870696	
	1,00E-012	0.04735	0.05190	-4,5508016322	
	5,00E-012	0.04735	0.10070	-53,3478127468	
d/o40	**1,6180601447E-015**	0.06458	0.06458	0,0026440288	
	1,00E-016	0.06458	0.06458	0,0001657358	
	1,00E-015	0.06458	0.06458	0,00164355	
	5,00E-015	0.06458	0.06457	0,0079114856	
	1,00E-014	0.06458	0.06457	0,0150599552	
	5,00E-014	0.06458	0.06453	0,045297297	**0,0701410547**
	1,00E-013	0.06458	0.06456	0,0180811735	
	5,00E-013	0.06458	0.06696	-2,383439056	
	1,00E-012	0.06458	0.07384	-9,2616012018	
	5,00E-012	0.06458	0.16132	-96,7351559319	
d/o45	**1,6180601447E-015**	0.11404	0.114026	0,0132775515	
	1,00E-016	0.11404	0.11404	0,0008236016	
	1,00E-015	0.11404	0.11403	0,0082181258	
	5,00E-015	0.11404	0.11400	0,0406936931	
	1,00E-014	0.11404	0.11396	0,0803980058	
	5,00E-014	0.11404	0.11368	0,3629934898	
	1,00E-013	0.11404	0.11341	0,6312713515	**0,5535537399**
	5,00E-013	0.11404	0.11420	-0,1606757005	
	1,00E-012	0.11404	0.12076	-6,7170681014	
	5,00E-012	0.11404	0.23169	-117,6487022115	
d/o50	**1,6180601447E-015**	0.21106	0.21103	0,0303251049	
	1,00E-016	0.21106	0.21106	0,0018795121	
	1,00E-015	0.21106	0.21104	0,0187634092	
	5,00E-015	0.21106	0.21097	0,0931135217	
	1,00E-014	0.21106	0.21088	0,1844737361	
	5,00E-014	0.21106	0.21021	0,8533161662	
	1,00E-013	0.21106	0.20952	1,5392194118	
	5,00E-013	0.21106	0.20915	1,9060217699	**0,9030725742**
	1,00E-012	0.21106	0.21806	-7,001850567	
	5,00E-012	0.21106	0.37271	-161,6461736969	
d/o55	**1,6180601447E-015**	0.28650	0.28645	0,0460548716	
	1,00E-016	0.28650	0.28649	0,0028577014	
	1,00E-015	0.28650	0.28647	0,0285094055	**0,0099510248**
	5,00E-015	0.28650	0.28636	0,1410489889	
	1,00E-014	0.28650	0.28622	0,2783734352	
	5,00E-014	0.28650	0.28525	1,2468568067	
	1,00E-013	0.28650	0.28435	2,1498102116	
	5,00E-013	0.28650	0.28665	-0,1513800869	
	1,00E-012	0.28650	0.30446	-17,9610731982	
	5,00E-012	0.28650	0.52396	-237,4677990862	
d/o60	**1,6180601447E-015**	0.38539	0.38529	0,0936170519	
	1,00E-016	0.38539	0.38538	0,0058103196	
	1,00E-015	0.38539	0.38533	0,0579575183	
	5,00E-015	0.38539	0.38510	0,2865617747	
	1,00E-014	0.38539	0.38482	0,5651117574	
	5,00E-014	0.38539	0.38287	2,5152800133	
	1,00E-013	0.38539	0.38108	4,3026513741	**1,1164522028**
	5,00E-013	0.38539	0.38574	-0,3544681215	
	1,00E-012	0.38539	0.41762	-32,2357290188	
	5,00E-012	0.38539	0.73392	-348,5375031365	

Table 21: November+ December 2009: RMSE for combined gravity field solution for different relative weights of GRACE SST-ll and GOCE SGG normal equations at different d/o of the spherical harmonic expansion

November / December 2009 (in-house)	Relative weight of NEQ (σ_{GRACE}^2 / σ_{GOCE}^2)	RMS in [m] equivalent water height		RMS [mm]	RMS Improvement
		GRACE only	GRACE + SGG	Difference	[%]
d/o 30	**1,5946185677E-015**	0.03489	0.03490	-0,0067559345	
	1,00E-016	0.03489	0.03489	-0,000410799	**-0,0011773903**
	1,00E-015	0.03489	0.03489	-0,0041855205	
	5,00E-015	0.03489	0.03491	-0,0226466143	
	1,00E-014	0.03489	0.03494	-0,0495725521	
	5,00E-014	0.03489	0.03531	-0,4150355997	
	1,00E-013	0.03489	0.03612	-1,225067955	
	5,00E-013	0.03489	0.05163	-16,7360839995	
	1,00E-012	0.03489	0.07858	-43,6891771572	
	5,00E-012	0.03489	0.27266	-237,767666124	
d/o 35	**1,5946185677E-015**	0.04735	0.04736	-0,0139677855	
	1,00E-016	0.04735	0.04735	-0,0008346601	**-0,0017627444**
	1,00E-015	0.04735	0.04736	-0,0085952429	
	5,00E-015	0.04735	0.04740	-0,048480402	
	1,00E-014	0.04735	0.04746	-0,1106211957	
	5,00E-014	0.04735	0.04843	-1,0770241185	
	1,00E-013	0.04735	0.05068	-3,3340394445	
	5,00E-013	0.04735	0.08820	-40,8492085193	
	1,00E-012	0.04735	0.14249	-95,1398663938	
	5,00E-012	0.04735	0.46981	-422,4631259583	
d/o40	**1,5946185677E-015**	0.06458	0.06457	0,0074716202	
	1,00E-016	0.06458	0.06458	0,0005478887	
	1,00E-015	0.06458	0.06458	0,0050009684	
	5,00E-015	0.06458	0.06457	0,0144190226	**0,0223272804**
	1,00E-014	0.06458	0.06458	0,0025405242	
	5,00E-014	0.06458	0.06558	-0,9983777243	
	1,00E-013	0.06458	0.06885	-4,265645799	
	5,00E-013	0.06458	0.12871	-64,1251626816	
	1,00E-012	0.06458	0.21114	-146,5628118485	
	5,00E-012	0.06458	0.65235	-587,7684801561	
d/o45	**1,5946185677E-015**	0.11404	0.11393	0,1123170925	
	1,00E-016	0.11404	0.11403	0,0071465694	
	1,00E-015	0.11404	0.11397	0,070844941	
	5,00E-015	0.11404	0.11370	0,3404600048	
	1,00E-014	0.11404	0.11339	0,6466508343	
	5,00E-014	0.11404	0.11214	1,8966755613	**1,6631704383**
	1,00E-013	0.11404	0.11337	0,6747064536	
	5,00E-013	0.11404	0.18028	-66,2407204942	
	1,00E-012	0.11404	0.28617	-172,1286280756	
	5,00E-012	0.11404	0.83483	-720,7903825773	
d/o50	**1,5946185677E-015**	0.21106	0.21062	0,4383616434	
	1,00E-016	0.21106	0.21103	0,0281162193	
	1,00E-015	0.21106	0.21078	0,2773847866	
	5,00E-015	0.21106	0.20976	1,3042472105	
	1,00E-014	0.21106	0.20865	2,407545139	
	5,00E-014	0.21106	0.20598	5,0781568675	**2,4060292842**
	1,00E-013	0.21106	0.21365	-2,585698822	
	5,00E-013	0.21106	0.36080	-149,7452723516	
	1,00E-012	0.21106	0.51645	-305,3903116388	
	5,00E-012	0.21106	1.15187	-940,8144884632	
d/o55	**1,5946185677E-015**	0.28650	0.28604	0,4534310613	
	1,00E-016	0.28650	0.28647	0,0303504911	
	1,00E-015	0.28650	0.28621	0,2919489937	
	5,00E-015	0.28650	0.28529	1,2070292614	
	1,00E-014	0.28650	0.28470	1,8015215462	**0,6288095185**
	5,00E-014	0.28650	0.29790	-11,3990415027	
	1,00E-013	0.28650	0.34148	-54,9821118275	
	5,00E-013	0.28650	0.72243	-435,9320380118	
	1,00E-012	0.28650	1.00150	-715,0057573739	
	5,00E-012	0.28650	1.79492	-1508,4186172235	
d/o60	**1,5946185677E-015**	0.38539	0.38429	1,0973214988	
	1,00E-016	0.38539	0.38531	0,0725382936	
	1,00E-015	0.38539	0.38468	0,702913742	
	5,00E-015	0.38539	0.38236	3,02330901	
	1,00E-014	0.38539	0.38053	4,8572073189	**1,2603484082**
	5,00E-014	0.38539	0.39997	-14,5800195516	
	1,00E-013	0.38539	0.47138	-85,9986477579	
	5,00E-013	0.38539	1.01817	-632,7857564161	
	1,00E-012	0.38539	1.36883	-983,4488936542	
	5,00E-012	0.38539	2.22921	-1843,8199903891	

Table 22: November+ December 2009 (in-house): RMSE for combined gravity field solution for different relative weights of GRACE SST-ll and GOCE SGG normal equations at different d/o of the spherical harmonic expansion

May / June 2010	Relative weight of NEQ (σ_{GRACE}^2 / σ_{GOCE}^2)	RMS in [cm] equivalent water height		RMS [mm]	RMS Improvement
		GRACE only	GRACE + SGG	Difference	[%]
d/o 30	**1,2013269749E-013**	5.28440	5.27914	0.053	
	1,00E-014	5.28440	5.28183	0.026	
	5,00E-014	5.28440	5.27560	0.088	
	8,00E-014	5.28440	5.27497	0.094	**0,1784143811**
	1,00E-013	5.28440	5.27635	0.080	
	2,00E-013	5.28440	5.30293	-0.185	
	3,00E-013	5.28440	5.35832	-0.739	
	5,00E-013	5.28440	5.53901	-2.546	
	8,00E-013	5.28440	5.94130	-6.569	
	1,20E-012	5.28440	6.64082	-13.564	
d/o 35	**1,2013269749E-013**	7.89036	7.96072	-0.704	
	1,00E-014	7.89036	7.89039	0.000	**-0,0004481097**
	5,00E-014	7.89036	7.90151	-0.112	
	8,00E-014	7.89036	7.92089	-0.305	
	1,00E-013	7.89036	7.93880	-0.484	
	2,00E-013	7.89036	8.08342	-1.931	
	3,00E-013	7.89036	8.30842	-4.181	
	5,00E-013	7.89036	8.94449	-10.541	
	8,00E-013	7.89036	10.20334	-23.130	
	1,20E-012	7.89036	12.16479	-42.744	
d/o40	**1,2013269749E-013**	10.50394	10.63561	-1.317	
	1,00E-014	10.50394	10.50158	0.024	**0,0225064403**
	5,00E-014	10.50394	10.51739	-0.134	
	8,00E-014	10.50394	10.55450	-0.506	
	1,00E-013	10.50394	10.59058	-0.866	
	2,00E-013	10.50394	10.89308	-3.891	
	3,00E-013	10.50394	11.36628	-8.623	
	5,00E-013	10.50394	12.66801	-21.641	
	8,00E-013	10.50394	15.09883	-45.949	
	1,20E-012	10.50394	18.63039	-81.264	
d/o45	**1,2013269749E-013**	14.91319	15.08757	-1.744	
	1,00E-014	14.91319	14.90730	0.059	**0,0395129019**
	5,00E-014	14.91319	14.92263	-0.094	
	8,00E-014	14.91319	14.97277	-0.596	
	1,00E-013	14.91319	15.02342	-1.102	
	2,00E-013	14.91319	15.45992	-5.467	
	3,00E-013	14.91319	16.14770	-12.345	
	5,00E-013	14.91319	18.02693	-31.137	
	8,00E-013	14.91319	21.48060	-65.674	
	1,20E-012	14.91319	26.40237	-114.892	
d/o50	**1,2013269749E-013**	24.87069	24.89353	-0.228	
	1,00E-014	24.87069	24.87030	0.004	
	5,00E-014	24.87069	24.77208	0.986	**0,3964948354**
	8,00E-014	24.87069	24.78921	0.815	
	1,00E-013	24.87069	24.83003	0.407	
	2,00E-013	24.87069	25.34495	-4.743	
	3,00E-013	24.87069	26.28173	-14.110	
	5,00E-013	24.87069	28.98251	-41.118	
	8,00E-013	24.87069	34.02524	-91.545	
	1,20E-012	24.87069	41.13869	-162.680	
d/o55	**1,2013269749E-013**	33.54892	33.52850	0.204	
	1,00E-014	33.54892	33.48780	0.611	
	5,00E-014	33.54892	33.35839	1.905	**0,567913728**
	8,00E-014	33.54892	33.37344	1.755	
	1,00E-013	33.54892	33.43239	1.165	
	2,00E-013	33.54892	34.22842	-6.795	
	3,00E-013	33.54892	35.67025	-21.213	
	5,00E-013	33.54892	39.68642	-61.375	
	8,00E-013	33.54892	46.79139	-132.425	
	1,20E-012	33.54892	56.26079	-227.119	
d/o60	**1,2013269749E-013**	41.31785	41.43931	-1.215	
	1,00E-014	41.31785	41.22600	0.919	
	5,00E-014	41.31785	41.05844	2.594	**0,6278422556**
	8,00E-014	41.31785	41.12496	1.929	
	1,00E-013	41.31785	41.25142	0.664	
	2,00E-013	41.31785	42.69192	-13.741	
	3,00E-013	41.31785	45.10223	-37.844	
	5,00E-013	41.31785	51.36432	-100.465	
	8,00E-013	41.31785	61.63266	-203.148	
	1,20E-012	41.31785	74.43617	-331.183	

Table 23: May + June 2010: RMSE for combined gravity field solution for different relative weights of GRACE SST-ll and GOCE SGG normal equations at different d/o of the spherical harmonic expansion

May / June 2010 (repr)	Relative weight of NEQ (σ_{GRACE}^2 / σ_{GOCE}^2)	RMS in [m] equivalent water height		RMS [mm]	RMS Improvement
		GRACE only	GRACE + SGG	Difference	[%]
d/o 30	**5,0091088030E-015**	0.05284	0.05283	0,0103336111	
	1,00E-016	0.05284	0.05284	0,0002076782	
	1,00E-015	0.05284	0.05284	0,0020742393	
	5,00E-015	0.05284	0.05283	0,0103149478	
	1,00E-014	0.05284	0.05282	0,0204901562	
	5,00E-014	0.05284	0.05275	0,0970314654	
	1,00E-013	0.05284	0.05266	0,1813085731	
	5,00E-013	0.05284	0.05233	0,5128783047	**0,9705518021**
	1,00E-012	0.05284	0.05245	0,3927647123	
	5,00E-012	0.05284	0.05892	-6,0807961446	
d/o 35	**5,0091088030E-015**	0.07890	0.07888	0,02337054	
	1,00E-016	0.07890	0.07890	0,0004685229	
	1,00E-015	0.07890	0.07890	0,0046816229	
	5,00E-015	0.07890	0.07888	0,0233282237	
	1,00E-014	0.07890	0.07886	0,0464576823	
	5,00E-014	0.07890	0.07868	0,2245231483	
	1,00E-013	0.07890	0.07847	0,4304969024	
	5,00E-013	0.07890	0.07737	1,5375655251	
	1,00E-012	0.07890	0.07698	1,9283048536	**2,4438756147**
	5,00E-012	0.07890	0.09163	-12,7247385926	
d/o40	**5,0091088030E-015**	0.10504	0.10500	0,0353285854	
	1,00E-016	0.10504	0.10504	0,0007084055	
	1,00E-015	0.10504	0.10503	0,0070783237	
	5,00E-015	0.10504	0.10500	0,0352646312	
	1,00E-014	0.10504	0.10497	0,0702131686	
	5,00E-014	0.10504	0.10470	0,3386872352	
	1,00E-013	0.10504	0.10439	0,6476657381	
	5,00E-013	0.10504	0.10281	2,2341086089	
	1,00E-012	0.10504	0.10250	2,541504405	**2,4195713883**
	5,00E-012	0.10504	0.12933	-24,2897040497	
d/o45	**5,0091088030E-015**	0.14913	0.14906	0,0676995137	
	1,00E-016	0.14913	0.14913	0,001357188	
	1,00E-015	0.14913	0.14912	0,0135614805	
	5,00E-015	0.14913	0.14906	0,0675769299	
	1,00E-014	0.14913	0.14900	0,134579694	
	5,00E-014	0.14913	0.14848	0,6503212231	
	1,00E-013	0.14913	0.14789	1,2460322826	
	5,00E-013	0.14913	0.14480	4,3299479661	
	1,00E-012	0.14913	0.14424	4,8892090233	**3,2784455635**
	5,00E-012	0.14913	0.19292	-43,7865804132	
d/o50	**5,0091088030E-015**	0.24871	0.24859	0,1216825037	
	1,00E-016	0.24871	0.24870	0,0024411771	
	1,00E-015	0.24871	0.24868	0,024389819	
	5,00E-015	0.24871	0.24859	0,1214623407	
	1,00E-014	0.24871	0.24847	0,2417117291	
	5,00E-014	0.24871	0.24755	1,1608070782	
	1,00E-013	0.24871	0.24650	2,2059011284	
	5,00E-013	0.24871	0.24170	7,0078784604	**2,8177253424**
	1,00E-012	0.24871	0.24245	6,2528839134	
	5,00E-012	0.24871	0.33173	-83,0206013135	
d/o55	**5,0091088030E-015**	0.33549	0.33528	0,2136072845	
	1,00E-016	0.33549	0.33548	0,0042917717	
	1,00E-015	0.33549	0.33545	0,0428674095	
	5,00E-015	0.33549	0.33528	0,2132213887	
	1,00E-014	0.33549	0.33507	0,423664156	
	5,00E-014	0.33549	0.33348	2,0092403108	
	1,00E-013	0.33549	0.33173	3,7557441044	
	5,00E-013	0.33549	0.32552	9,9693172624	**2,9715765041**
	1,00E-012	0.33549	0.33108	4,4053614972	
	5,00E-012	0.33549	0.47579	-140,3045414426	
d/o60	**5,0091088030E-015**	0.41318	0.41286	0,3217595346	
	1,00E-016	0.41318	0.41317	0,0064824905	
	1,00E-015	0.41318	0.41311	0,0647164923	
	5,00E-015	0.41318	0.41286	0,3211798912	
	1,00E-014	0.41318	0.41254	0,6363834312	
	5,00E-014	0.41318	0.41023	2,9487565233	
	1,00E-013	0.41318	0.40784	5,3429764279	
	5,00E-013	0.41318	0.40391	9,2644774323	**2,2422456276**
	1,00E-012	0.41318	0.42141	-8,2342225298	
	5,00E-012	0.41318	0.63558	-222,3973215303	

Table 24: May + June 2010 (repr): RMSE for combined gravity field solution for different relative weights of GRACE SST-ll and GOCE SGG normal equations at different d/o of the spherical harmonic expansion